Two-Dimensional Minimum Free Energy Autoregressive Parametric Modelling and Spectral Estimation.

A thesis

by

Mr P Kiernan M Sc B Sc

Submitted to

Dublin City University,

School of Computer Applications

for the degree of

Doctor of Philosophy

Supervisor Dr M Scott Ph D

January 1995

Declaration

I hereby certify that this material, which I now submit for assessment on the programme of study leading to the award of Ph D is entirely my own work and has not been taken from the work of others save and to the extent that such work has been cited and acknowledged within the text of my work

Signed P Kiernan ID No 92700012

Date 28/2/95

Dedicated to my parents Charles and Imelda who taught me the virtue of self motivation, and to my wife Sylvia for her unrelenting support and constant encouragement

"Then to Silvia let us sing,
That Silvia is excelling
She excels each mortal thing
Upon the dull earth dwelling
To her let us garlands bring "

W Shakespeare

Acknowledgements

I would like to express my sincere gratitude to Professor M Ryan and Dr M Scott for their help and encouragement during this research project I would like to thank Mr J Doyle and Mr D O'Callahan for their friendly assistance on numerous occasions I would also like to thank the library staff in D C U and D I T for their fortitude in coping with my many demands Special thanks are due to Dr J Pimbley for his very kind and timely letter of encouragement A debt of gratitude is also owed to Mr C V Cowley, Mr C J Bruce and my departmental colleagues for their good humoured support Finally, I would like to thank the many researchers in this and related fields whose dedication and hard work has been a constant source of inspiration

Contents

Figures

Tables

Two-Dimensional Minimum Free Energy Autoregressive Parametric Modelling and Spectral Estimation

P Kiernan

Abstract

We present a new high resolution spectral estimation method This method is a 2-D extension of the Minimum Free Energy (MFE) parameter estimation technique based on extension of the multidimensional Levinson method Our 2-D MFE technique determines autoregressive (AR) models for 2-D fields MFE-AR models may be used for 2-D spectral estimation The performance of the technique for spectral estimation of closely spaced 2-D sinusoids in white noise is demonstrated by numerical example

Experimental results from tests on spectral resolution, estimator bias and variance, and tolerance to change in signal processing temperature are examined The effects on spectral estimation of signal to noise ratio, data set size, model size, autocorrelation type, and dynamic range difference are illustrated The spectral estimates from combined and single quarter plane estimates are contrasted The results illustrate that MFE provides accurate low model order spectral estimation

The performance of the method is compared to the multidimensional Levinson, conventional transform, modified covariance (MCV), hybrid, and maximum entropy methods It is seen that our MFE method provides superior spectral estimation over that which can be achieved with the Levinson algorithm with equivalent computational burden Superior spectral resolution is achieved at lower data set size than that provided by the Fourier transform method In terms of spectral resolution, the MFE method performs just as well as the MCV method for snapshot data It is seen that MFE provides spectral estimates that are as good as if not better than that provided by hybrid and maximum entropy methods

The computational expense, stability, and accuracy of spectral estimation over a number of mdependent simulation trials are examined for both MFE and MCV methods The bias and variance statistics for MFE are comparable to those for MCV However, the computational expense is far less than that of MCV and maximum likelihood methods

Models generated by our method give rise to stable and causal systems that are recursively computable Hence they may also be used for correlation extension and for field modelling applications such as texture generation

Abbreviations

ACS	Autocorrelation sequence
AR	Autoregressive
ARMA	Autoregressive moving average
CGI	Computer generated imagery
CRB	Cramer-Rao bound
GRF	Gibbs random field
LMS	Least mean square
MA	Moving average
m-D	Multidimensional
MCV	Modified covariance method
MDSP	Multidimensional digital signal processing
MEM	Maximum entropy method
MFE	Minimum free energy
MLE	Maximum likelihood estimation
MRF	Markov random field
MV	Minimum variance
NSHP	Non-symmetric half plane
PSD	Power spectral density
QP	Quarter plane
SAR	Simultaneous autoregressive
SNR	Signal to noise ratio
SPA	Single peak area

Chapter 1. Introduction

1.1 Introduction

The areas of multidimensional digital signal processing (MDSP) and multidimensional spectral estimation are introduced We describe various multidimensional spectral estimation techniques and reference is made to application areas We outline our 2-D minimum free energy (MFE) method and its connections with both the multidimensional Levinson algorithm [52] and 1-D MFE [66], [67] We comment on the originality of our technique and on its advantages over other methods We discuss the requirement for parametric spectral estimation techniques Comment is also made on the necessity for ongoing research in the area of multidimensional spectral estimation

1.2 Multidimensional spectral estimation

Digital signal processing (DSP) has been an active field of research for more than twenty-five years It is concerned with the processing of sampled temporal signals MDSP is concerned with the processing of signals that can be represented as multidimensional arrays such as sampled images or sampled temporal waveforms received simultaneously from a number of sensors in some spatial dimension Such signals are multidimensional (m-D, where m ≥ 2) in the variable sense There is a substantial difference between the theories for the processing of 1-D and 2-D signals However apart from the issue of computational complexity there is little difference between the 2-D and higher-dimensional cases [17], [54] The 2-D case is the most prevalent case in applications

DSP may be divided into the two major areas of digital filtering and spectral analysis Spectral analysis or estimation is the process of characterizing the frequency content of a measured signal Marple [52] provides an interesting historical account of the developments in spectral estimation from early times The aim of multidimensional spectral estimation is to derive an estimate of the power spectral density (PSD) of an observed or measured multidimensional signal Specifically, the 2-D PSD function describes the distribution of power with spatial frequency of a 2-D process The spatial frequency (f_x, f_y) may be thought of as the fraction of the sampling frequency used in obtaining the data samples from a continuous process The autocorrelation at some lag $(k\ l)$ in 2-D is the mean product of observed field values at points of distance (k, l) from one another Since the PSD is based on an infinite number of autocorrelation values and we have a finite observed field, we may at best only determine an estimate of the PSD

The various techniques for multidimensional spectral estimation are reviewed by Dudgeon and Mersereau [17], and McClellan [54] The two main classes of spectral estimators are classical methods based on the Fourier transform, and modern spectral estimation methods Modern

methods include autoregressive (AR), maximum entropy (MEM) and minimum variance (MV) techniques These techniques generally produce higher resolution spectral estimates than classical methods In determining spectral resolution it is important to differentiate between close spurious peaks caused by noise, and valid peaks Spectral resolution is defined as the closeness of the closest valid spectral components that the method can resolve It is an indication of the ability of a spectral estimator to display spectral fine detail

It is possible to derive parametric models of an observed process The model parameters may be used to estimate the spectral characteristics of the process The process may also be classified and synthesized using the model parameters Examples of parametric models include AR and autoregressive moving average (ARMA) models [7], [85] These models are a direct extension of linear time series models [38] Parametric spectral estimation in the 2-D variable case essentially involves determination of a set of parameters in multidimensional parameter space which may be used to generate a spectral estimate on the 2-D spatial frequency plane for a 2-D process

Cadzow and Ogino [7] have developed a 2-D ARMA model spectral estimation method However the overall resolution capability of this procedure is predominantly influenced by the AR parameter selection AR models have dominated the research effort to date and are finding much use in industry [52] In 1-D it has been found that moving average (MA) models characterize broad spectral peaks well but produce poor spectral estimates of narrowband peaks Hence MA parametric spectral estimators are not classed as high resolution estimators The use of 2-D MA models for spectral estimation has not been studied in the literature

The key AR spectral methods are the modified covariance method (MCV) [38] and that due to solution of the Yule-Walker equations by the Levinson algorithm These methods produce causal, recursively computable systems [3] The output of such systems is calculated from spatial or temporal past outputs and the spatial or temporal present input The efficient multichannel

Levinson algorithm has been extended and modified to produce the multidimensional Levinson algorithm [52] This algorithm determines a set of parameters in multidimensional parameter space for a 2-D process In multichannel signal processing there are a number of simultaneous temporal processes each on a different channel Multichannel spectral estimation is concerned with the problem of estimating the auto-spectra of the individual channels and the cross-spectra between channels

The MEM is a popular high resolution technique for 1-D spectral estimation However this method does not extend easily from the 1-D case to 2-D The MEM maximizes the entropy of an observed field subject to the constraint that the inverse Fourier transform of the resultant PSD equals the known autocorrelation values of the observed field Unlike the 1-D case, 2-D AR spectral estimation does not yield identical results to that given by MEM This is because the 2-D process does not possess the autocorrelation sequence (ACS) matching property In other words the inverse Fourier transform of the PSD estimate is not necessarily equal to the known autocorrelation function [50] Hence the relationship between these alternative representations of a 2-D AR process is not one to one This may be attributed to the lack of a factorisation theorem for 2-D polynomials This means that 'the inverse polynomial of the 2-D maximum entropy PSD cannot be factored, requiring non-linear means of solution to find the 2-D maximum entropy PSD, which is not always guaranteed to exist given any arbitrary set of 2-D ACS values' [52] Hence the existence of the MEM estimate is not always certain The MEM method may also produce poorly resolved or negative power spectra for closely spaced sinusoids in both the temporal and spatial frequency domains This is also due to the type of estimated autocorrelation used and is discussed in Section 2 5

A 2-D hybrid technique uses a Fourier transform for one dimension along with a higher resolution 1-D spectral estimator for the other dimension It is generally used when the required resolution for a spectral estimate in one dimension is achievable using a Fourier transform estimator MEM is often used as the high resolution estimator An application example which uses the hybrid

method for frequency wavenumber estimation in array processing is given by Kay in [38] and is discussed in more detail in Section 1 3 on applications

The high resolution performance of some 1-D spectral estimators [38] has promoted an interest in 2-D versions of these estimators In general MDSP can be quite different from 1-D DSP This is because mathematics in the multidimensional case is less complete than in the 1-D case and the computational load imposed at higher dimension is far greater Our method is based on extension of the multidimensional Levinson algorithm It is also based on a 2-D extension of the MFE method developed by Pinbley [66], and Pinbley and Silverstein [67]

Choice of the most suitable method of spectral estimation depends on the particular application 2-D AR parametric estimation may be better suited to a particular application 'In many areas of application, treatment of m-d random fields is unnecessarily general considering that their PSD may not be arbitrary but instead a low-order parametric rational function However if the parametric form of such fields is ignored, then much is lost in estimating their power spectrum In other words, if the given random field is better described by a finite set of parameters which is much smaller than the total number of observations, then parametric spectrum estimation approach will be more accurate than any of the standard approaches '[60]

As only an estimate of the PSD may be determined, the bias and variance of spectral estimates are commonly used statistical measures of estimator performance These measures are calculated over a number of simulation trials Analytical determination of bias and variance of spectral estimates is usually not mathematically tractable even in 1-D [52] Resolution and computational expense may also be used as performance measures for comparison of various spectral estimation methods In comparing spectral estimators the same data set should be used for snapshot or single data record comparison Alternatively, if statistical tests are carried out to determine the bias or variance over a number of simulation runs, the same set of snapshots should be used for each estimator This ensures that one estimator does not enjoy an unfair advantage 'Only very limited

experimental results have been reported in the literature regarding 2-D spectral estimators, so performance comparisons are difficult to make' [52] We address this issue by comparing the performance of MFE spectral estimation with a number of other methods These include the modified covariance, Levinson, hybrid, maximum entropy, and conventional transform methods

1.3 Applications

Successful extensions of 1-D spectral estimators will find application in many areas of multidimensional systems High resolution spectral estimation of 2-D homogeneous fields is becoming increasingly important because of its role in various areas Such areas include analysis of space-space, space-time, and time-time data arrays Space-space data arrays may be used in image processing [30], whereas space-time applications include sonar, seismic [8] and biomedical signal processing [68], [61] Time-time arrays are typically used in the analysis of radar pulse repetition versus arrival time [55] As stated by McClellan [54] 'The operation of spectral analysis arises in many fields of application Situations in which signals are inherently multidimensional can be found in geophysics, radio astronomy, sonar, and radar, to mention a few These multidimensional problems present a challenging set of theoretical and computational difficulties that must be tackled' Other areas where spectrum estimation techniques are essential include geophysics [70], radio astronomy [57], and biomedical imaging [31] In short, any field in which the frequency spectrum of a directly measured quantity is of interest will benefit from continuing advances in power spectrum estimation [66]

As seen in Section 1 2, an application example of frequency wavenumber estimation for space-time array processing is given in [38] A spectral estimator with higher spectral resolution in one dimension than the other may be used in applications where there is a wealth of time data and a lack of spatial data The lack of spatial data may be due to the small number of spatial sensors relative to the number of time samples available for each sensor A full high-resolution 2-D technique is needed if the temporal data is too small to allow adequate temporal frequency

resolution using Fourier techniques Another example of frequency wavenumber spectral analysis where there is lack of symmetry in the spatio-temporal functions is in the biomedical signal processmg area [68]

Besides spectral estimation, parametric representations of 2-D random fields are useful in many applications such as texture modelling and synthesis [56] In [44] we model and synthesise the random field element of a number of texture fields using maximum likelihood AR and ARMA models Spectral estimates based on these parametric models are also given References to applications of random field models in image processing and analysis are given m [37] These include areas such as design of image enhancement or restoration algorithms, image coding and segmentation, and texture characterisation

1.4 Active research

There are three main reasons that explain why 2-D spectral estimation contmues to be an active area of research

Firstly, there are inherent mathematical difficulties associated with MDSP This is due m part to differences m 1-D and 2-D linear systems theory in the inability to factor a 2-D polynomial into polynomials of lower degrees The mathematics for describing 2-D systems is less complete than for 1-D systems and there is no fundamental theory of algebra for polynomials of dimension greater than unity Bose [2], [4] concentrates on some of the mathematical limitations encountered in MDSP and on the progress that has been made to overcome these limitations This goes some of the way to bridge the gap between DSP and polydisc algebra [71] This algebra is concerned with the study of functions on m-D complex space [48], [49], [9] as opposed to functions on 1-D complex space such as temporal processes

Secondly the computational burden imposed by advanced 2-D spectral estimation methods have in general limited their testing and application to small 2-D data sets Such data sets typically

consist of simple signal scenarios, such as a few sinusoids in spatially white noise The computational burden has also limited the dimension of the parameter space that can be used Only the 2-D periodogram, 2-D hybrid methods and the 2-D minimum variance method have seen practical application to extensive 2-D data sets [52]

Finally, in many of the applications cited above in Section 1 3 one of the major performance criteria is high resolution [47] at small data set size This is reiterated by Nikias and Raghuveer [60] They state that 'Important requirements to be satisfied by the spectrum estimation method are high resolution/good spectrum matching, and tolerance towards inhomogeneities in the data field while making use of small sized data set' Small data sets or limited data sequences often occur in practice 'For example, to study intra pulse modulation characteristics of a radar, only a few time samples may be taken from a single very short radar pulse In sonar, many data samples are available, but target motion necessitates that the analysis interval be short in order to assume that the target statistics are effectively unchanging within the analysis interval ' [52]

'Digital spectral estimation continues to be an active area of research for better estimation methods and faster computational algorithms ' [52] The search continues for an efficient high resolution multidimensional parametric spectral estimation technique that is computationally efficient and capable of operatmg with small data sets and at low signal to noise ratio (SNR) This is due to the plethora of applications in which 2-D spectral estimators are used, the problems associated with multidimensional mathematical difficulties, and the high computational burden of existing advanced 2-D spectral estimation techniques Furthermore the efficiency and high resolution of 1-D techniques make extension of these techniques to 2-D an attractive option

1.5 Minimum Free Energy Autoregressive Spectral Estimation

We present a new high resolution 2-D spectral estimation method Our concentration is on causal 2-D AR models with quarter plane (QP) parameter region of support These models are a direct

extension of the linear time series seasonal analysis models of Box and Jenkins [5] A causal system is one for which the output is derived from the present input and past outputs To obtain a stable and causal system [38] the region of support for the AR model must be in the non-symmetric half plane (NSHP) This region may be expressed for a $p_1 \times p_2$ order model as

$$\{a(m,n)\} \text{ for } -(p_1-1) \le m \le (p_1-1) \text{ if } 1 \le n \le (p_2-1),\ 1 \le m \le (p_1-1) \text{ if } n = 0 \quad (1)$$

This ensures recursive computability Bose [3] defines recursive computability 'Recursibility (recursive computability) is defined to be a property of certain difference equations which allows one to iterate the equation by choosing an indexing scheme so that every output sample can be computed from outputs that have already been found, from initial conditions and from samples of the input sequence' The definition of causality assumes that the output is calculated in a way that is analogous to that of a raster screen where lines are scanned top to bottom moving left to right NSHP spectral estimators perform poorly for data fields comprising sinusoids in noise This may be due to the high model orders required [52] For this reason much of the discussion on AR spectral estimation is based on models with QP region of support The first QP region is a subset of the NSHP region given in expression (1) above The first and fourth QP region of support for a $p_1 \times p_2$ order model may be expressed as

$$\{a_1(m,n)\} \text{ for } 0 \le m \le (p_1-1) \text{ if } 1 \le n \le (p_2-1),\ 1 \le m \le (p_1-1) \text{ if } n = 0 \quad (2)$$

$$\{a_4(m,n)\} \text{ for } 0 \le m \le (p_1-1) \text{ if } -(p_2-1) \le n \le -1,\ 1 \le m \le (p_1-1) \text{ if } n = 0 \quad (3)$$

The multidimensional Levinson recursion is an established autocorrelation based method for deriving the parameters of a causal QP AR model [29] In this algorithm, reflection coefficient matrices and hence the AR parameters are determined by the minimization of the forward and backward linear prediction error energy The reflection coefficients are analogous to physical parameters in a seismic model or acoustic tube model of speech An estimation technique that chooses model parameters commensurate with the global minimum of a prediction error energy

objective function falls within the general class referred to as least mean square (LMS) algorithms If the observed field is contaminated by noise or the data set size is too small LMS algorithms often produce unreliable estimates 'It is well known, that some LMS based algorithms work well at high signal to noise ratios (SNR's), but invariably suffer severe degradation at low SNR's ' [67]

We show how the AR model parameters for 2-D fields may be determined by the solution of Yule-Walker equations by an MFE based modified multidimensional Levinson algorithm Our extension [39], [40], [41], [42], [43] to the Levinson algorithm [52] is based on determination of the reflection coefficient matrices by minimisation of the free energy rather than by minimisation of the prediction error energy alone The MFE method through a signal entropy or smoothness measure compensates for noise or incomplete data and thereby provides better spectral estimation than that provided by the LMS approach

The choice of a cost function based on free energy is motivated by the desire to conceptually model a stochastic signal analysis system in a way that is analogous to statistical thermodynamic models used in physical systems [67] Hence, the connection between thermodynamic systems and parameter estimation comes from a common conceptual approach to solving a problem for a complicated stochastic process The free energy in a physical system is the combination of energy and entropy At any temperature there is a balance between energy and entropy Fluctuations in a thermodynamic system are analogous to noise in a signal processing system Minimizing the free energy at some entropy energy level compensates for system noise

The QP models generated by our method give rise to stable and causal systems Hence in addition to spectral estimation they may be used for field synthesis and correlation extension [50] An example of the use of field synthesis is for texture generation in computer generated imagery (CGI) Correlation extension is used to provide improved spectral estimation by extending the

autocorrelation and subsequently applying a Fourier transform The cost of the improved spectral estimation by correlation extension is added computational expense

Our 2-D MFE spectral estimation method is an original and unique extension of a 1-D method We are encouraged by the support expressed by Pimbley [65] for our extension of the 1-D concept to 2-D There have been no previous publications apart from the author's that extend the MFE method of parameter estimation to 2-D and provide combmed quarter plane spectral estimation of closely spaced sinusoids based on such an extension In [12] a 1-D MFE method is used along with a 1-D periodogram as part of a hybrid separable algorithm for 2-D spectral estimation Our method responds to the call in this paper for an efficient 2-D MFE algorithm

The 2-D MFE method provides accurate spectral estimates and is particularly useful for low SNR data sets even at low data set size Hence, our research also responds to the call by Marple [52] for more effort to be directed towards signals buried deeper in noise MFE provides accurate spectral estimation over broad temperature ranges, rendering determination of specific critical temperatures unnecessary The resolution quality of MFE spectral estimates and accuracy of peak location in the spatial frequency plane improve with model order

The 2-D MFE method may be preferred over the Levinson algorithm because it can outperform the Levinson technique producing superior spectral estimates with similar computational burden The method may also be preferred over MCV as it is significantly faster and can produce spectral estimates with variance and bias comparable to that of MCV MFE performs accurate spectral estimation at low SNR and low data set size producing estimates with superior resolution over those produced by the conventional Fourier transform method. The MFE method performs as well as if not better than the hybrid dual 1-D method [47] and the maximum entropy method [51]

Chapter 2. 2-D MFE Theory

2.1 Introduction

In Chapter 2 we discuss simultaneous autoregressive models giving their descriptions in the spatial and frequency domains We provide the theoretical development of 2-D MFE from Yule-Walker equations [52] through to the cost functions required for the optimisation in our algorithm Implementation issues concerning optimisation and associated MFE cost functions are studied We outline the benefit of using combined QP spectral estimators over the use of single QP estimators The exact, biased and unbiased forms of the autocorrelation function are examined and compared Finally we provide details concerning the implementation environment for 2-D MFE and the simulations that follow in Chapters 3 and 4

2.2 AR Models

A discrete 2-D signal is any function $y(m,n)$ that is an array of real or complex numbers defined for the ordered integer pair (m,n) over $-\infty < m,n < \infty$ This discrete signal may represent a sampled continuous 2-D function in space or time and may typically be assumed to have a region of support over $1 \leq m \leq N,\ 1 \leq n \leq N$

A simultaneous AR (SAR) model [7] may be represented by

$$\sum_{i=0}^{p1}\sum_{j=0}^{p2} a(i,j)y(m-i,n-j) = u(m,n) \tag{4}$$

where $\{y(m,n)\}$ is a finite set of observations on $1 \leq m \leq N,\ 1 \leq n \leq N$ and is a homogeneous random field A homogeneous random field will have an autocorrelation function that is mdependent of where on the field it is evaluated and is dependent only on the distance between the points or the lag employed The autocorrelation is therefore not a function of position Finite observation sets may be considered to be locally stationary hence permitting spectral estimation techniques to be used [52] $\{u(m,n)\}$ is uncorrelated Gaussian white noise with zero mean and variance σ^2 A toroidal model is assumed on this $N \times N$ lattice [36] This means that the 2-D field may be regarded as doubly periodic and that $y(1, n)$ is the east neighbour of $y(N, n)$ and that $y(m, N)$ is the north neighbour of $y(m, 1)$

A causal system is one for which the model region of support is in the NSHP or QP Spectral factorization, which is a feature of 1-D systems, generalizes to 2-D when these regions of support are used Hence the SAR model in (4) is factorable and a special case of the conditional AR model [34], [32] m which $\{u\}$ is correlated The autoregressive model parameters are given by $\{a\}$ over the $p_1 \times p_2$ QP region of support where $a(0,0) = 1$ The first QP PSD of this model [85] may be written in normalised spatial frequency terms (f_x, f_y) where $|f_x| \leq 1/2,\ |f_y| \leq 1/2$ as

$$S(f_x,f_y)=\frac{\sigma^2}{\left|\sum_{k=0}^{p1}\sum_{l=0}^{p2}a_{kl}e^{-j(2\pi f_x k+2\pi f_y l)}\right|^2} \tag{5}$$

or $$S(f_x,f_y)=\beta\Big/|D(f_x,f_y)|^2 \quad \text{where} \quad \beta=\sigma^2 \tag{6}$$

2.3 Single and Combined QP spectral estimators

Using a single quarter plane spectral estimator may result in elliptical contours of constant PSD level This is due to the directional dependency of the resolution characteristics of quarter plane estimators [86] This may be overcome to some extent by using a combined quarter plane estimator Quarter plane estimates are combined in parallel resistor fashion to form a combined estimate Single quadrant spectra may also suffer from spurious peaks at high SNR or at high model order [86] Hence another motivation for the use of a combined estimator is that spurious peaks are less likely to occur if quarter plane estimates are combined [38] In Chapter 3 we examine how the directional dependency and spurious peaks of single quadrant spectra may be overcome by the use of combined spectra Unless otherwise stated we combine first and fourth quarter plane estimates for all PSD estimates

2.4 2-D MFE

The Yule-Walker equations are derived by multiplying expression (4) by *y(m-k, n-l)* and taking the expectation These equations are therefore based on the autocorrelation estimates of the observed field and are given by

$$\sum_{i=0}^{p1}\sum_{j=0}^{p2}a(i,j)r_{yy}(k-i,l-j)=(\sigma^2 \text{ for } (k,l)=(0,0),\ 0 \text{ for } (k,l)\in \text{QP}')$$

where $$\text{QP} = \text{QP}' \cup (0,0) \tag{7}$$

or in matrix form [38] as $\mathbf{R}\underline{\mathbf{a}} = \underline{\boldsymbol{\rho}}$ (8)

where $\underline{\mathbf{a}} = \begin{bmatrix} \mathbf{a}[0] \\ \mathbf{a}[1] \\ \\ \\ \mathbf{a}[p_1 - 1] \end{bmatrix}$ (9) with $\mathbf{a}[l] = \begin{bmatrix} a(l, 0) \\ a(l, 1) \\ \\ \\ a(l, p_2 - 1) \end{bmatrix}$ (10)

and $\underline{\boldsymbol{\rho}} = \begin{bmatrix} \boldsymbol{\rho} \\ \mathbf{0} \\ \\ \\ \mathbf{0} \end{bmatrix}$ (11) with $\boldsymbol{\rho} = \begin{bmatrix} \sigma^2 \\ 0 \\ \\ \\ 0 \end{bmatrix}$ (12)

$\mathbf{R}$ is a block Toeplitz matrix which is symmetric and positive semi-definite The positive semi-definiteness of the matrix ensures its eigenvalues are nonnegative Furthermore the matrix is made up of blocks $\mathbf{R}_{yy}$ that are also Toeplitz in structure though not symmetric and have elements r_{yy} that are derived from the correlation of the observed field *{y(m,n)}* The matrix in expression (13) below is of order $p_1 p_2$ x $p_1 p_2$ $\mathbf{R}_{yy}$ are the observed field autocorrelation matrices

$$\mathbf{R} = \begin{bmatrix} \mathbf{R}_{yy}[0] & \mathbf{R}_{yy}[-1] & & \mathbf{R}_{yy}[-(p1-1)] \\ \mathbf{R}_{yy}[1] & \mathbf{R}_{yy}[0] & & \mathbf{R}_{yy}[-(p1-2)] \\ & & & \\ & & & \\ \mathbf{R}_{yy}[p1-1] & \mathbf{R}_{yy}[p1-2] & & \mathbf{R}_{yy}[0] \end{bmatrix} \quad (13)$$

$$\mathbf{R}_{yy}[l] = \begin{bmatrix} r_{yy}[l, 0] & r_{yy}[l, -1] & & r_{yy}[l, -(p_2-1)] \\ r_{yy}[l, 1] & r_{yy}[l, 0] & & r_{yy}[l, -(p_2-2)] \\ & & & \\ & & & \\ r_{yy}[l, p_2-1] & r_{yy}[l, p_2-2] & & r_{yy}[l, 0] \end{bmatrix} \quad (14)$$

The multidimensional Levinson algorithm may be used to solve (8) for the AR parameters and the white driving noise variance The reflection coefficients in Levinson type algorithms may be interpreted as the negative normalized correlation coefficients between the forward and backward linear prediction errors with one unit of delay Prediction is forward in the sense that the estimate at some spatial point is based on a number of points that are spatially before the point, and backward in the sense that the estimate is based on a number of points that are after the point. The reflection coefficients at stage m of the recursion are represented by a set of reflection matrices $\mathbf{A}_m[m]$ If the order of the model used is $p1$ x $p2$, then from the multidimensional, row ordered, Levinson algorithm [52] at the last of $(p1-1)$ recursions

$$\mathbf{A}_{p1}[p1]\,\mathbf{P}^{f}_{p1-1} + \Delta_{p1} = \mathbf{O} \tag{15}$$

where as in the 1-D case the Toeplitz structure of the autocorrelation matrices ensure that the covariance of the prediction error process is identical for the backward and forward AR process

$$\mathbf{P}^{f}_{p1} = \mathbf{P}^{b}_{p1} \tag{16}$$

The partial correlation matrix [52] may be expressed as

$$\Delta_{p1} = \left[\mathbf{I}\ \mathbf{A}_{P1-1}[1]\ \ \mathbf{A}_{P1-1}[2]\ \ \ \mathbf{A}_{P1-1}[p1-1]\right]\left[\mathbf{R}_{yy}[p1-1]\,\mathbf{R}_{yy}[p1-2]\ \ \ \mathbf{R}_{yy}[0]\right]^{T} \tag{17}$$

and the prediction error covariance matrices may be expressed as

$$\mathbf{P}^{f}_{p1} = \left[\mathbf{I} - \mathbf{A}_{p1}[p1]\mathbf{A}^{T}_{p1}[p1]\right]\mathbf{P}^{f}_{p1-1}, \tag{18}$$

with initial condition

$$\mathbf{P}^{f}_{1} = \mathbf{R}_{yy}[0] \tag{19}$$

The reflection coefficient matrices [52] may be expressed as

$$\mathbf{A}_{p1}[q] = \mathbf{A}_{p1-1}[q] + \mathbf{A}_{p1}[p1]\mathbf{A}^{T}_{p1-1}[p1-q-1] \quad \text{for} \quad 1 \le q \le p1-1 \tag{20}$$

Matrices in expressions (14) through (20) are of order p_2 x p_2 The derivation of these equations for the 2-D case is based on the multichannel case [81] for a p_2 channel AR process of order p_1 There is a direct correspondence between $\mathbf{A}_m[m]$ in the multichannel case and the reflection coefficients k_m in the single channel case

Expression (15) gives optimisation of the reflection coefficients based on minimisation of prediction error energy The AR parameters and white driving noise variance $\{a_1, \rho_1, a_2, \rho_2\}$ of the first and fourth QP model respectively are determined from the reflection coefficient and the prediction error covariance matrices For $1 \leq l \leq p1\text{-}1$ the row ordered vectors are given by

$$\rho_1^r = \mathbf{P}_{p1-1}^f \mathbf{a}_1^r[0] \quad (21) \qquad \text{and} \qquad \mathbf{a}_1^r[l] = \mathbf{A}_{p1-1}^H[l]\mathbf{a}_1^r[0] \quad (22)$$

where

$$\mathbf{a}_1^r[l] = \begin{bmatrix} a_1(l,0) \\ a_1(l,1) \\ \\ \\ a_1(l,p2-1) \end{bmatrix} \quad (23) \qquad \text{and} \qquad \rho_1^r = \begin{bmatrix} \rho_1 \\ 0 \\ \\ \\ 0 \end{bmatrix} \quad (24)$$

and

$$\rho_2^r = \mathbf{P}_{p1-1}^f \mathbf{a}_2^r[0] \quad (25) \qquad \text{and} \qquad \mathbf{a}_2^r[l] = \mathbf{A}_{p1-1}^H[l]\mathbf{a}_2^r[0] \quad (26)$$

where

$$\mathbf{a}_2^r[l] = \begin{bmatrix} a_2(l,p2-1) \\ a_2(l,p2-2) \\ \\ \\ a_2(l,0) \end{bmatrix} \quad (27) \qquad \text{and} \qquad \rho_2^r = \begin{bmatrix} 0 \\ 0 \\ \\ \\ \rho_2 \end{bmatrix} \quad (28)$$

We extend this method by including an extra cost function based on entropy In our method the cost function is given by (15) and the differential of a 2-D entropy term with respect to the reflection matrices The motivation behind this comes from statistical thermodynamics There is a direct analogy between statistical thermodynamics and stochastic signal analysis If the temperature m a physical system is reduced to absolute zero the system is forced into its lowest energy state In this case fluctuations disappear and physical systems condense into their ground state This ground state corresponds to the case in signal processing where parameter estimation is carried out on the basis of minimisation of the prediction error energy alone with zero input from the entropy term

At nonzero temperature there is a balance between low energy and high entropy with the result that physical systems are neither in minimum energy nor maximum entropy states An increase in system temperature causes an increase in entropy and a decrease in energy Temperature, therefore, acts as a control parameter for the entropy or fluctuations in the system [76] Temperature driven fluctuations in thermodynamic systems correspond to noise in signal analysis systems

'In statistical physics, the probability density function that a system will occupy a specific state of energy E is represented by a Gibbs distribution function of the form $\omega(E) = exp[(F-E)/kT]$ Here T is the system equilibrium temperature, k is Boltzmann's constant, and F is the free energy The system entropy is defined in terms of the ensemble average of the logarithm of the distribution function $S \equiv -k\langle log\omega(E)\rangle$ Hence the free energy is a linear combination of the entropy and the average energy, $F = \langle E\rangle - TS$' [76] In signal analysis systems the free energy is given as the difference between the prediction error energy and the entropy energy The equilibrium parameters of a system are associated with the global minimum of the free energy function An example is given in the annealing of a crystalline solid As the temperature is slowly reduced, the lattice spacing continuously changes so that the free energy is at a minimum for every temperature The parameters of the lattice correspond to model parameters in a signal analysis context [77]

The cost function in the 1-D MFE parameter estimation algorithm is based on an extension of the LMS criterion to include a noisy data cost element This extra cost element minimises the free energy and suppresses estimation errors caused by noise It is due to the entropy term and is given in [66], [67] by differentiation of the entropy energy with respect to reflection coefficients Hence MFE is based on determination of model parameters associated with minimization of the free energy function MFE extends LMS methods into the realm of noisy or incomplete data

We may gain further insight into the formulation of MFE by considering that estimation results can be improved by inserting a priori knowledge into the cost function [74] If prior knowledge about the probability of some properties of the spectrum, expressible in terms of the model parameters, exists, then by adding a penalty to the cost function this knowledge can be incorporated effectively into the estimation The spectra of sinusoids in noise at high SNR exhibit sharp peaks corresponding to the sinusoidal components with smooth valleys, whereas the spectrum of a single snapshot of random noise characteristically exhibits roughness If a noise spectrum probability distribution is determined from a number of independent snapshot data samples, then a smoother noise spectrum will have far higher probability than a highly distorted noise spectrum [77] Similar arguments may be made for spectra of sinusoids that are corrupted by noise or have small data set size Hence, the penalty measure should be a spectral smoothing measure This measure should add to the estimation problem some knowledge of signals and noise that is not present in the LMS scheme and thus compensate for the effect of added noise at low SNR As signal entropy is a measure of a priori probability the penalty function should be a decreasing function of entropy

In the 2-D case we now extend the multidimensional Levinson algorithm to include an extra, noisy data, cost function based on entropy This results in the minimisation of the resultant free energy, thereby providing better spectral estimation than that provided by minimization of prediction error energy alone Different forms of entropy functions are given in [57] The Shannon-Burg entropy measure is defined to within an arbitrary constant For 1-D methods this form of entropy results in an all-pole spectral estimate [76] We use a 2-D Shannon-Burg entropy type field H as in [17], [54] and [51] This may be expressed as

$$H \propto \int_{-1/2}^{1/2} \int_{-1/2}^{1/2} \ln\left[\beta / |D(f_x, f_y)|^2 \right] df_x df_y \tag{29}$$

We require the differential of the 2-D entropy term with respect to the reflection coefficient matrix $\mathbf{A}_m[m]$ at stage m For real fields the reflection coefficient matrix $\mathbf{A}$ is real and we may express the differential of the entropy energy term, with respect to $\mathbf{A}$ as

$$\partial \alpha H / \partial \mathbf{A} = \alpha \left[\partial \ln(\beta) / \partial \mathbf{A} - \partial \left[\int_{-1/2}^{1/2} \int_{-1/2}^{1/2} \ln[|D(f_x, f_y)|^2] df_x df_y \right] / \partial \mathbf{A} \right] \tag{30}$$

The entropy proportionality constant is absorbed into the signal processing temperature parameter α

At stage m of the recursion the double integral in expression (30) becomes

$$-\int_{-1/2}^{1/2} \int_{-1/2}^{1/2} \partial \left[\ln[D_m(f_x, f_y) D_m^*(f_x, f_y)] \right] / \partial \mathbf{A}_m[m] \, df_x df_y \tag{31}$$

or

$$-\int_{-1/2}^{1/2} \int_{-1/2}^{1/2} \partial \ln D_m(f_x, f_y) / \partial \mathbf{A}_m[m] + \partial \ln D_m^*(f_x, f_y) / \partial \mathbf{A}_m[m] \, df_x df_y \tag{32}$$

At any frequency (f_x, f_y) the differential

$$\partial \ln D_m(f_x, f_y) / \partial \mathbf{A}_m[m] \tag{33}$$

is the differential of a scalar quantity with respect to a matrix Applying matrix calculus [26] this may be expressed as a *(p2,p2)* matrix, any element $\mu(i, j)$ of which may be given by

$$\mu(i, j) = \partial \ln D_m(f_x, f_y) / \partial \tau(i, j) = D_m^{-1} \partial D_m(f_x, f_y) / \partial \tau(i, j) \tag{34}$$

where $\tau(i,j)$ is an element of the reflection matrix $\mathbf{A}_m[m]$ The integration in expression (32) becomes

$$\begin{aligned} &\int_{-1/2}^{1/2} \int_{-1/2}^{1/2} \left[\partial D_m(f_x, f_{yt}) / \partial \mathbf{A}_m[m] \right] / D_m(f_x, f_y) \, df_x df_y \\ &+ \int_{-1/2}^{1/2} \int_{-1/2}^{1/2} \left[\partial D_m^*(f_x, f_{yt}) / \partial \mathbf{A}_m[m] \right] / D_m^*(f_x, f_y) \, df_x df_y \end{aligned} \tag{35}$$

The first part of expression (35) becomes

$$\int_{-1/2}^{1/2}\int_{-1/2}^{1/2}\left(\partial\sum_{k=0}^{p1}\sum_{l=0}^{p2}a_{kl}[m]e^{-j(f_xk+f_yl)}\,/\,\partial\mathbf{A}_m[m]\right)/\,D_m(f_x,f_y)\,df_xdf_y \tag{36}$$

This integral may be performed by taking a contour integral about a surface in the 2-D complex frequency hyperplane The two analogues of the unit disc in 2-D complex z space $\mathbf{C}^2$ [49] are the

unit bidisc expressed as $$\left\{(z_x,z_y)\in\mathbf{C}^2\;|z_x|<1,|z_y|<1\right\} \tag{37}$$

and the unit ball expressed as $$\left\{(z_x,z_y)\in\mathbf{C}^2\;|z_x|^2+|z_y|^2<1\right\} \tag{38}$$

We use the bidisc analogue and carry out contour integration on the lower half of the associated complex frequency planes We extend the Cauchy Goursat based argument [66], [18] that the symmetry in the contour path reduces the contour integration to integrations at (a) and (b)

$$\text{(a)}\begin{Bmatrix}[-1/2\le \mathrm{Re}(f_x)\le +1/2,\mathrm{Im}(f_x)=-\infty]\\ [-1/2\le \mathrm{Re}(f_y)\le +1/2,\mathrm{Im}(f_y)=-\infty]\end{Bmatrix},\text{(b)}\begin{Bmatrix}[-1/2\le \mathrm{Re}(f_x)\le +1/2,\mathrm{Im}(f_x)=0]\\ [-1/2\le \mathrm{Re}(f_y)\le +1/2,\mathrm{Im}(f_y)=0]\end{Bmatrix} \tag{39}$$

The integration at (a) goes to zero as the numerator of the expression (36) contains a multiplicative exponential term This suggests that for $f_x=-j\infty$ and $f_y=-j\infty$ the integral vanishes, because the numerator goes to zero, while the denominator reduces to unity

We now examine the integration at (b) The multidimensional Levinson method [52] which is a minimum prediction error method yields solutions to the Yule-Walker equations These solutions may not be stable even for a positive definite autocorrelation matrix Hence $D(f_x,f_y)$ may not always be minimum phase In the case of a homogeneous random field [44] $D(f_x,f_y)$ is minimum phase If this is not the case the input field may be whitened sufficiently to ensure that the autocorrelation falls off fast enough so that $D(f_x,f_y)$ is minimum phase This results in a stable model However, by appropriate choice of signal processing temperature range MFE ensures that stable AR parameters may be found whether the autocorrelation matrix is positive

definite or not MFE models are stable, causal, and recursively computable [17], [38], [3] and hence they may also be used for field synthesis applications such as texture generation [44], [46], or data or correlation extension [50] With minimum phase $D(f_x, f_y)$ all singularities, that is solutions of the equation $D(z_x, z_y) = 0$, or zeroes of $D(z_x, z_y)$, are within the unit bicircle In the 2-D complex z space C^2 this may be expressed by Shanks theorem [17] as

$$D(z_x, z_y) \neq 0 \text{ for } \{ |z_x| \geq 1, |z_y| \geq 1 \} \tag{40}$$

Hence there are no zeroes outside the unit bicircle, or in the lower half of the 2-D complex frequency hyperplane Minimum phase placement of zeroes corresponds to pole placement for reciprocal functions Therefore, the function $D(z_x, z_y)$ and its reciprocal or transfer function have no singularities and are analytic in this domain [69]

We now examine extension of the residue theorem to 2-D Bose [3] shows that the test for a bivariate polynomial $B(z_1, z_2) \neq 0$ can be simplified to

$$\{[B(0, z_2) \neq 0, |z_2| \leq 1], [B(z_1, z_2) \neq 0, |z_1| \leq 1, |z_2| = 1]\} \tag{41}$$

and that $$N(z) = (1/2\pi j) \oint_{c2} \partial B(z_1, z_2) / \partial z_2 \; B(z_1, z_2)^{-1} dz_2 = 0 \tag{42}$$

where $N(z)$ is the number of z_2 zeroes in $B(z_1, z_2)$ for any fixed z_1 and contour $c2$ $|z_2| = 1$ This is also seen in [71] Generally the test for a bivariate polynomial can be simplified to testing for each variable when the other is fixed The number of zeroes in each z plane may be determined by fixing one variable and performing the contour integration with respect to the other This effectively means applying Cauchy's residue theorem twice [17] In performing double contour integration one variable is fixed and the contour integral is evaluated with respect to the other variable Therefore the integral residue formula [9]

$$(1/2\pi j) \oint_c f'(z) / f(z) dz = N - P \tag{43}$$

for the case of no poles P or zeros N inside an area enclosed by contour c of the complex plane applies, giving the double contour integral

$$\oint_{c1}\oint_{c2} f'(z_x,z_y)/f(z_x,z_y)\,dz_x dz_y = 0 \tag{44}$$

Hence the integration on the region specified by (39) (b) goes to zero

This may also be seen in that Krantz [49] gives us the Cauchy integral formula for $\mathbf{C}^2$ $D(z_x,z_y)$ is analytic in the domain of interest The integrand of expression (36) has no poles in the lower half of the 2-D complex frequency plane Therefore, there are no nonessential singularities of the first or second kind Hence by the $\mathbf{C}^2$ Cauchy integral theorem [1] the integral specified by (39) (b) goes to zero A similar argument may be made for the second integral in expression (35)

Continuing with expression (30), in terms of Levinson algorithm parameters at stage m of the recursion

$$\ln\beta_m = \ln[\mathbf{P}_m^f] = \ln\left[(\mathbf{I}-\mathbf{A}_m[m]\mathbf{A}_m^T[m])\mathbf{P}_{m-1}^f\right] \tag{45}$$

hence

$$\partial(\ln\beta_m)/\partial\mathbf{A}_m[m] = \partial\ln\left[(\mathbf{I}-\mathbf{A}_m[m]\mathbf{A}_m^T[m])\mathbf{P}_{m-1}^f\right]/\partial\mathbf{A}_m[m] \tag{46}$$

If

$$\mathbf{B}_m = \partial(\ln\beta_m)/\partial\mathbf{A}_m[m] \tag{47}$$

then for model order p_1 x p_2 matrix$\mathbf{B}$ has p_2 x p_2 elements each of which itself is a p_2 x p_2 matrix For example for a 3 x 3 order model any element of the 3 x 3 $\mathbf{B}$ matrix $\mathbf{B}(a,b)$ is itself given by the 3 x 3 matrix

$$\begin{bmatrix}
\left(1/\mathbf{P}_m^f(1,1)\right)\left(-\mathbf{P}(a,1)\mathbf{A}(1,b)+(a\&1)\left(-\mathbf{P}(1,1)\mathbf{A}(1,b)-\mathbf{P}(2,1)\mathbf{A}(2,b)-\mathbf{P}(3,1)\mathbf{A}(3,b)\right)\right) \\
\left(1/\mathbf{P}_m^f(1,2)\right)\left(-\mathbf{P}(a,2)\mathbf{A}(1,b)+(a\&1)\left(-\mathbf{P}(1,2)\mathbf{A}(1,b)-\mathbf{P}(2,2)\mathbf{A}(2,b)-\mathbf{P}(3,2)\mathbf{A}(3,b)\right)\right) \\
\left(1/\mathbf{P}_m^f(1,3)\right)\left(-\mathbf{P}(a,3)\mathbf{A}(1,b)+(a\&1)\left(-\mathbf{P}(1,3)\mathbf{A}(1,b)-\mathbf{P}(2,3)\mathbf{A}(2,b)-\mathbf{P}(3,3)\mathbf{A}(3,b)\right)\right) \\
\left(1/\mathbf{P}_m^f(2,1)\right)\left(-\mathbf{P}(a,1)\mathbf{A}(2,b)+(a\&2)\left(-\mathbf{P}(1,1)\mathbf{A}(1,b)-\mathbf{P}(2,1)\mathbf{A}(2,b)-\mathbf{P}(3,1)\mathbf{A}(3,b)\right)\right) \\
\left(1/\mathbf{P}_m^f(2,2)\right)\left(-\mathbf{P}(a,2)\mathbf{A}(2,b)+(a\&2)\left(-\mathbf{P}(1,2)\mathbf{A}(1,b)-\mathbf{P}(2,2)\mathbf{A}(2,b)-\mathbf{P}(3,2)\mathbf{A}(3,b)\right)\right) \\
\left(1/\mathbf{P}_m^f(2,3)\right)\left(-\mathbf{P}(a,3)\mathbf{A}(2,b)+(a\&2)\left(\mathbf{P}(1,3)\mathbf{A}(1,b)-\mathbf{P}(2,3)\mathbf{A}(2,b)-\mathbf{P}(3,3)\mathbf{A}(3,b)\right)\right) \\
\left(1/\mathbf{P}_m^f(3,1)\right)\left(-\mathbf{P}(a,1)\mathbf{A}(3,b)+(a\&3)\left(-\mathbf{P}(1,1)\mathbf{A}(1,b)-\mathbf{P}(2,1)\mathbf{A}(2,b)-\mathbf{P}(3,1)\mathbf{A}(3,b)\right)\right) \\
\left(1/\mathbf{P}_m^f(3,2)\right)\left(-\mathbf{P}(a,2)\mathbf{A}(3,b)+(a\&3)\left(-\mathbf{P}(1,2)\mathbf{A}(1,b)-\mathbf{P}(2,2)\mathbf{A}(2,b)-\mathbf{P}(3,2)\mathbf{A}(3,b)\right)\right) \\
\left(1/\mathbf{P}_m^f(3,3)\right)\left(-\mathbf{P}(a,3)\mathbf{A}(3,b)+(a\&3)\left(\mathbf{P}(1,3)\mathbf{A}(1,b)-\mathbf{P}(2,3)\mathbf{A}(2,b)-\mathbf{P}(3,3)\mathbf{A}(3,b)\right)\right)
\end{bmatrix} \tag{48}$$

where $\mathbf{A} = \mathbf{A}_m[m]$ and $\mathbf{P} = \mathbf{P}^f_{m-1}$ (49)

We minimise the cost function at recursion m and signal processing temperature α by determining a reflection matrix $\mathbf{A}_m[m]$ such that

$$\mathbf{A}_m[m]\mathbf{P}^f_{m-1} + \Delta_m - \alpha \mathbf{B}_m = \mathbf{0} \tag{50}$$

When $\alpha = 0$ the method reverts to the multidimensional Levinson algorithm

2.5 Autocorrelation functions

The autocorrelation function used in the equations above may be exact or an unbiased or biased estimate We examine the differences in these correlation functions The result of MFE spectral estimation using different correlation measures is detailed in Chapters 3 and 4 and in particular in Section 3 5

The exact autocorrelation generated by T sinusoids in white noise [85], [47], [86], [51] is given by

$$r(k,l) = \sigma^2\delta(k,l) + \sum_{i=1}^{T} a_i^2 \cos(2\pi f_{xi}k + 2\pi f_{yi}l) \tag{51}$$

This k x l point autocorrelation corresponds to the exact correlation from a data set over an M x N rectangular region of support where $-M < k < M$ and $-N < l < N$ a_i^2 is the power and (f_{xi}, f_{yi}) is the spatial frequency of the i^{th} sinusoid of T sinusoids

The exact correlation is somewhat artificial as it is not relevant to any practical problem despite its popular use in numerical simulation [85], [47], [51] It also ignores the statistical variability aspect of the problem The autocorrelation resulting from a single realisation of sinusoids plus noise would display cross-terms between sinusoids and would depend on the relative phases of the sinusoids However the exact autocorrelation helps to identify errors that occur as a result of using some form of estimated autocorrelation as opposed to errors that occur due to the spectral

method itself An example of errors occurring due to an estimated unbiased autocorrelation at low data set size is given in Section 3 8 on data length

The biased and unbiased autocorrelation functions are estimated from a realisation of sinusoids plus white noise of the form [50]

$$x(m,n) = \sum_{i=1}^{T} \sqrt{2} a_i \cos(2\pi f_{xi} \mathrm{m} + 2\pi f_{yi} n + \phi_i) + w(m,n) \tag{52}$$

where $w(m,n)$ denotes zero mean noise of power σ^2 The power and spatial frequency of the i^{th} sinusoid of T sinusoids are given as a_i^2 and (f_{xi}, f_{yi}) The phase of the i^{th} sinusoid is given by ϕ_i

The unbiased autocorrelation estimate [52] at lag (k,l) for a M x N data set over a rectangular region of support $0 \le m \le M-1$ and $0 \le n \le N-1$ is given over lag range $|k| \le M-1$ and $|l| \le N-1$ by

$$\hat{r}_{xx}(k,l) = \begin{cases} \dfrac{1}{(M-k)(N-l)} \displaystyle\sum_{m=0}^{M-1-k} \sum_{n=0}^{N-1-l} x(m+k,n+l)x^*(m,n) & \text{for } k \ge 0, l \ge 0 \\ \dfrac{1}{(M-k)(N-l)} \displaystyle\sum_{m=0}^{M-1-k} \sum_{n=-l}^{N-1} x(m+k,n+l)x^*(m,n) & \text{for } k \ge 0, l < 0 \\ \hat{r}_{xx}^*(-k,-l) & \text{for } k \le 0, \text{ any } l \end{cases} \tag{53}$$

and the biased autocorrelation is given by

$$\check{r}_{xx}(k,l) = \begin{cases} \dfrac{1}{MN} \displaystyle\sum_{m=0}^{M-1-k} \sum_{n=0}^{N-1-l} x(m+k,n+l)x^*(m,n) & \text{for } k \ge 0, l \ge 0 \\ \dfrac{1}{MN} \displaystyle\sum_{m=0}^{M-1-k} \sum_{n=-l}^{N-1} x(m+k,n+l)x^*(m,n) & \text{for } k \ge 0, l < 0 \\ \check{r}_{xx}^*(-k,-l) & \text{for } k \le 0, \text{ any } l \end{cases} \tag{54}$$

The biased estimate suffers from nonequitable weighting of the correlation lag terms The long correlation lag terms are responsible for resolving spectral fine structure, hence the biased form can result in loss of resolution However the Fourier transform of the biased estimated is always nonnegative, whereas this is not the case for the unbiased estimate For this reason the biased form is more generally used even though the unbiased estimate may give superior results In 1-D MFE the unbiased ACS may be used as MFE provides a self-regularization function in addition to compensation for noise [76]

For both exact autocorrelation and autocorrelation estimated from a realisation of sinusoids in white noise the SNR [50] may be expressed as $$SNR = \frac{\sum_{i=1}^{T} a_i^2}{\sigma^2} \qquad (55)$$

Unless otherwise stated we have used the unbiased autocorrelation estimated from a realisation of sinusoids in white noise with fixed relative initial phase Statistical studies have been carried out on the use of the 1-D MFE ACS algorithm [78] for estimating two isolated and two close spectral sources These have shown that the two isolated source peaks are unbiased while the close peaks are slightly biased rendering them slightly inaccurate 'This slight bias is due to the fixed relative initial phases of closely separated sources, it is an effect which is common in all coherent imaging situations If the relative phase had been chosen to be random and uncorrelated for each snapshot, the bias would disappear in multi-look averaging ' [78] We see therefore that the relative phase affects the resultant estimate for closely spaced sinusoids We may therefore expect some biasing of spectral estimates of closely spaced sinusoids

2.6 Optimisation and cost functions

A Nedler-Mead simplex [14] or Newton gradient [15] technique may be used to perform the minimisation of the left hand side of expression (50) The technique used depends upon the model order and width of the temperature range of interest The time required for the simplex to converge is far greater than that for the Newton method However the simplex avoids problems such as starting guess dependence and convergence at a local rather than the global minimum

For model order $p_1 x p_2$ the matrix $\mathbf{B}_m$ in expression (50) has elements each of which itself is a $p_2 x p_2$ matrix, however the matrices $\mathbf{A}_m[m]$, $\mathbf{P}_{m-1}^f$ and Δ_m are all of order $p_2 x p_2$ We average the $p_2 x p_2$ submatrices of $\mathbf{B}_m$ to ensure all matrices in expression (50) are of the same order We then determine the resultant matrix from expression (50) and generate a cost figure by taking the sum of the squared elements in this matrix This cost figure is minimised by the Nedler-Mead simplex or Newton method The fundamental steps of the MFE algorithm are given in Table 2 1

Cost figures may be assigned to the entropy term matrix $\mathbf{B}_m$ and the matrix due to the error energy term $\left[\mathbf{A}_m[m]\mathbf{P}_{m-1}^f + \Delta_m\right]$ as above We may then monitor the interaction between the entropy term and the error energy term by plotting these figures at each iteration or as an average over a number of iterations over the entire minimisation Figure 2 1 (a), (b), and (c) show the cost figures for the free energy, error energy, and entropy terms The minimization is for the final iteration in the MFE determination of a 5 x 5 model for an 80 x 80 point data set The data set consists of two sinusoids at normalised frequencies (0 1, 0 2) and (0 3, 0 4) in white Gaussian noise at 0 dB SNR When the cost functions due to the entropy term and error energy term are of the same order then the free energy is being minimised This provides an early indication within the algorithm of temperature range suitability, before AR parameter and PSD generation Experimental results on temperature range determination through calculation of the cost function order difference are given in the results Section 3 6 2 on temperature determination

2.7 Implementation environment

We have predominantly used the MATLAB fourth generation programming language [53] to implement the algorithms This language contains many high level functions that are particularly suitable for digital signal processing It therefore represents an ideal cost effective environment for algorithm development The package is available for a variety of platforms including 386/486 PCs to Cray All simulation results were printed using a Hewlett Packard LaserJet IIIp printer

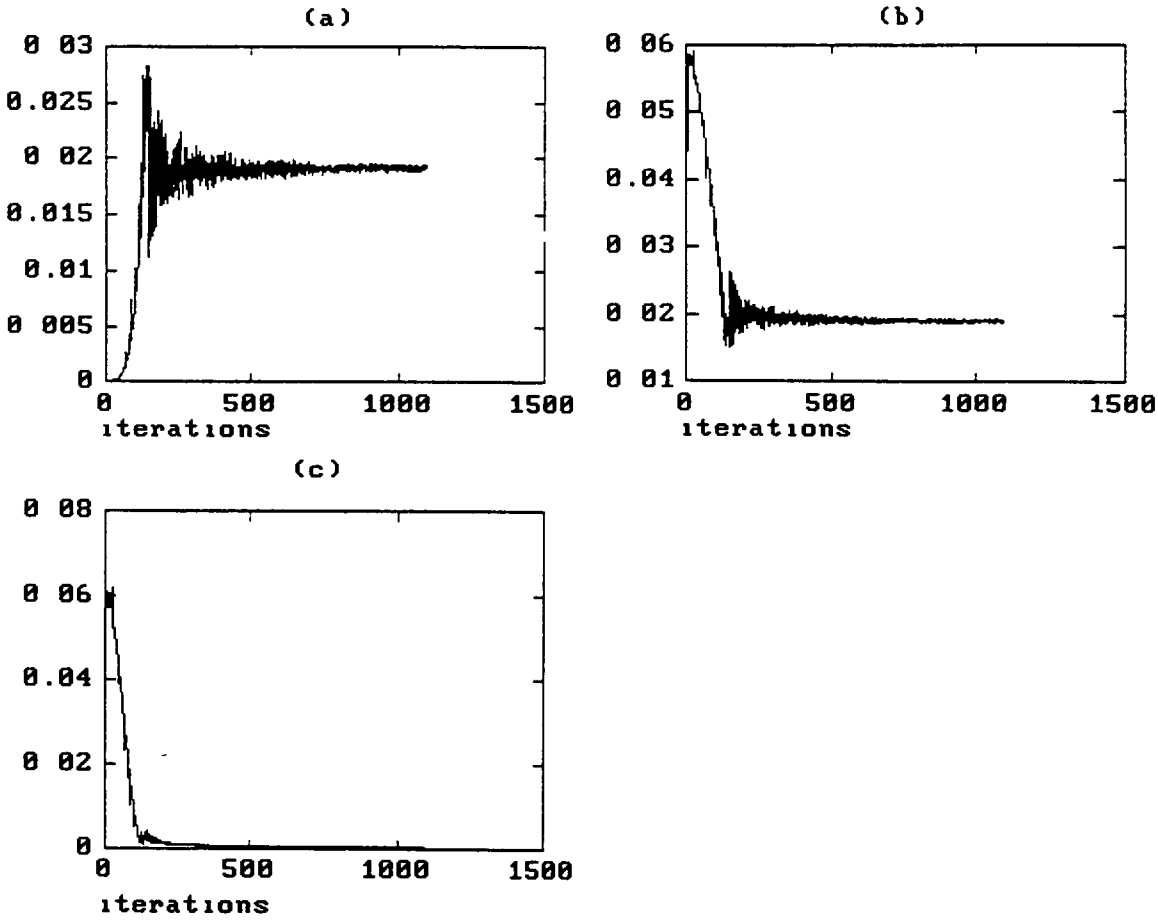

Figure 2 1 Cost figures for (a) error energy, (b) entropy, and (c) free energy for the minimization at the final iteration for MFE determination of a 5 x 5 model at temperature 0 05 for a data set consisting of two sinusoids at normalised frequencies (0 1, 0 2) and (0 3, 0 4) in white Gaussian noise at 0 dB SNR

Table 2 1

The Algorithm for Computing MFE AR parameters and PSD from Exact or Estimated Autocorrelation Data for Model Order p1 x p2, Temperature α and Data Set Size M x N

---

1. Begin algorithm

2. Generate autocorrelation data over k x l points where $-M < k < M$ and $-N < l < N$

2.1 Generate the exact autocorrelation for T sinusoids in white noise of power σ^2 where a_i^2 is the power and (f_{xi}, f_{yi}) is the spatial frequency of the i^{th} sinusoid using

$$r(k,l) = \sigma^2\delta(k,l) + \sum_{i=1}^{T} a_i^2 \cos(2\pi f_{xi}k + 2\pi f_{yi}l) \qquad (51)$$

or

2.2 Generate or acquire data and estimate autocorrelation

2.2.1 Generate data from a realisation of T sinusoids plus zero mean white noise $w(m,n)$ of power σ^2, where the power, spatial frequency, and phase of the i^{th} sinusoid are a_i^2, (f_{xi}, f_{yi}), and ϕ_i.

$$x(m,n) = \sum_{i=1}^{T} \sqrt{2}a_i \cos(2\pi f_{xi}m + 2\pi f_{yi}n + \phi_i) + w(m,n) \qquad (52)$$

or

2.2.2 Acquire data from other source such as homogeneous random texture field

2.2.3 Compute the unbiased autocorrelation estimate at lag (k,l)

$$\hat{r}_{xx}(k,l) = \begin{cases} \dfrac{1}{(M-k)(N-l)} \displaystyle\sum_{m=0}^{M-1-k} \sum_{n=0}^{N-1-l} x(m+k,n+l)x^*(m,n) & \text{for } k \geq 0,\ l \geq 0 \\ \dfrac{1}{(M-k)(N-l)} \displaystyle\sum_{m=0}^{M-1-k} \sum_{n=-l}^{N-1} x(m+k,n+l)x^*(m,n) & \text{for } k \geq 0, l < 0 \\ \hat{r}_{xx}^*(-k,-l) & \text{for } k \leq 0, \text{ any } l \end{cases} \qquad (53)$$

or

2.2.4 Compute the biased autocorrelation at lag *(k,l)*

$$\tilde{r}_{xx}(k,l) = \begin{cases} \dfrac{1}{MN} \sum_{m=0}^{M-1-k} \sum_{n=0}^{N-1-l} x(m+k,n+l)x^*(m,n) & \text{for } k \geq 0, l \geq 0 \\ \dfrac{1}{MN} \sum_{m=0}^{M-1-k} \sum_{n=-l}^{N-1} x(m+k,n+l)x^*(m,n) & \text{for } k \geq 0, l < 0 \\ \tilde{r}_{xx}^*(-k,-l) & \text{for } k \leq 0, \text{ any } l \end{cases} \quad (54)$$

3. Place the autocorrelation data into a matrix format

$\mathbf{R}_{yy}[l]$ are Toeplitz though not symmetric

$$\mathbf{R}_{yy}[l] = \begin{bmatrix} r_{yy}[l,\ 0] & r_{yy}[l,\ -1] & & r_{yy}[l,\ -(p2-1)] \\ r_{yy}[l,\ 1] & r_{yy}[l,\ 0] & & r_{yy}[l,\ -(p2-2)] \\ & & & \\ r_{yy}[l,\ p2-1] & r_{yy}[l,\ p2-2] & & r_{yy}[l,\ 0] \end{bmatrix} \quad (14)$$

$\mathbf{R}$ is block Toeplitz and symmetric

$$\mathbf{R} = \begin{bmatrix} \mathbf{R}_{yy}[0] & \mathbf{R}_{yy}[-1] & & \mathbf{R}_{yy}[-(p1-1)] \\ \mathbf{R}_{yy}[1] & \mathbf{R}_{yy}[0] & & \mathbf{R}_{yy}[-(p1-2)] \\ & & & \\ \mathbf{R}_{yy}[p1-1] & \mathbf{R}_{yy}[p1-2] & & \mathbf{R}_{yy}[0] \end{bmatrix} \quad (13)$$

4 for $m = 1$ to $p1-1$

4.1 Compute the order $p2 \times p2$ correlation matrix

$$\Delta_m = \left[\mathbf{I}\ \mathbf{A}_{m-1}[1]\ \mathbf{A}_{m-1}[2] \quad \mathbf{A}_{m-1}[m-1]\right] \left[\mathbf{R}_{yy}[m]\ \mathbf{R}_{yy}[m-1] \quad \mathbf{R}_{yy}[1]\right]^T \quad (17)$$

4.2 Select multivariate unconstrained optimisation method e g Nedler-Mead simplex or Newton method

4.2.1 Minimise a cost figure based on the sum of the squared elements in the resultant matrix from the left hand side of expression (50) by determination of the reflection matrix $\mathbf{A}_m[m]$ Hence $\mathbf{A}_m[m]$ which is order $p_2 \times p_2$ is chosen such that

$$\mathbf{A}_m[m]\mathbf{P}_{m-1}^f + \Delta_m - \alpha \mathbf{B}_m = \mathbf{0} \qquad (50)$$

where $\mathbf{B}_m = \partial \ln[(\mathbf{I} - \mathbf{A}_m[m]\mathbf{A}_m^T[m])\mathbf{P}_{m-1}^f] / \partial \mathbf{A}_m[m]$

and $\mathbf{P}_0^f = \mathbf{R}_{yy}[0]$ (19)

$\mathbf{B}_m$ has $p2$ x $p2$ elements each of which is a $p2$ x $p2$ submatrix Average these submatrices to ensure all matrices in expression (50) are of the same order

4.3 Compute the order $p2$ x $p2$ prediction error covariance matrices

$$\mathbf{P}_m^f = [\mathbf{I} - \mathbf{A}_m[m]\mathbf{A}_m^T[m]]\mathbf{P}_{m-1}^f \qquad (18)$$

4.4 Compute the reflection coefficient matrices

$$\mathbf{A}_m[q] = \mathbf{A}_{m-1}[q] + \mathbf{A}_m[m]\mathbf{A}_{m-1}^T[m-q] \quad \text{for} \quad 1 \le q \le m-1 \quad (20)$$

end of for m

5. Compute the AR parameters and white driving noise variance $\{\mathbf{a}_1, \rho_1\}$of the first QP model

5.1 Determine ρ_1 from $\rho_1^r = \mathbf{P}_{p1-1}^f \mathbf{a}_1^r[0]$ (21)

where $a(0,0) = 1$, and $\mathbf{a}_1^r[1] = \begin{bmatrix} a_1(1,0) \\ a_1(1,1) \\ \\ \\ a_1(1,p2-1) \end{bmatrix}$ (23) and $\rho_1^r = \begin{bmatrix} \rho_1 \\ 0 \\ \\ \\ 0 \end{bmatrix}$ (24)

5.2 For $i = 1$ to $p1-1$

determine the row ordered vectors $\mathbf{a}_1^r[i] = \mathbf{A}_{p1-1}^H[i]\mathbf{a}_1^r[0]$ (22)

end of for i

6. Compute the AR parameters and white driving noise variance $\{\mathbf{a}_2\ \rho_2\}$ of the fourth QP model

6.1 Determine ρ_2 from $\rho_2^r = \mathbf{P}_{p1-1}^f \mathbf{a}_2^r[0]$ (25)

where $a_2(0,0) = 1$, $\mathbf{a}_2^r[l] = \begin{bmatrix} a_2(l, p2-1) \\ a_2(l, p2-2) \\ \\ \\ a_2(l,0) \end{bmatrix}$ (27) and $\rho_2^r = \begin{bmatrix} 0 \\ 0 \\ \\ \\ \rho_2 \end{bmatrix}$ (28)

6.2 For $l = 1$ to $p1-1$

determine the row ordered vectors $\mathbf{a}_2^r[l] = \mathbf{A}_{p1-1}^H[l]\mathbf{a}_2^r[0]$ (26)

end of for l

7. Compute the power spectral density for each QP over a suitable region F^2 of the frequency plane

for $f_x = 1$ to F

for $f_y = 1$ to F

$$S_{qp1}(f_x, f_y) = \frac{\rho_1}{\left| \sum_{k=0}^{p1-1} \sum_{l=0}^{p2-1} a_1(k,l) \exp(-j((2\pi / F)(f_x - F/2)k + (2\pi / F)(f_y - F/2)l) \right|^2} \quad (5)$$

$$S_{qp4}(f_x\ f_y) = \frac{\rho_2}{\left| \sum_{k=-(p1-1)}^{0} \sum_{l=0}^{p2-1} a_2(k,l) \exp(-j((2\pi / F)(f_x - F/2)k + (2\pi / F)(f_y - F/2)l)) \right|^2}$$

where $|f_x| \le 1/2$, $|f_y| \le 1/2$ for normalised frequency

end of for f_y

end of for f_x

8. End algorithm

Chapter 3. Numerical Simulations and Experimental Results

3.1 Introduction

In this Chapter we provide numerical examples in which the method outlined above has been applied These examples show power spectral estimates determined directly using MFE based AR model parameters Spectral estimates determined by other techniques are used for comparative purposes The resolution of sinusoids in white noise is a widely used standard simulation exercise for spectral estimation techniques including AR model based techniques [50], [86], [77], [84], [83] Generally, we used an unbiased autocorrelation function estimated from a realisation of sinusoids plus white noise Various data set sizes ranging from 160 x 160 to 5 x 5 points have been used over the full set of tests The size of the region of autocorrelation

estimates used depends only on the model order For example a 5 x 5 order model will use only 5 x 5 autocorrelation points, giving a 5 x 5 region of autocorrelation support

We performed a wide variety of tests on the MFE method outlined above These may be divided into two classes of simulations The first class relates to tests carried out on the technique itself to evaluate its performance These included resolution directional dependency, estimator bias and variance over a number of independent trials, and sensitivity of spectral estimates to signal processing temperature The effects on spectral estimation of SNR, data length, model size, and type of autocorrelation function used were also examined We performed spectral estimation on a number of examples of very closely spaced sinusoids as a test in spectral resolution We examine the directional bias and standard deviation over a number of independent trials for spectral estimates generated by models with non-symmetric region of support Tests were also carried out on the effect of dynamic range difference between sinusoids

The second class of tests involving comparison of MFE spectral estimation results with those of other techniques are detailed in Chapter 4

Spectral estimates are plotted as normalised amplitude PSD plots or as log plots on the x frequency axis $psd(f_x,0)$ $0 \le f_x \le 0.5$ and on the y frequency axis $psd(0,f_y)$ $0 \le f_y \le 0.5$ Contour plots showing the spectral estimate on both frequency axes of the (f_x, f_y) frequency plane are also used The highest contour level is normalised to 0 dB Where possible the contours are labelled in dB below the maximum value of 0 dB The contours are equally spaced and the contour increment is given in all cases The data is real, resulting in spectral estimates that are symmetric with respect to the origin Hence only one half of the frequency axes is generally displayed

3.2 Pair of sinusoids

We took a 80 x 80 point data snapshot consisting of sinusoids at arbitrary unity normalised frequencies (0 1, 0 2) and (0 3, 0 4) The sinusoids are of equal amplitude at arbitrary SNR of 6 dB in white Gaussian noise The parameters are given in Table 3 1 below An unbiased autocorrelation estimate was used

Table 3 1 Data set parameters

Number of sinusoids M	White noise power σ^2	Sinusoid power a_i^2	Spatial frequencies
2	0 5	1 1	(0 1, 0 2) (0 3, 0 4)

We determined the spectral estimate at temperatures 0 074 and zero This has special significance because at zero temperature our technique reverts to the multidimensional Levinson or Burg type technique The temperature of 0 074 was the optimal temperature for spectral estimation based on the average autocorrelation over 10 noise seeds This temperature also falls within a broad range of temperatures ($\sim 10^2$) within which accurate spectral estimation was obtained

Figure 3 1 (a) shows the combined first and fourth quarter plane normalised amplitude PSD plot on the x frequency axis $psd(f_x,0)$ $0 \le f_x \le 05$ This spectral estimate was derived using the MFE based AR models of order 5 x 5 at temperature 0 074 The region of autocorrelation support is only 5 x 5 points coinciding with the model order Figure 3 1 (b) is the corresponding contour plot showing the spectral estimate on both f_x and f_y frequency axes The corresponding plots for the spectral estimates at temperature zero are shown in Figure 3 1 (c) and (d)

Sharp peaks are evident in Figure 3 1 (a) at $f_x = 0\ 1$ and $f_x = 0\ 3$ The spatial frequency peaks at (0 1, 02) and (0 3, 0 4) are clearly visible in the contour plot of Figure 3 1 (b) The sharpness of the peaks is illustrated by the 10 dB contours A number of peaks in the x frequency direction can be seen in Figure 3 1 (c) None are at the correct frequencies of $f_x = 0\ 1$ and $f_x = 0\ 3$ The contour plot of Figure 3 1 (d) clearly shows that the peaks are not located at spatial frequencies (0 1, 0 2) and (0 3, 0 4) and therefore are incorrectly resolved We conclude that both frequency components are accurately resolved at temperature 0 074 and are not accurately resolved at temperature zero using the Levinson method

It should also be noted that the zero temperature model has reflection coefficients of value greater than unity This results in autoregressive parameters that are not unity bounded Hence, the zero temperature system is unstable and unsuitable for field synthesis or autocorrelation extension

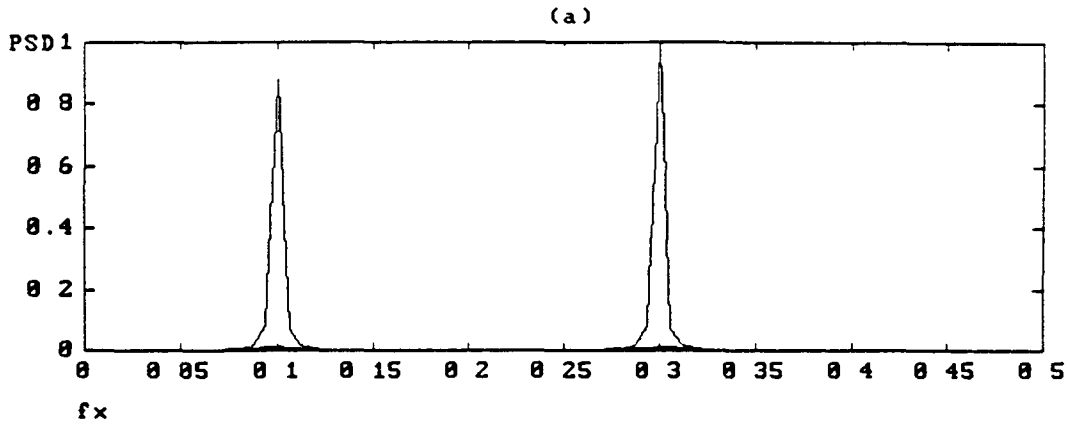
(a)
PSD 1
0 8
0 6
0.4
0 2
0
0 0 05 0 1 0 15 0 2 0 25 0 3 0 35 0 4 0 45 0 5
fx

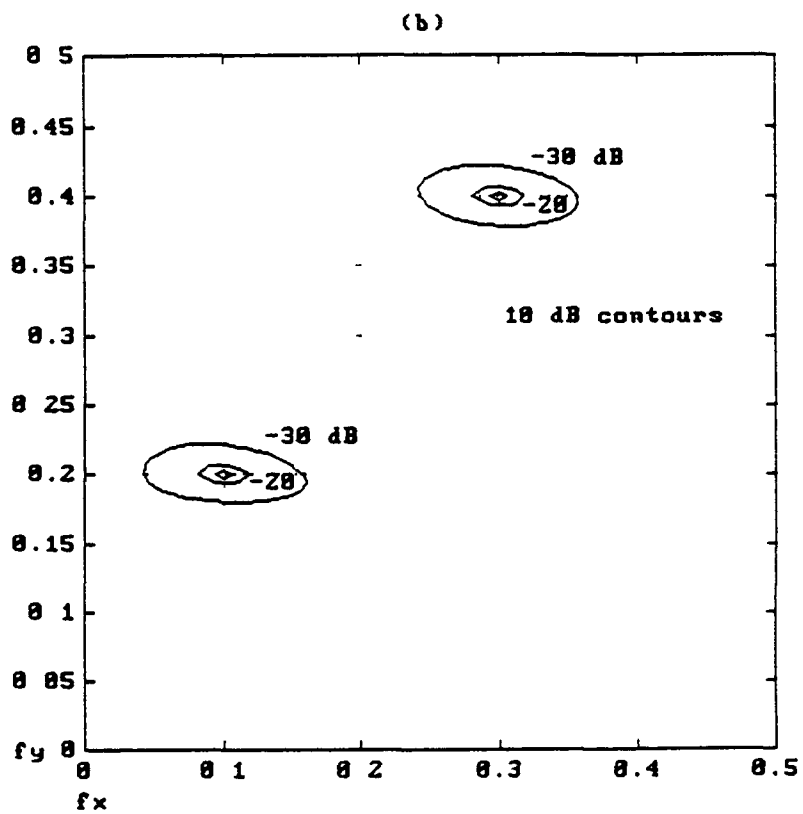
(b)
0 5
0.45
0.4
0.35
0.3
0 25
0.2
0.15
0 1
0 05
fy 0
0 0 1 0 2 0.3 0.4 0.5
fx
-30 dB
-20
10 dB contours
-30 dB
-20

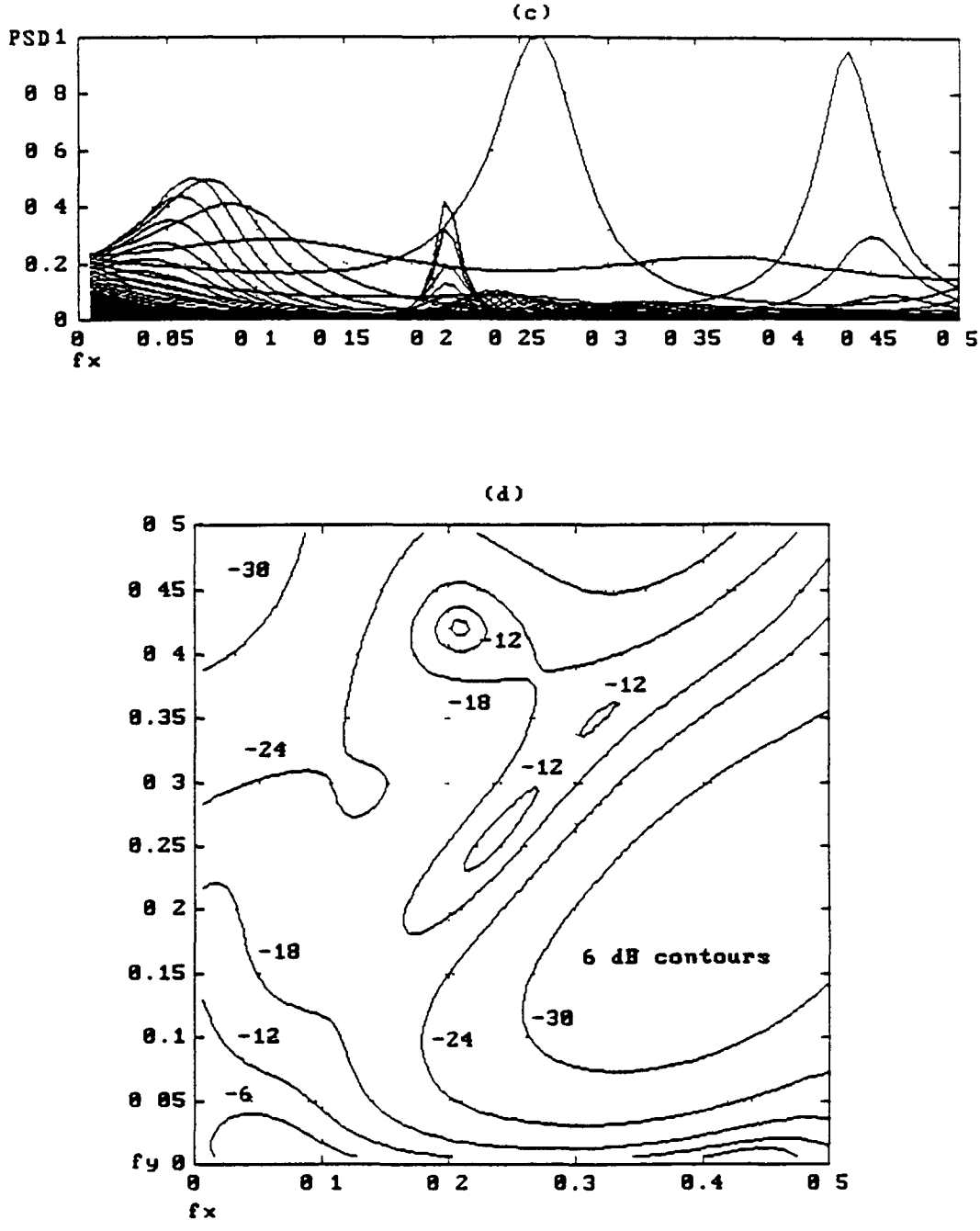

Figure 3 1 MFE spectral estimates of sinusoids at normalised frequencies (0 1, 0 2) and (0 3, 0 4) in white noise at SNR of 6 dB at temperature (a), (b) 0 074 and (c), (d) zero

(a)(c)Normalised amplitude spectral estimate on the x frequency axis, (b) (d) Contour plot in dB on x and y frequency axes

3.3 Single sinusoid at high SNR

A sinusoid at normalised frequency (0 1, 0 2) at 27 dB SNR in white noise was used This data set is detailed in Table 3 2 A 160 x 160 point unbiased autocorrelation was estimated from the 80 x 80 point data set

Table 3 2 Data set parameters

Number of sinusoids M	White noise power σ^2	Sinusoid power a_i^2	Spatial frequencies
1	0 002	1	(0 1, 0 2)

Figure 3 2 (a) is a plot of the normalised amplitude spectral estimate on the x frequency axis The 2-D contour plot of the estimate is given in Figure 3 2 (b) The spectral estimate was obtained using an MFE based AR model of order 5 x 5 at temperature zero No spectral peak occurs at the correct frequency and several spurious peaks occur Figure 3 2 (c) and (d) gives the normalised amplitude plot and corresponding contour plot for the spectral estimate derived using an MFE AR model of order 5 x 5 at temperature 0 5 They show that the spectral component is accurately resolved at (0 1, 0 2) It is seen that the MFE method outperforms the multidimensional Levinson method

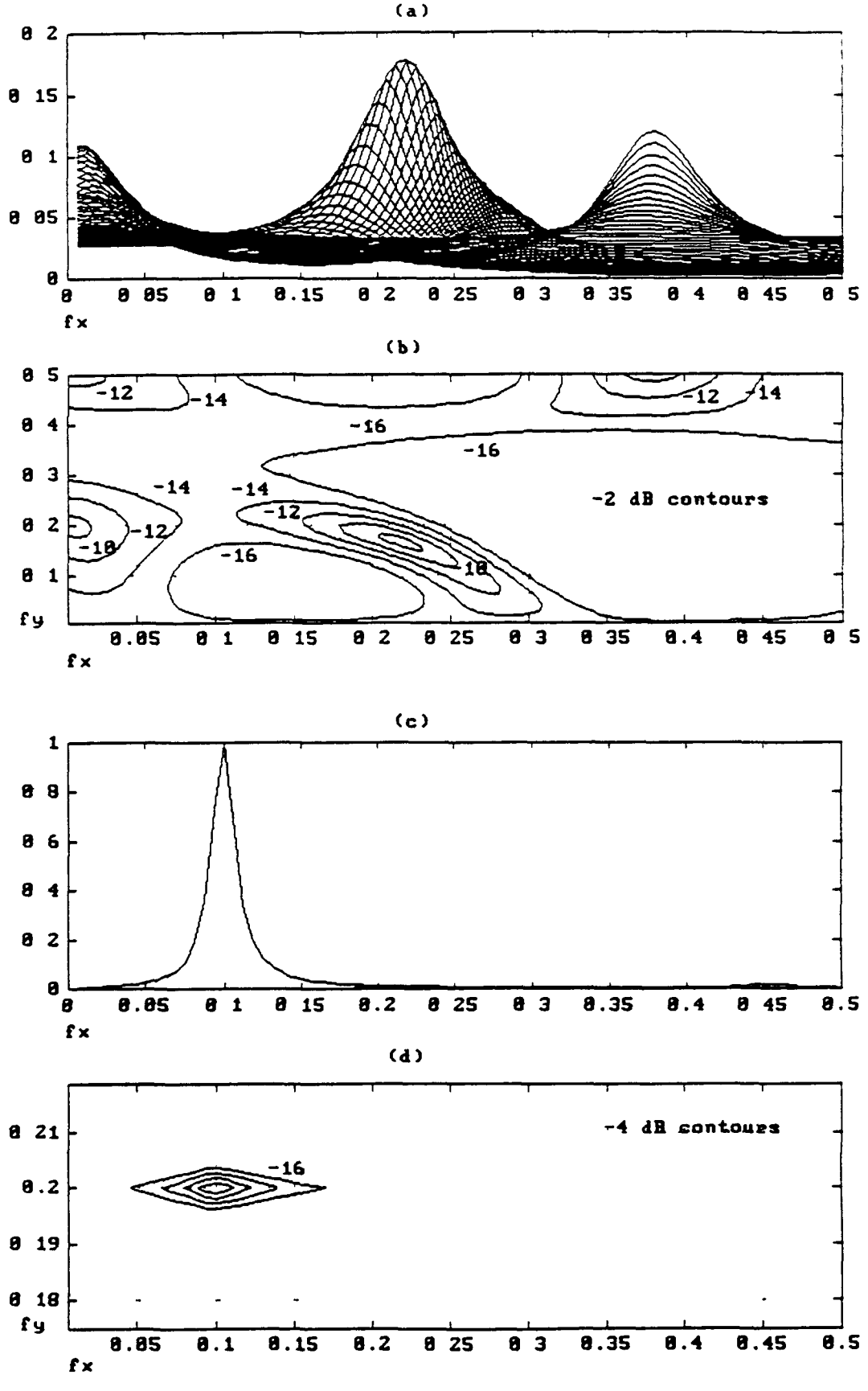

Figure 3 2 MFE spectral estimates of a single sinusoid at normalised frequency (0 1, 0 2) in white noise at SNR of 27 dB at temperature (a), (b) zero and (c), (d) 0 5

(a)(c) Normalised amplitude spectral estimate on the x frequency axis, (b)(d) Contour plot in dB

3.4 Combined QP estimates

Single quadrant spectral estimators have directional dependent resolution capabilities [86] This means that the estimator has better resolution capability in some directions in the frequency plane than in others The resulting spectral estimate is dependent on the positions of sinusoids in the frequency plane and their relative positions to each other The effect on the resolution caused by relative position dependency of sinusoids to each other may be due to interference that may occur between these sinusoids This may occur when the signal contains two or more sinusoids [86] This directional dependency also applies to MFE spectral estimates

The net result is that a single quarter plane spectral estimator may produce spectral estimates with elliptical contours of constant PSD level Whether this occurs or not depends on the location and power of sinusoids in a particular data set This may be overcome to some extent leading to circular contours by using a combined quarter plane estimator Figure 3 3 shows the contour plots for MFE spectral estimates based on a biased autocorrelation of the 80 x 80 data set in Table 3 3 below The first and fourth quarter plane model spectral estimates, as seen in (a) and (b) have opposing elliptical skews The combined estimate (c) yields a circular response

Table 3 3 Data set parameters

Number of sinusoids M	White noise power σ^2	Sinusoid power a_i^2	Spatial frequencies
2	2	1 0 5	(0 3333, 0 2) (0 1, 0 222)

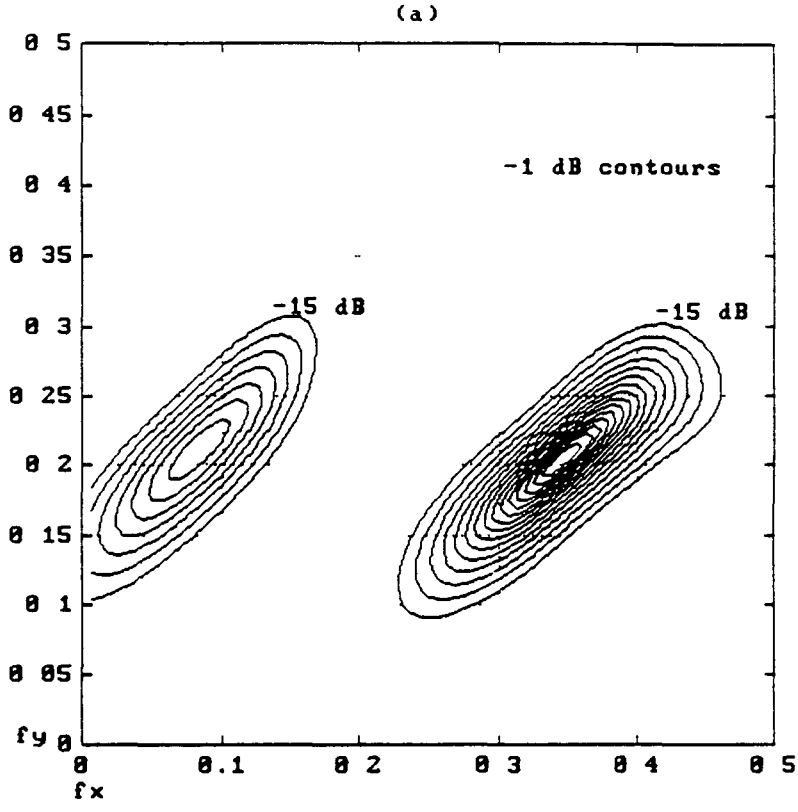
(a)
-1 dB contours
-15 dB
-15 dB
0 5
0 45
0 4
0 35
0 3
0 25
0 2
0 15
0 1
0 05
fy 0
0
0 1
0 2
0 3
0 4
0 5
fx

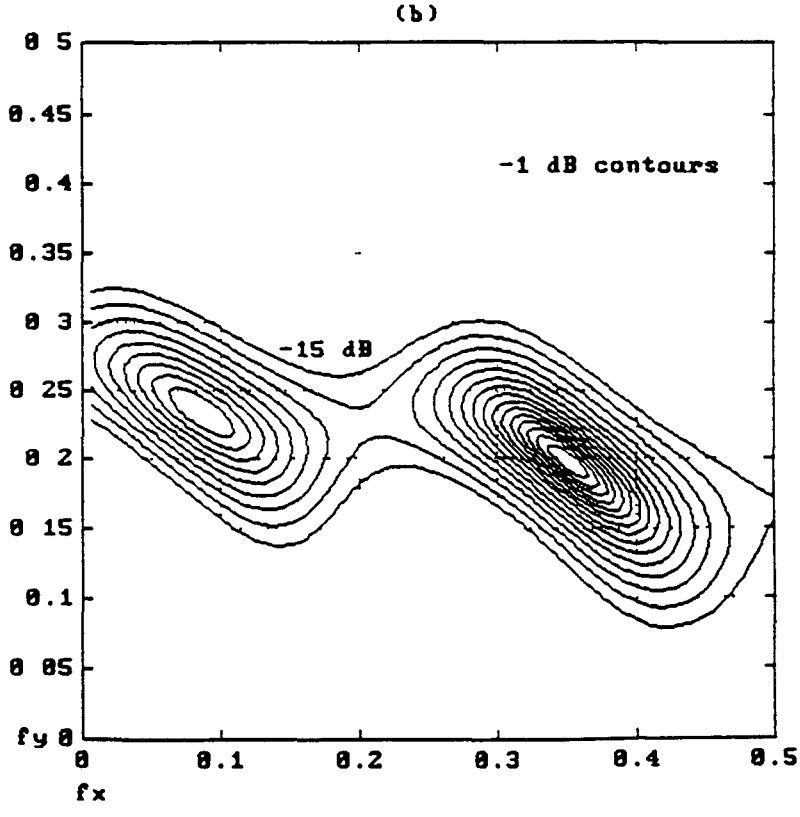
(b)
-1 dB contours
-15 dB
0 5
0.45
0.4
0.35
0 3
0 25
0 2
0 15
0.1
0 05
fy 0
0
0.1
0.2
0.3
0.4
0.5
fx

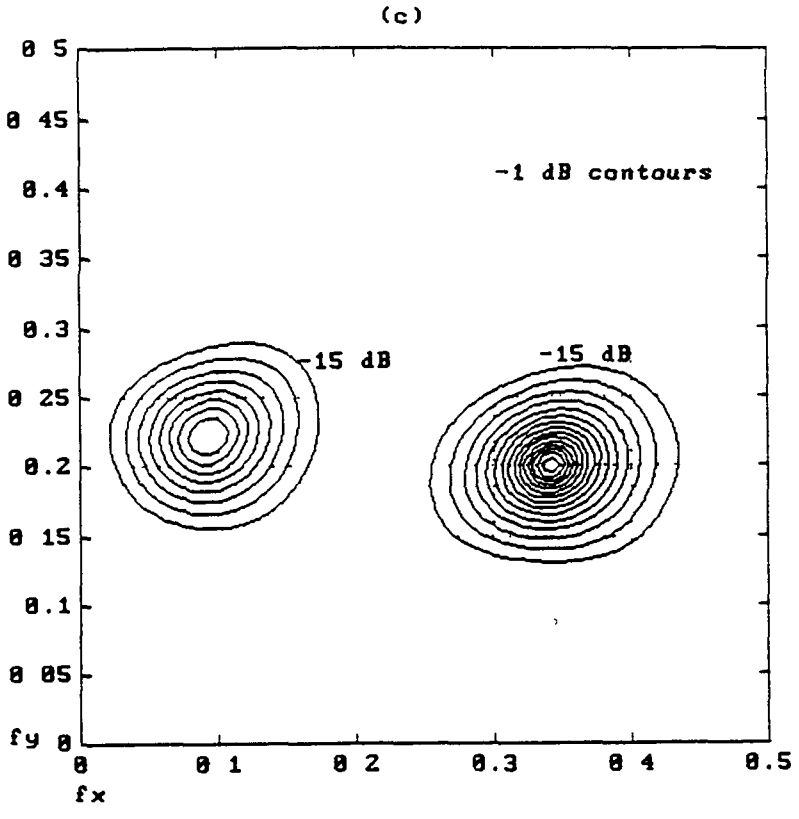

Figure 3 3 MFE temperature 0 05 spectral estimates of sinusoids at normalised frequencies (0 3333, 0 2) and (0 1, 0 222) in white noise at SNR of -1 25 dB

Contour plot in dB on x and y frequency axes of (a) first quarter plane spectral estimate, (b) fourth quarter spectral estimate, and (c) combined quarter plane spectral estimate

The shape of the combined estimate may not always be circular As with other quarter plane methods the shape of the combined estimate depends on the relative strengths of the first QP and fourth QP spectral estimates Figure 3 4 (a), (b) and (c) shows the first QP, fourth QP and combined QP spectral estimates for a 40 x 40 data snapshot the details of which are specified in Table 3 1 An AR modified covariance technique (MCV) with model order 5 x 5 is used

Depending on the relative locations of sinusoidal components the interference may lead to bias in peak location, spurious peaks and peak splitting Hence another motivation for the use of a combined estimator is that spurious peaks are less likely to occur if quarter plane estimates are combined in 'parallel resistor' fashion [38] Single quadrant AR spectra also suffer from spurious peaks at high SNR or high model order [86] In 1-D spectral estimation the spurious peaks are caused by extra poles close to the unity circle in the z plane [38] Figure 3 5 (a), (b), and (c) shows the first QP, fourth QP and combined first and fourth QP spectral estimates on the x frequency axis This spectral estimate is based on models of order 7 x 7 derived by MFE at temperature 0 05 The 80 x 80 data set is given in Table 3 4 An unbiased autocorrelation estimate was used The Figure in (a) shows peaks occurring at the required frequencies $fx = 0\ 1$ and $fx = 0\ 3$ However spurious peaks occur about the required frequencies thus obscuring accurate spectral estimation The situation for the fourth QP model spectral estimate in the x frequency direction is similar, with the correct components accompanied by spurious components A similar case exists on the y frequency axis These spurious peaks are eliminated by combining the QP estimates as shown in the Figure 3 5 (c)

Table 3 4 Data set parameters

Number of sinusoids M	White noise power σ^2	Sinusoid power a_i^2	Spatial frequencies
2	2	1	(0 1, 0 2)
		1	(0 3, 0 4)

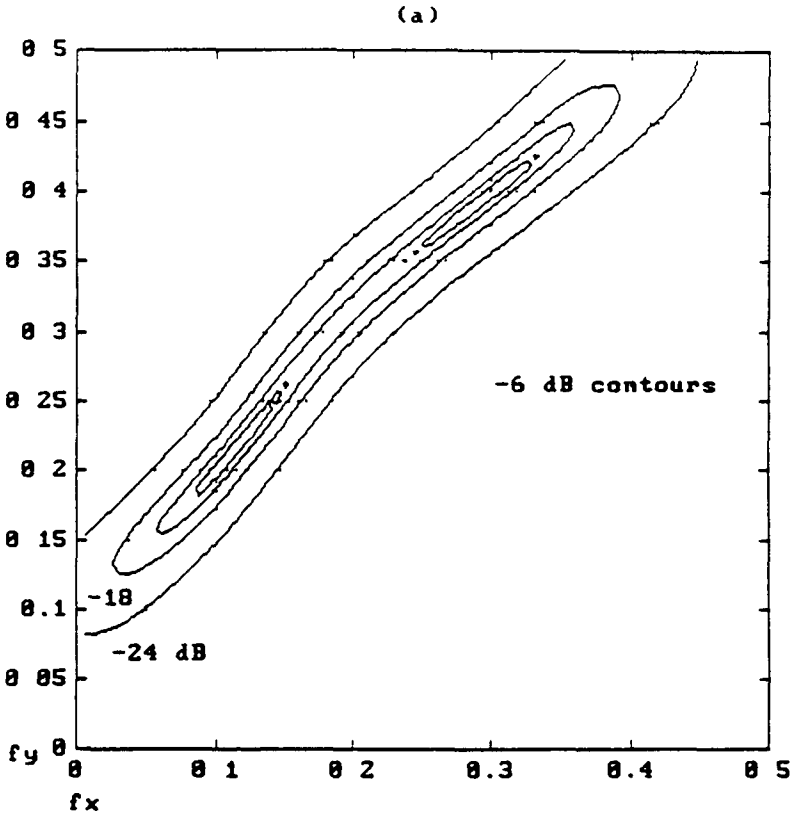
(a)
0 5
0 45
0 4
0 35
0 3
0 25
0 2
0 15
0.1
0 05
fy 0
0
0 1
0 2
0.3
0.4
0 5
fx
-6 dB contours
-18
-24 dB

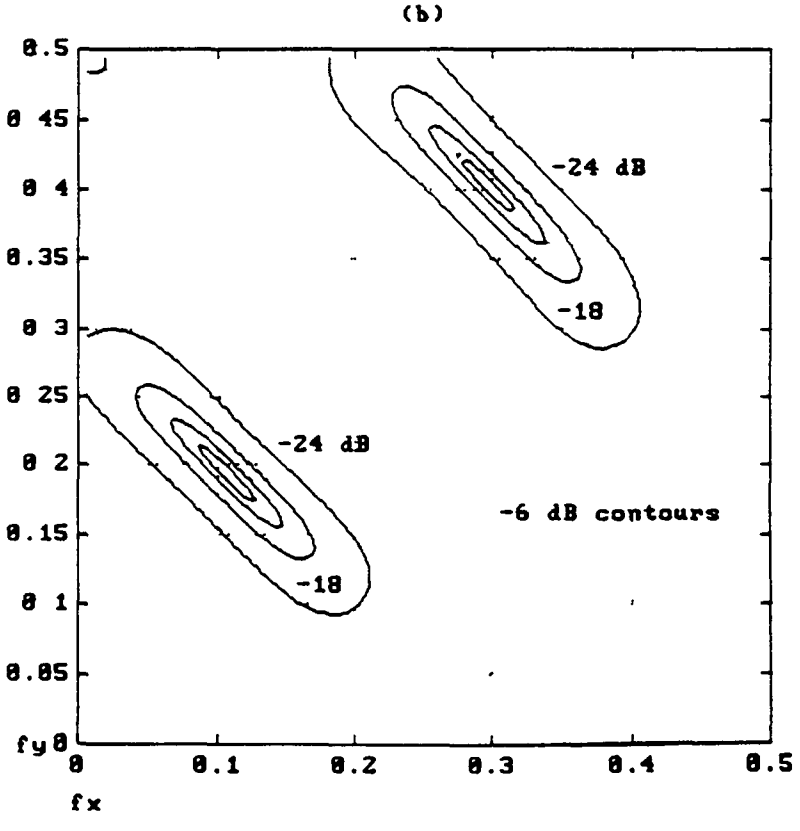
(b)
0.5
0 45
0 4
0.35
0 3
0 25
0 2
0.15
0 1
0.05
fy 0
0
0.1
0.2
0.3
0.4
0.5
fx
-24 dB
-18
-24 dB
-18
-6 dB contours

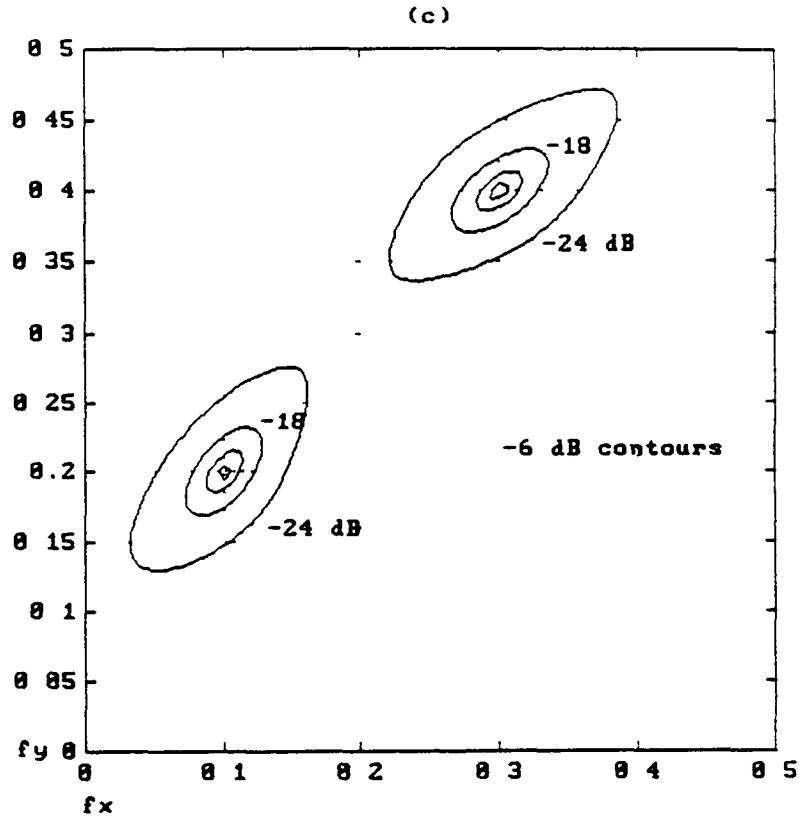

Figure 3 4 MCV spectral estimates of sinusoids at normalised frequencies (0 1, 0 2) and (0 3, 0 4) in white noise at SNR of 6 dB

Contour plot in dB on x and y frequency axes of (a) first quarter plane spectral estimate, (b) fourth quarter spectral estimate, and (c) combined quarter plane spectral estimate

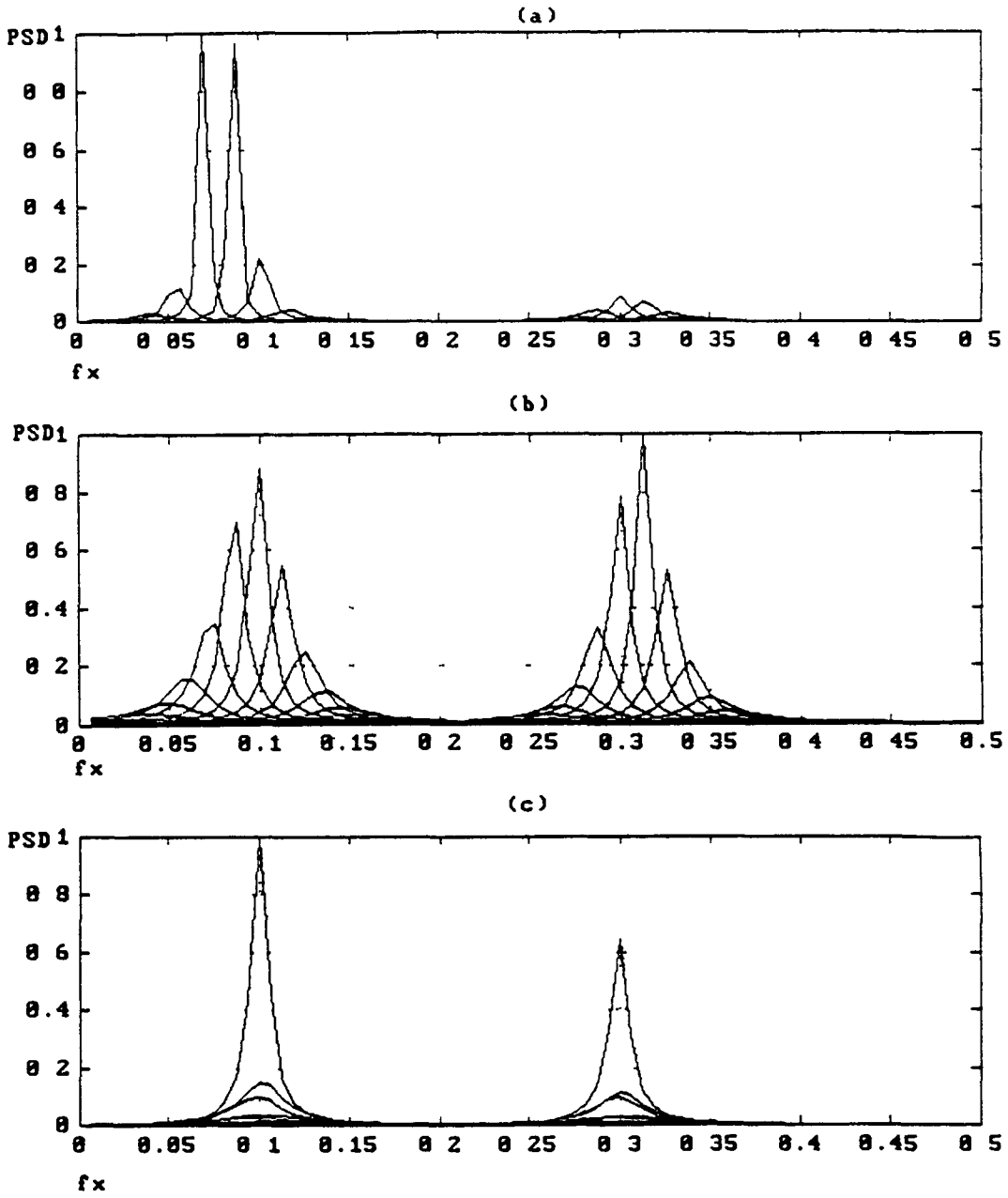

Figure 3 5 MFE temperature 0 05 spectral estimates of sinusoids at normalised frequencies (0 1, 0 2) and (0 3, 0 4) in white noise at SNR of 0 dB

Normalised amplitude spectral estimate on the x frequency axis based on (a) first QP, (b) fourth QP and (c) combined first and fourth QP models

Further evidence of spurious peak elimination can be seen in the x frequency plots of Figure 3 6 These show an order 5 x 5 model MFE spectral estimate at temperature 0 074 of the 80 x 80 point data set detailed in Table 3 1 In Figure 3 6 (a) the first QP spectral estimate m dB has spectral peaks at $fx = 0\ 1$ and $fx = 0\ 3$ which are accompanied and overshadowed by spurious peaks The situation for the fourth QP is similar However in Figure 3 6 (c) we see that the combined first and fourth QP spectral estimate exhibits distinct spectral peaks at only the required frequencies

Hence, we see that spurious peaks that may occur for single quarter plane models are very effectively eliminated by using a combined quarter plane model Third quadrant model spectra are identical to first, and second quadrant model spectra are identical to fourth We combine first and fourth quarter plane PSD estimates for all simulations and tests unless otherwise stated

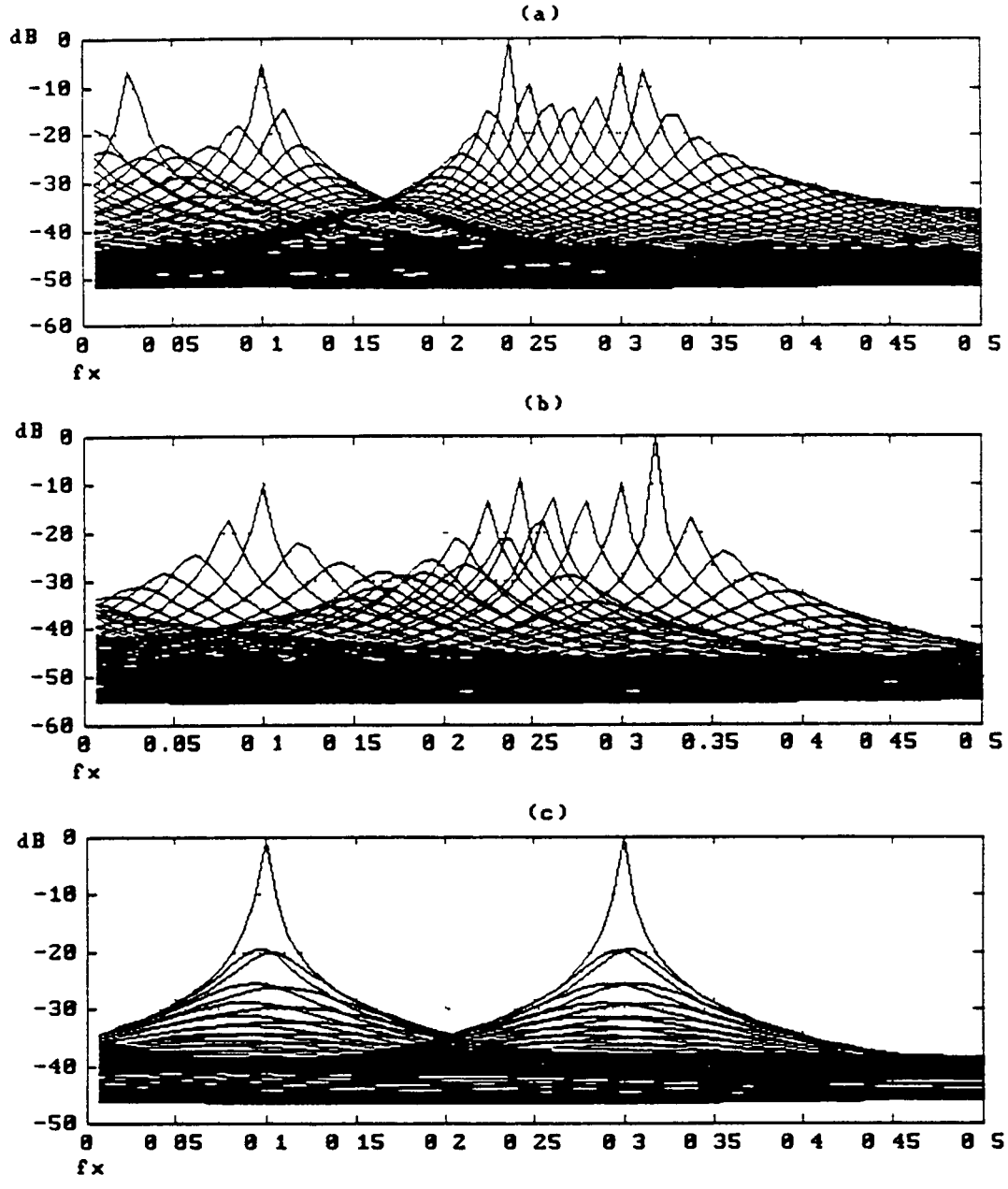

Figure 3 6 MFE temperature 0 074 spectral estimates of sinusoids at normalised frequencies (0 1, 0 2) and (0 3, 0 4) in white noise at SNR of 6 dB

Log plots of spectral estimates on the x frequency axis based on (a) first QP, (b) fourth QP, and (c) combined first and fourth QP models

3.5 Autocorrelation type

The difference in spectral estimation based on exact, biased and unbiased autocorrelation estimates may be examined This may be achieved by comparing the resulting MFE spectral estimates for a single snapshot of data consisting of a number of sinusoids in white noise Figure 3 7 (a), (b), and (c) show the exact, unbiased and biased forms of the autocorrelation function for the 80 x 80 data set of Table 3 5 The same white noise field was used in each case The resulting spectral estimates generated by MFE models of order 6 x 6 at temperature 0 5 for exact, biased and unbiased autocorrelation functions are shown in Figures 3 8, 3 9, and 3 10 (a) and (b) respectively In all three cases the spectral elements are resolved, however the dynamic range difference between the two sinusoids is preserved best by the exact correlation with the unbiased estimate being next best As in other AR methods the peak of the PSD is proportional to the square of the power of the sinusoid This is unlike Fourier methods where the peak is directly proportional to the sinusoid power

Table 3 5 Data set parameters

Number of sinusoids M	White noise power σ^2	Sinusoid power a_i^2	Spatial frequencies
2	2	2 1	(0 3333, 0 2) (0 1, 0 22)

We note from Section 2 5 on autocorrelation functions that the use of the exact autocorrelation helps identify errors that may occur in autocorrelation estimation rather than in the spectral estimation method itself In Section 3 8 on data length, we will see that if the unbiased autocorrelation estimate is used, then for low data set size errors in the peak location may occur These errors do not occur if the exact autocorrelation is used This represents an error in the autocorrelation estimate as opposed to an error in the MFE method itself Evidence of the independence of spectral estimates to data set size using the exact autocorrelation function is seen in Section 4 3 on conventional transform comparison

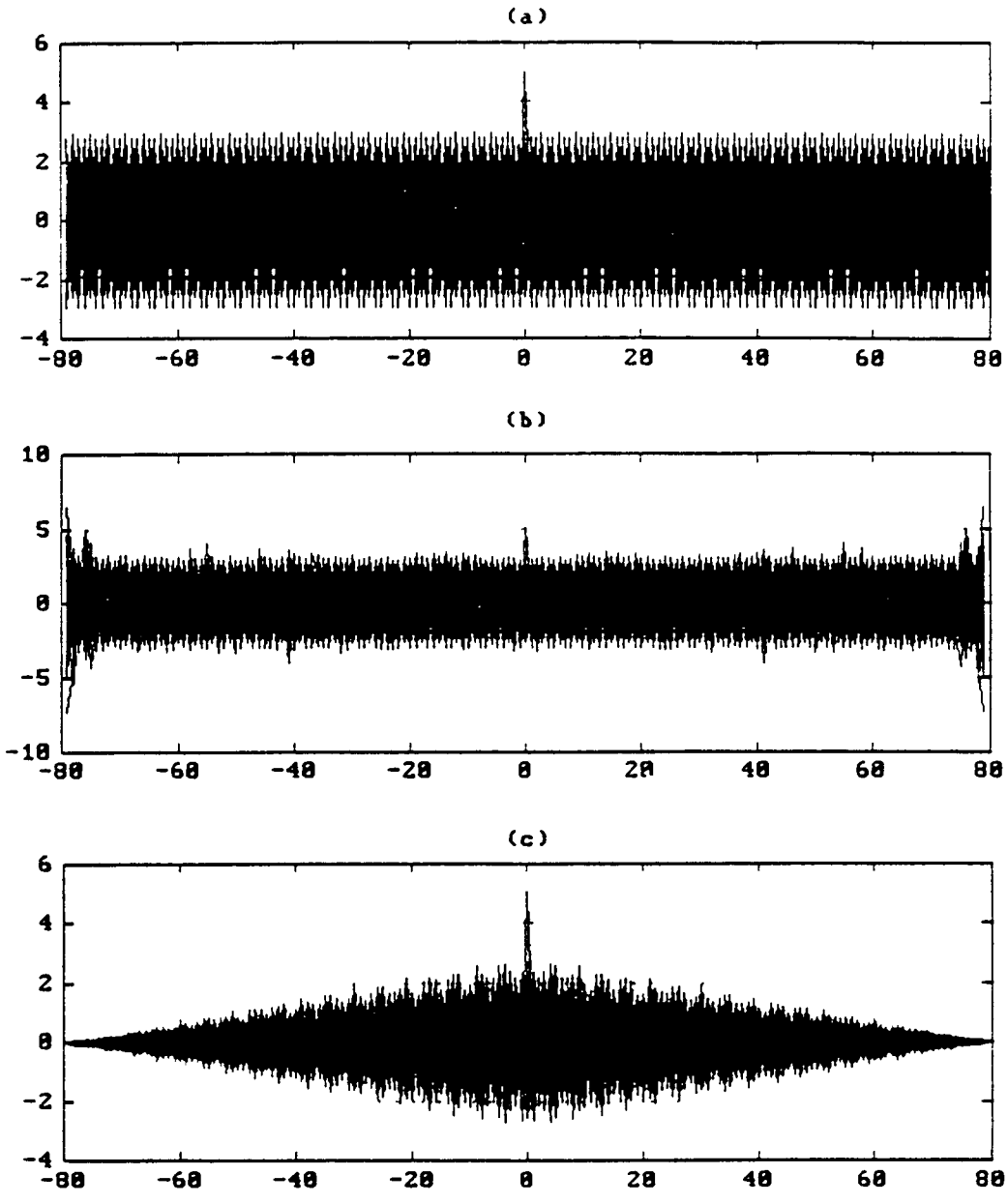

Figure 3 7 Autocorrelation functions for 80 x 80 data set consisting of sinusoids at normalised frequencies (0 3333, 0 2) and (0 1, 0 22) in white noise at SNR of 1 77 dB

(a) exact autocorrelation function, (b) unbiased autocorrelation function, and (c) biased autocorrelation function

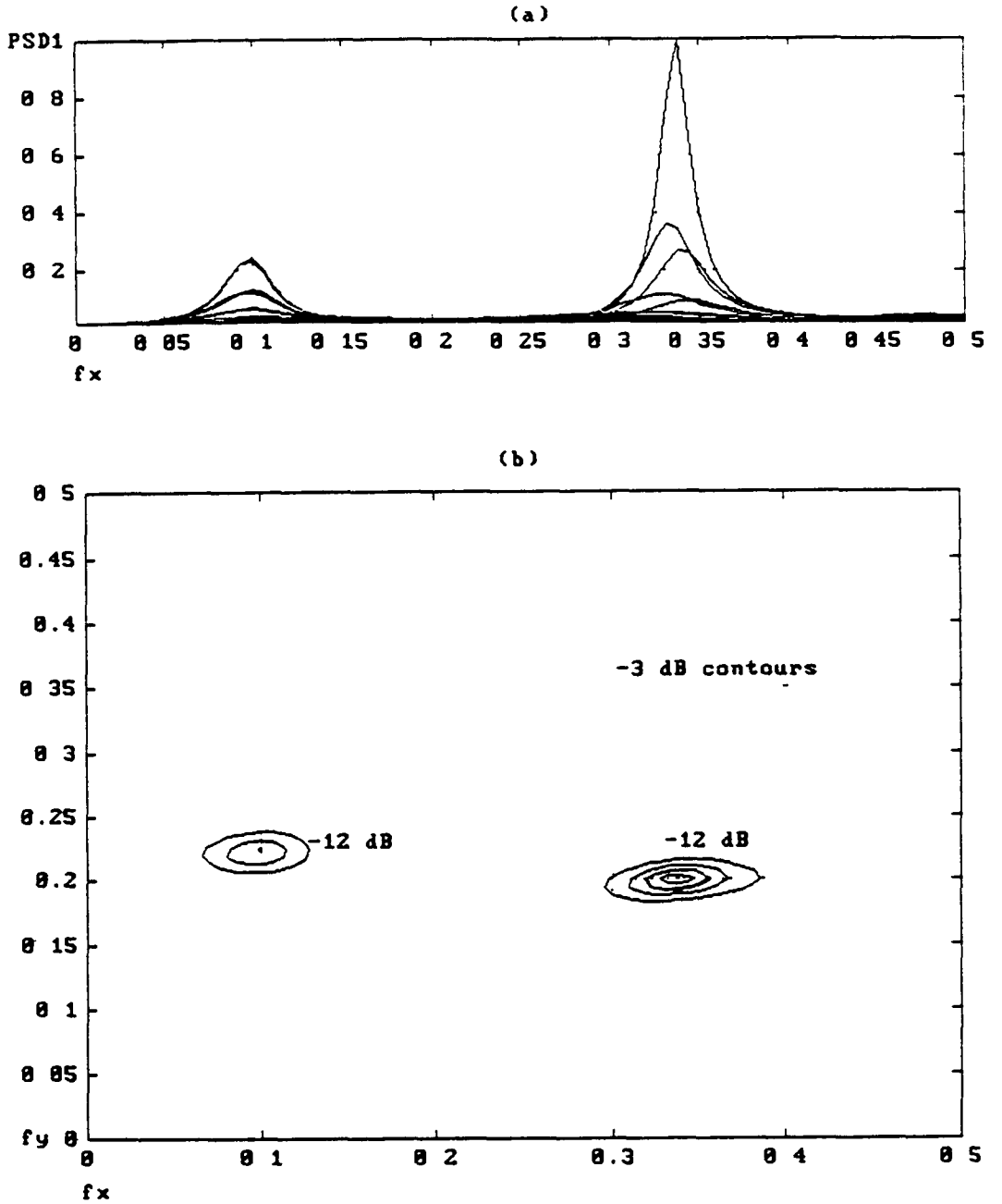

Figure 3 8 MFE temperature 0 5 spectral estimate of sinusoids at normalised frequencies (0 3333, 0 2) and (0 1, 0 22) in white noise at SNR of 1 77 dB based on the exact autocorrelation

(a) Normalised amplitude spectral estimate on the x frequency axis, and (b) Contour plot in dB on x and y frequency axes

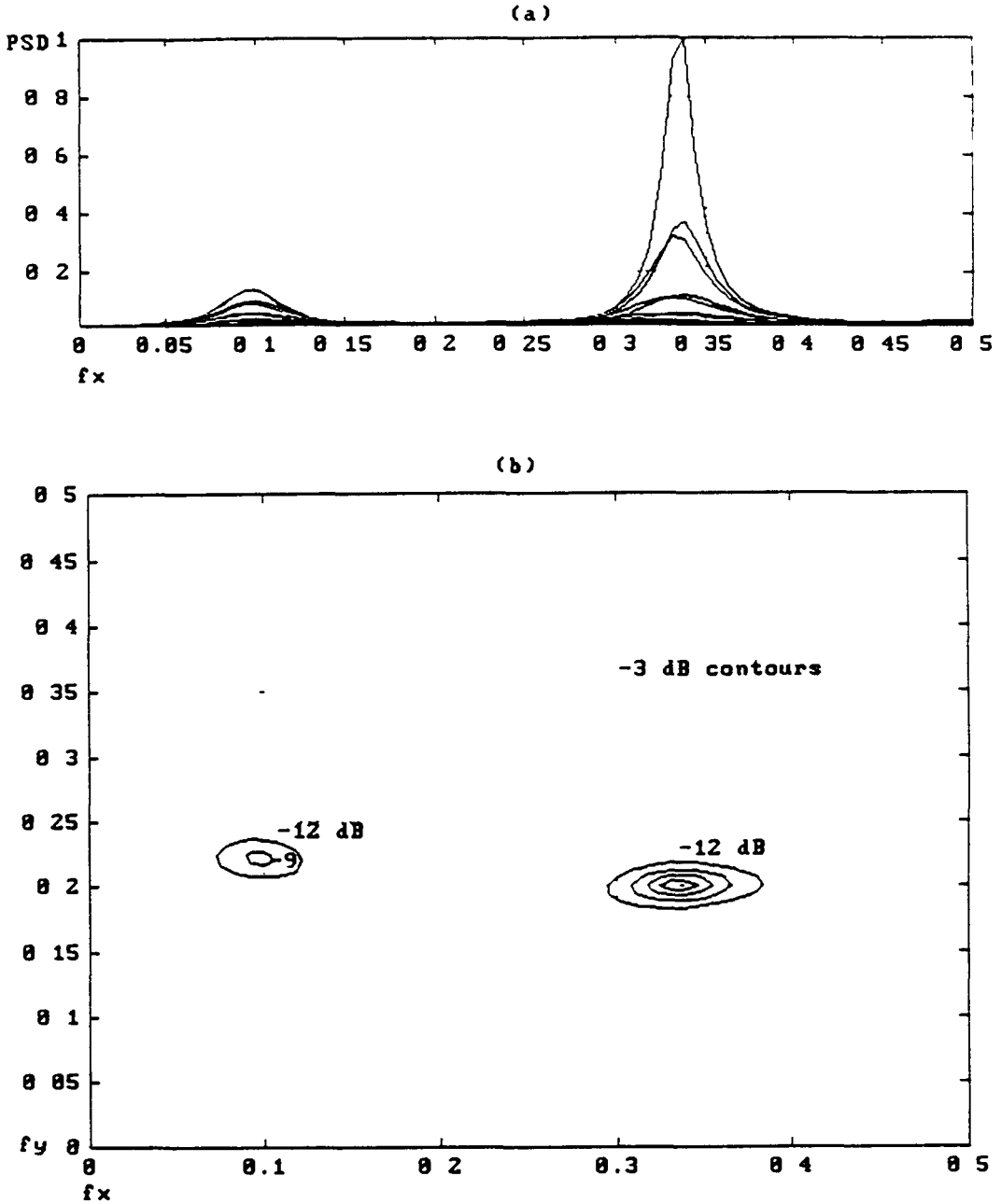

Figure 3 9 MFE temperature 0 5 spectral estimate of a single sinusoid at normalised frequencies (0 3333, 0 2) and (0 1, 0 22) in white noise at SNR of 1 77 dB based on the biased autocorrelation estimate

(a) Normalised amplitude spectral estimate on the x frequency axis, and (b) Contour plot in dB on x and y frequency axes

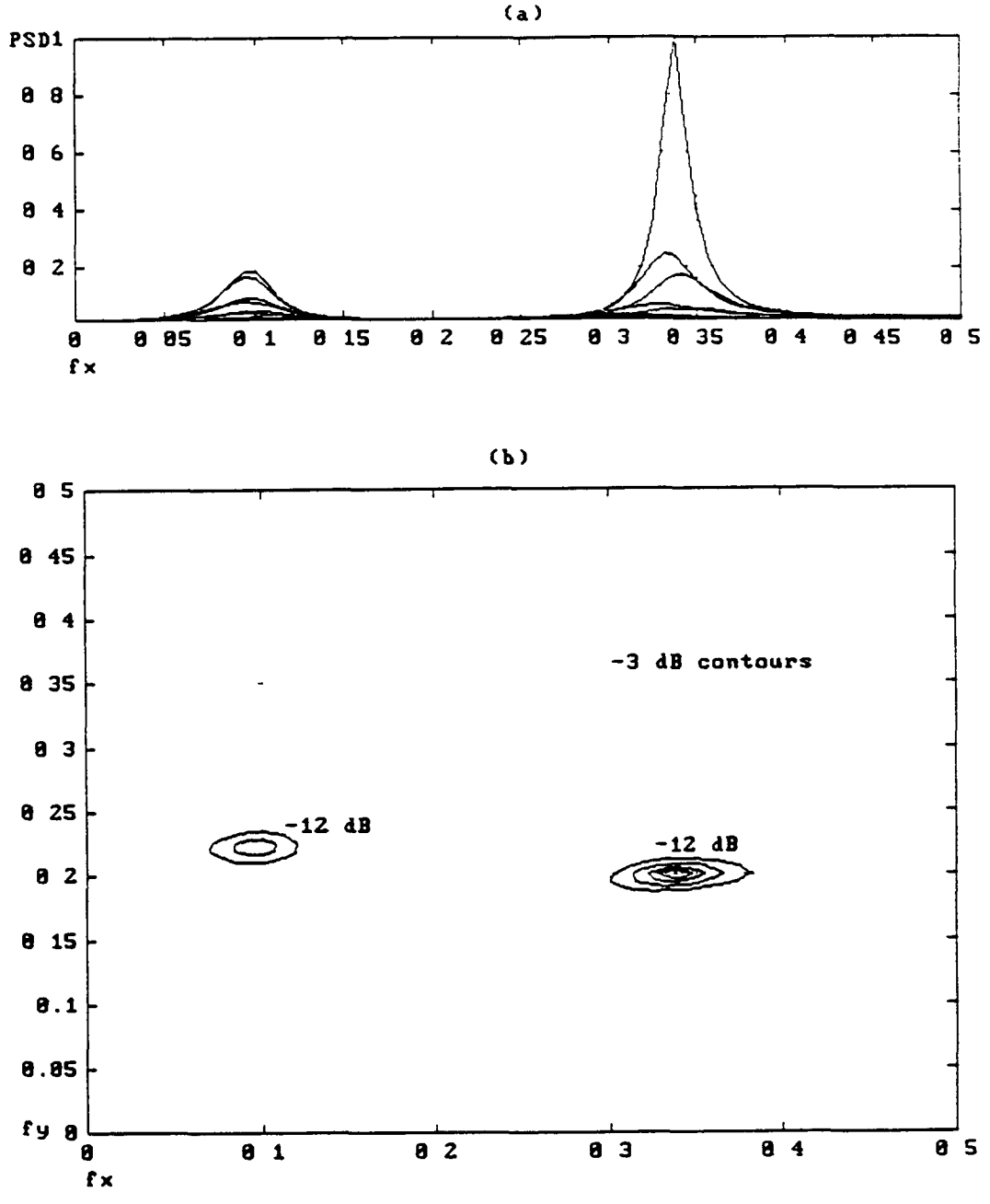

Figure 3 10 MFE temperature 0 5 spectral estimate of a single sinusoid at normalised frequencies (0 3333, 0 2) and (0 1, 0 22) in white noise at SNR of 1 77 dB based on the unbiased autocorrelation estimate

(a) Normalised amplitude spectral estimate on the x frequency axis, and (b) Contour plot in dB on x and y frequency axes

The second example is for three sinusoids of equal amplitude in white noise at an SNR of -6 dB The details for the data set are given in Table 3 6 below The temperature was set at 0 001 and 7 x 7 order MFE models were used The MFE spectral estimates based on all three autocorrelation types result in spectral peaks at the correct spatial frequency locations Figure 3 11 (a), (b), and (c) show the normalised amplitude spectral estimates on the x frequency axis for the unbiased, biased, and exact autocorrelations respectively

Table 3 6 Data set parameters

Number of sinusoids M	White noise power σ^2	Sinusoid power a_i^2	Spatial frequencies
3	6	0 5 0 5 0 5	(0 1, 0 1) (0 3, 0 1) (0 2, 0 2)

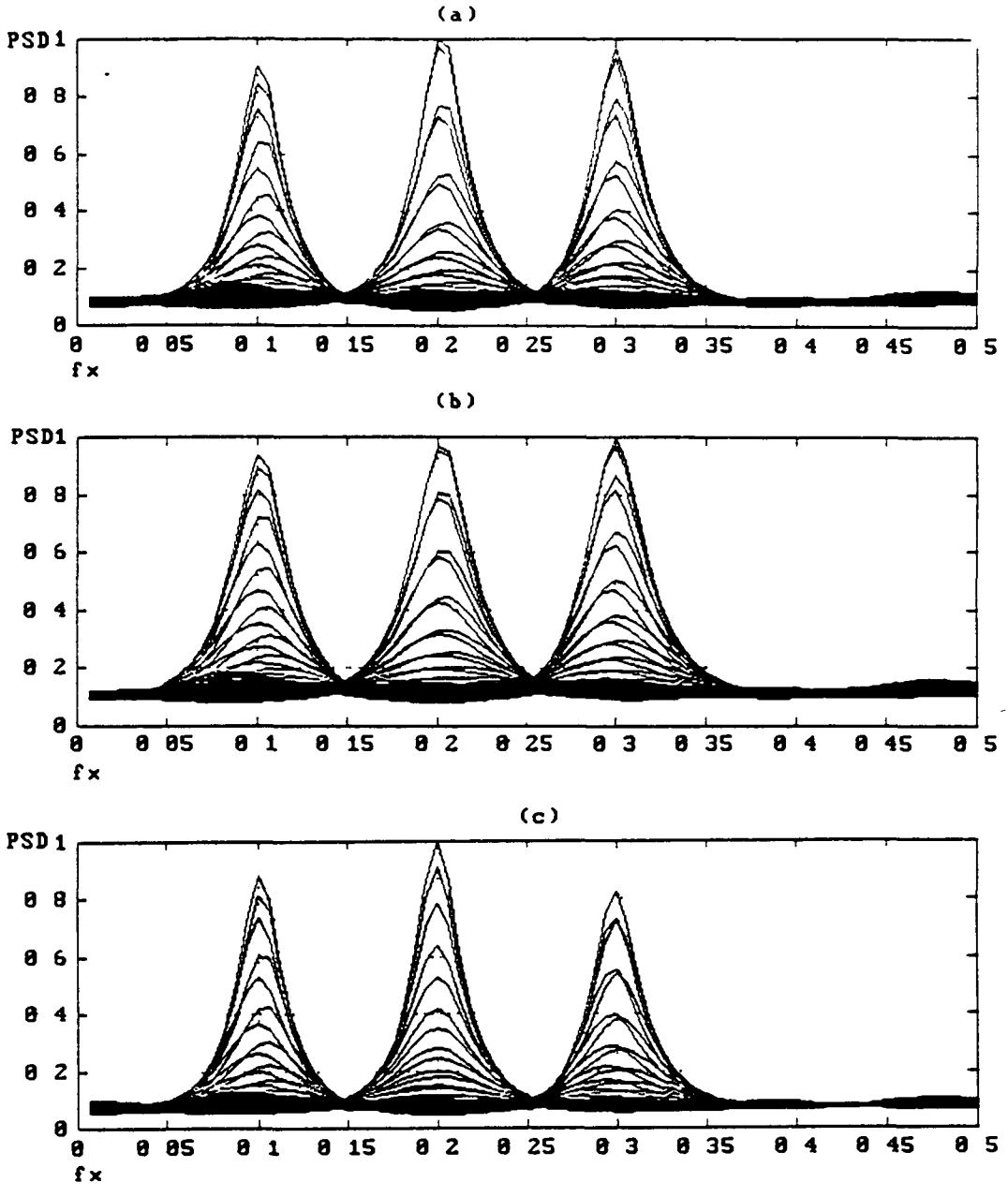

Figure 3 11 MFE temperature 0 001 spectral estimates of sinusoids at normalised frequencies (0 1, 0 1), (0 3, 0 1), and (0 2, 0 2) in white noise at SNR of -6 dB based on unbiased, biased and exact autocorrelation functions

Normalised amplitude spectral estimate on the x frequency axis based on (a) exact autocorrelation, (b) unbiased autocorrelation estimate, and (c) biased autocorrelation estimate

3.6.1 Temperature - Simulations

We investigate the variation with temperature of the spectral estimate of a single snapshot of data This snapshot consists of two sinusoids in white noise at fixed SNR of 6 dB An unbiased autocorrelation estimate was used The data set parameters are given in Table 3 1 above The model order used was 5 x 5 Figures 3 12, 3 13, 3 14 and 3 15 (a) and (b) show the normalised PSD and contour plots for the resulting spectral estimates at temperatures 0 0, 0 05, 0 5, and 5 0 respectively As discussed in Section 3 2, at zero temperature the spectral estimate is very poor and does not exhibit spectral peaks at the correct frequencies This is clearly illustrated in Figure 3 12 (a) and (b)

Figure 3 13 (a) shows a spectral estimate with sharp peaks at $f_x = 0\ 1$ and $f_x = 0\ 3$ It is evident from the contour plot of Figure 3 13 (b) that the spectral estimate at temperature 0 05 is accurate The 10 dB contours illustrate the sharpness of the peaks The spectral estimate is elliptical at very low dB value showing some directional bias However this directional bias is negligible from the -10 dB contour upwards

At temperature 0 5 the spectral peaks are not quite as sharp as they are at temperature 0 05 This is illustrated by the PSD plot in Figure 3 14 (a) and the contours in Figure 3 14 (b)

In Figure 3 15 (a) the spectral estimate at temperature 5 0 displays two very broad peaks The broadness of the peaks is further illustrated by the 1 dB contours shown in Figure 3 15 (b) Hence we see that the upper temperature limit is marked by a reduction m spectral resolution, whereas below the lower limit spectral estimation is poor This agrees with the discussion in [12] The poor results obtained near or at zero temperature are accompanied by negative driving noise variance or non-unity bounded autoregressive model parameters Extensive experimentation has shown that regardless of model size or data set size employed there is a reasonably broad range of temperature over which MFE provides good spectral estimates Hence precise determination of a critical signal processing temperature value is unnecessary

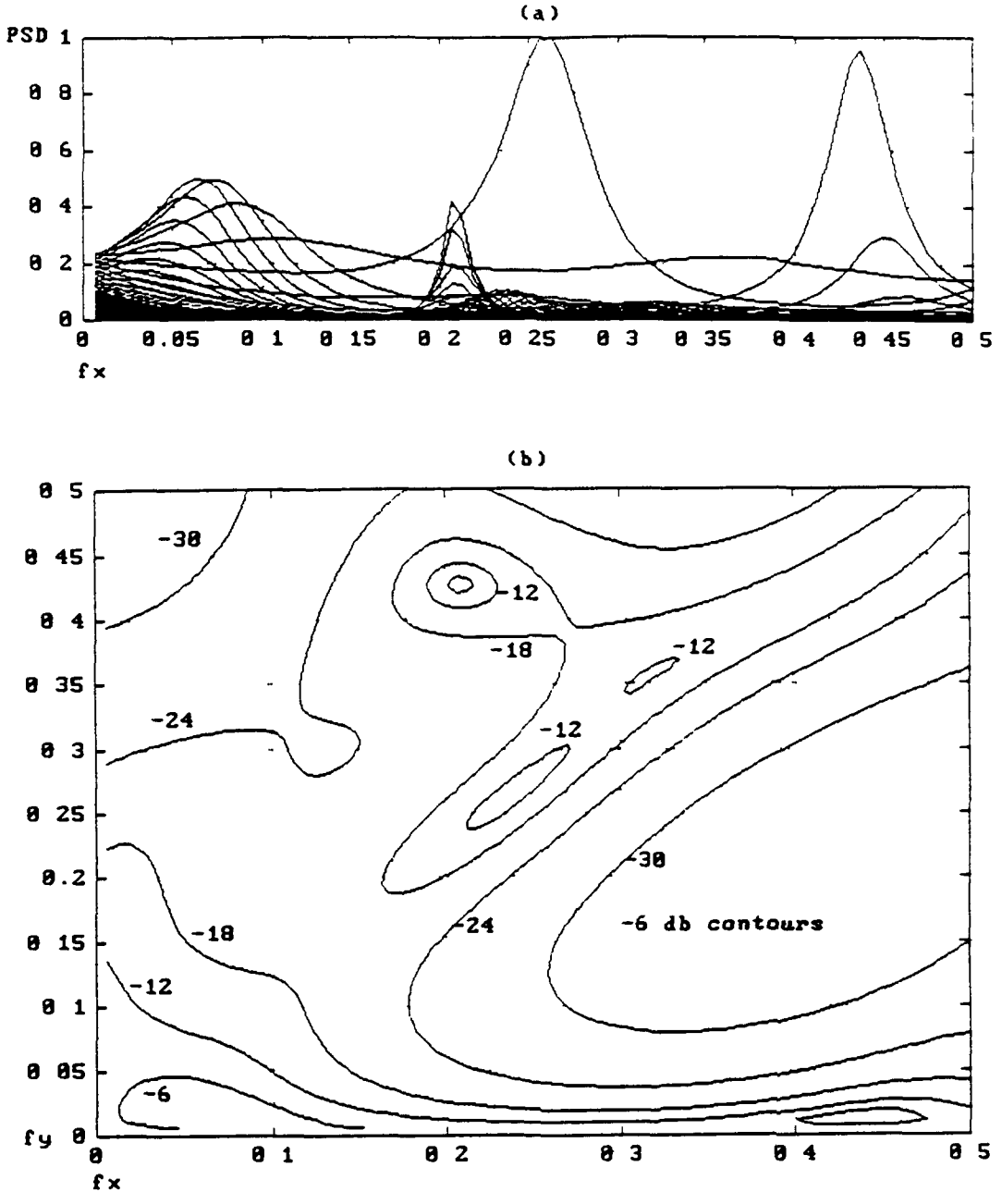

Figure 3 12 MFE temperature zero spectral estimate of sinusoids at normalised frequencies (0 1, 0 2) and (0 3, 0 4) in white noise at SNR of 6 dB

(a) Normalised amplitude spectral estimate on the x frequency axis, and (b) Contour plot in dB on x and y frequency axes

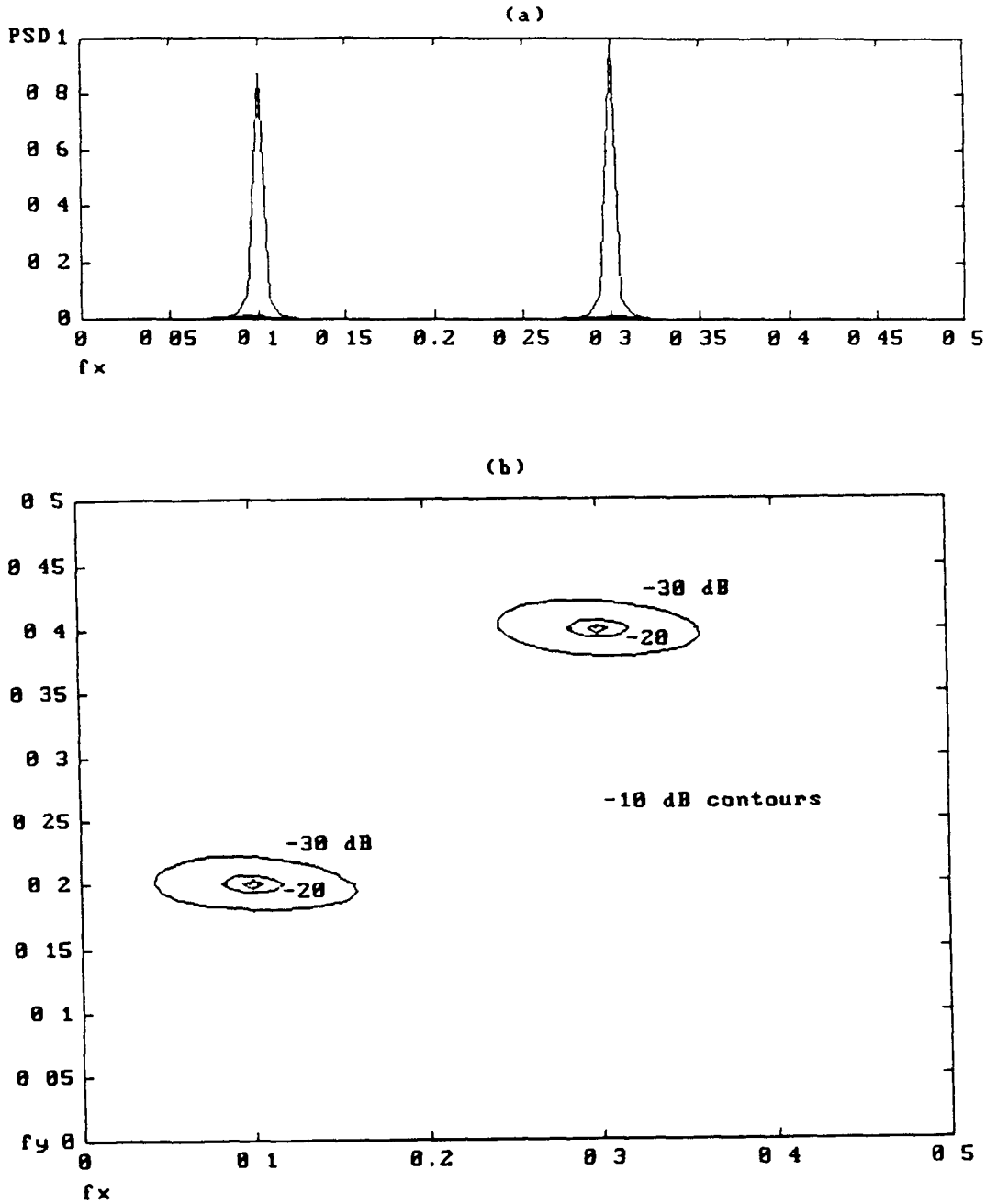

Figure 3 13 MFE temperature 0 05 spectral estimate of sinusoids at normalised frequencies (0 1, 0 2) and (0 3, 0 4) in white noise at SNR of 6 dB

(a) Normalised amplitude spectral estimate on the x frequency axis, and (b) Contour plot in dB on x and y frequency axes

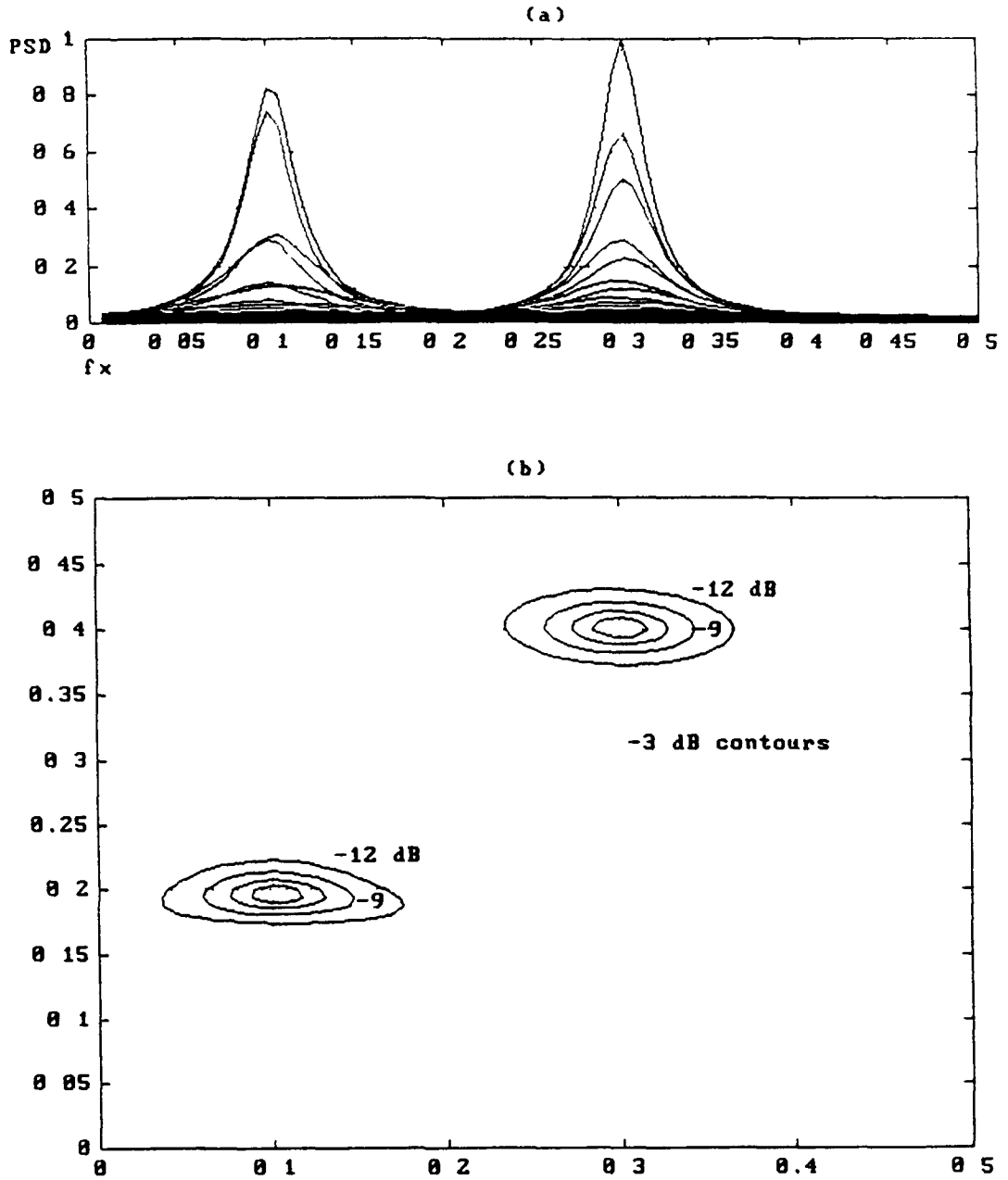

Figure 3 14 MFE temperature 0 5 spectral estimate of sinusoids at normalised frequencies (0 1, 0 2) and (0 3, 0 4) in white noise at SNR of 6 dB

(a) Normalised amplitude spectral estimate on the x frequency axis, and (b) Contour plot in dB on x and y frequency axes

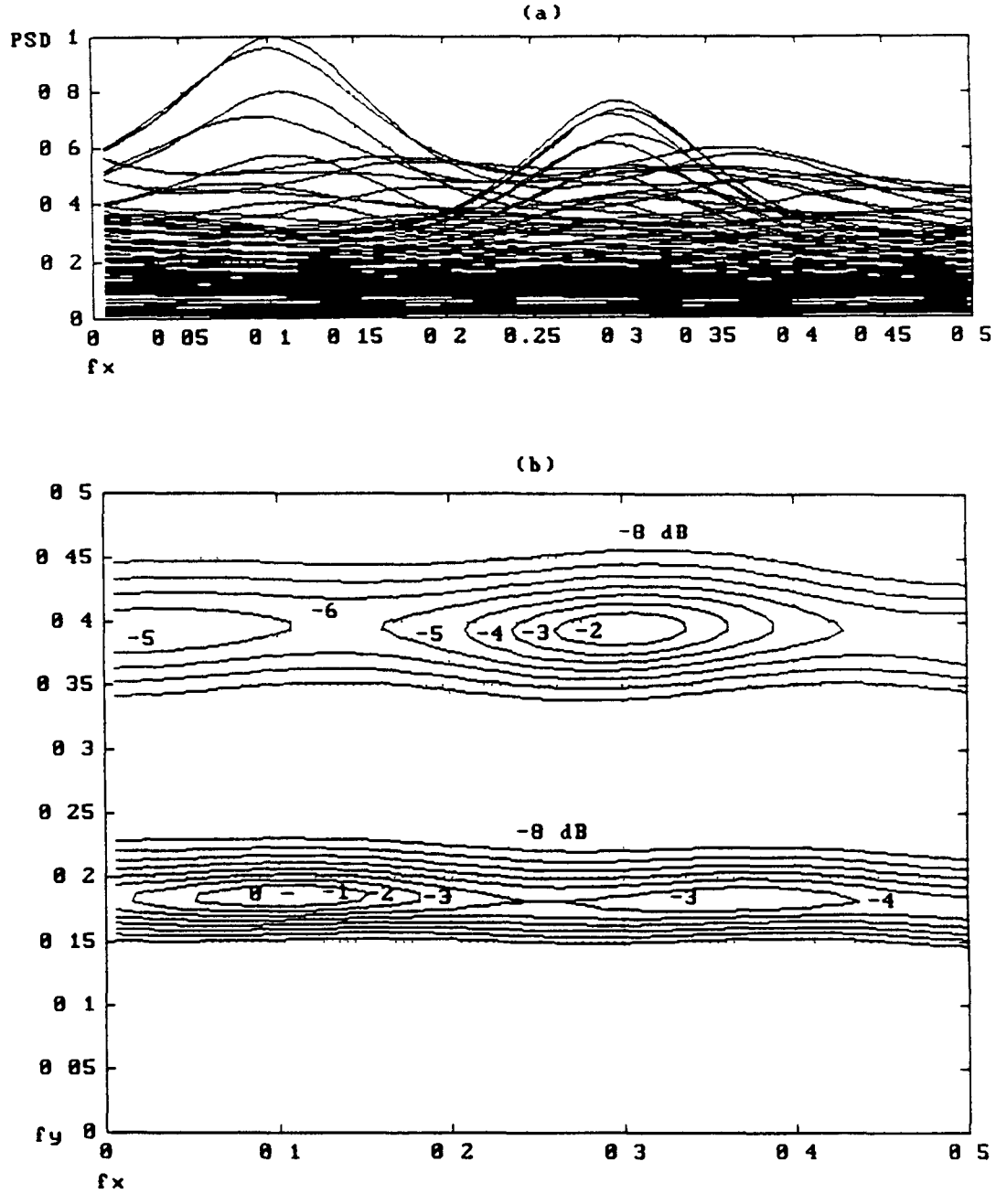

Figure 3 15 MFE temperature 5 0 spectral estimate of sinusoids at normalised frequencies (0 1, 0 2) and (0 3, 0 4) in white noise at SNR of 6 dB

(a) Normalised amplitude spectral estimate on the x frequency axis, and (b) Contour plot in dB on x and y frequency axes

3.6.2 Temperature - Determination

A method of identification of the best temperature range before or within the MFE parameter estimation algorithm should provide a computational advantage especially for high order models The alternative is to determine the temperature range empirically and to calibrate the system temperature with a known source that is subjected to a known level of noise as in 1-D [77] The cost function in 2-D MFE is minimised at $O((p_1-1)(2p_2^4))$ multiplies per iteration where the model order is $p_1 \times p_2$ MFE can provide accurate spectral estimation over a broad temperature range where the optimum temperature range depends on the model order and level of noise Hence a priori temperature determination would present an advantage at high model orders However, as stated in [78] 'We have no fundamental theory for the temperature' A priori temperature determination remains an open and unsolved question even for 1-D MFE [66] In Section 6 3 we highlight directions for ongoing research that may lead to a solution of this question

To get an early indication of temperature range suitability, we may investigate the relationship between the reflection coefficient matrices in 2-D MFE and optimal signal processing temperature For optimal temperature spectral estimation the entropy term in the MFE cost function should ensure reflection matrices with unity bounded elements Hence the condition of the reflection coefficient matrices gives an indicator of the quality of the resultant spectral estimates

Another method of early determination of the best temperature range is to monitor the order of magnitude difference between cost functions associated with expression (50) as discussed in Section 2 6 on optimisation and cost functions We define the cost function order difference (ord) as the absolute difference between the log of the cost function due to the error energy and that due to entropy Figure 3 16 is a plot of this order difference over temperature This example is from MFE model order 3 x 3 spectral estimation of the homogeneous random field constituent of texture D93 from the Brodatz album [6] In [44] and [45] we decompose scanned fields from the

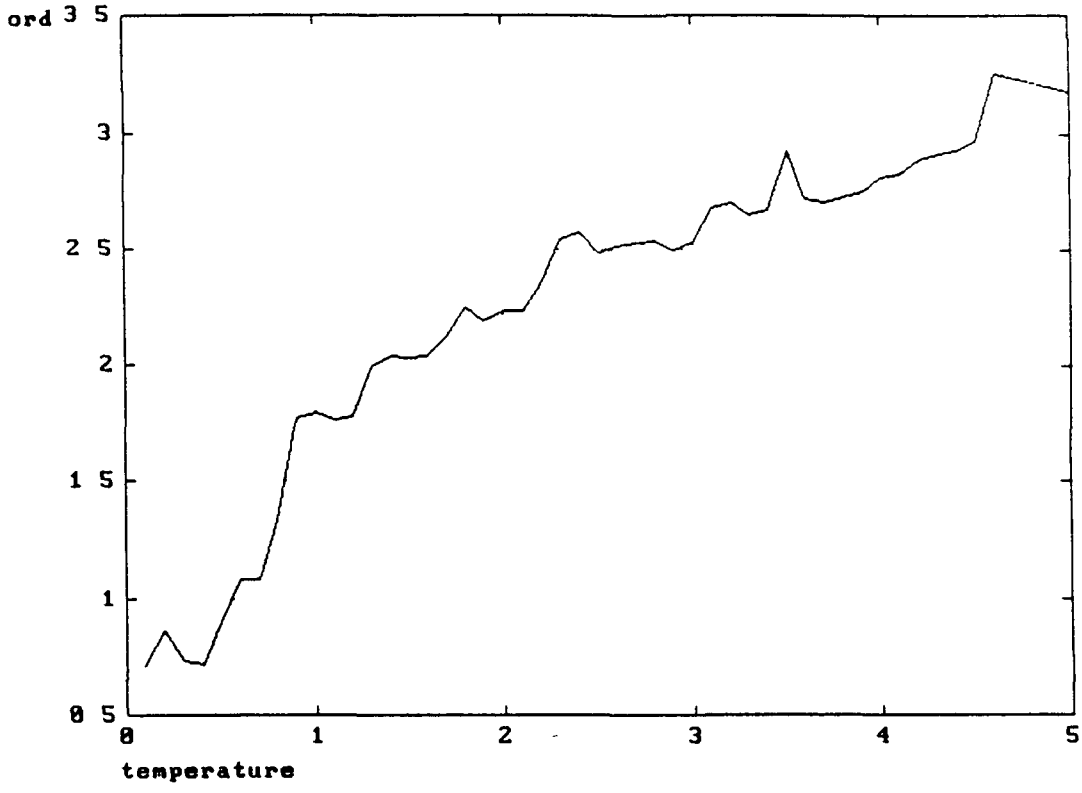

Figure 3 16 Cost function order difference (ord) as a function of temperature for MFE model order 3 x 3 spectral estimate of the homogeneous random field constituent of texture field D93

Brodatz album into constituent fields including homogeneous random fields The issue of wideband and mixed MFE spectra estimation is addressed in Section 6 5

3.7 Model order

It has been proposed by Pimbley [66] and more recently by Cooper and Pimbley [12] that it may be possible to determine the model order by use of the Akaike information criterion However the Akaike information criterion is not a consistent decision rule for estimating the order of AR models [35] We use a simple and effective method of increasing the model order as long as the resolution of the resultant spectral estimate is improving The computational expense of the method depends on model order, hence there is a simple trade off between added computational expense and higher resolution

Extensive experimentation into the effect of model order variation has shown that the width of the peaks corresponding to sinusoid components in a spectral estimate decreases as the model order increases In one test we took a 80 x 80 point single snapshot of data consisting of 2 equal amplitude sinusoids at 0 dB SNR The data set detailed in Table 3 4 was subjected to spectral estimation using MFE models of order 3 x 3, 5 x 5, 7 x 7 and 9 x 9 The corresponding temperatures used were 0 001, 0 001, 0 05 and 0 05 respectively Figure 3 17 shows the contour plots for the estimates In filter theory the Q-factor is used to determine the selectivity of filters by providing a measure of the peakiness of the spectral response of a filter We adapt this concept to 2-D and use a 2-D Q-factor to measure the sharpness of the peaks in the frequency domain This Q-factor is determined as the inverted product of the bandwidths in the x and y frequency direction across each spectral peak at a given amplitude We use the averaged Q-factor over the two spatial frequency components or peaks as a comparative measure of the sharpness of the peaks The average Q-factors at -21 dB for the 9 x 9, 7 x 7, and 5 x 5 model spectral estimates and at -3 dB for the 3 x 3 model spectral estimate are in the ratio 10 5 4 4 4 4 respectively Figures 3 18 and 3 19 (a) and (b) show the spectral estimates on the x and y frequency axes for the 5 x 5 and 3 x 3 cases The broad peaks of the 3 x 3 case are in stark contrast to the sharp peaks of the 5 x 5 case

We may apply a transformation [52], [38] on our 3x3 model PSD estimate and thereby produce a modified PSD with sharper peaks However in applying this transformation the amplitude of one of the spectral components is diminished significantly We conclude that better spectral estimation in terms of peak amplitude, and peak width as quantified by the Q-factor, is achieved as the model order increases The only known disadvantage of higher model order is added computational expense

There is a connection between model order and minimum signal processmg temperature for accurate spectral estimation Extensive experimental simulation shows that an increase m model order causes an increase in the minimum feasible value of signal processing temperature This agrees with the discussions of Cooper and Pimbley on their hybrid method in [12]

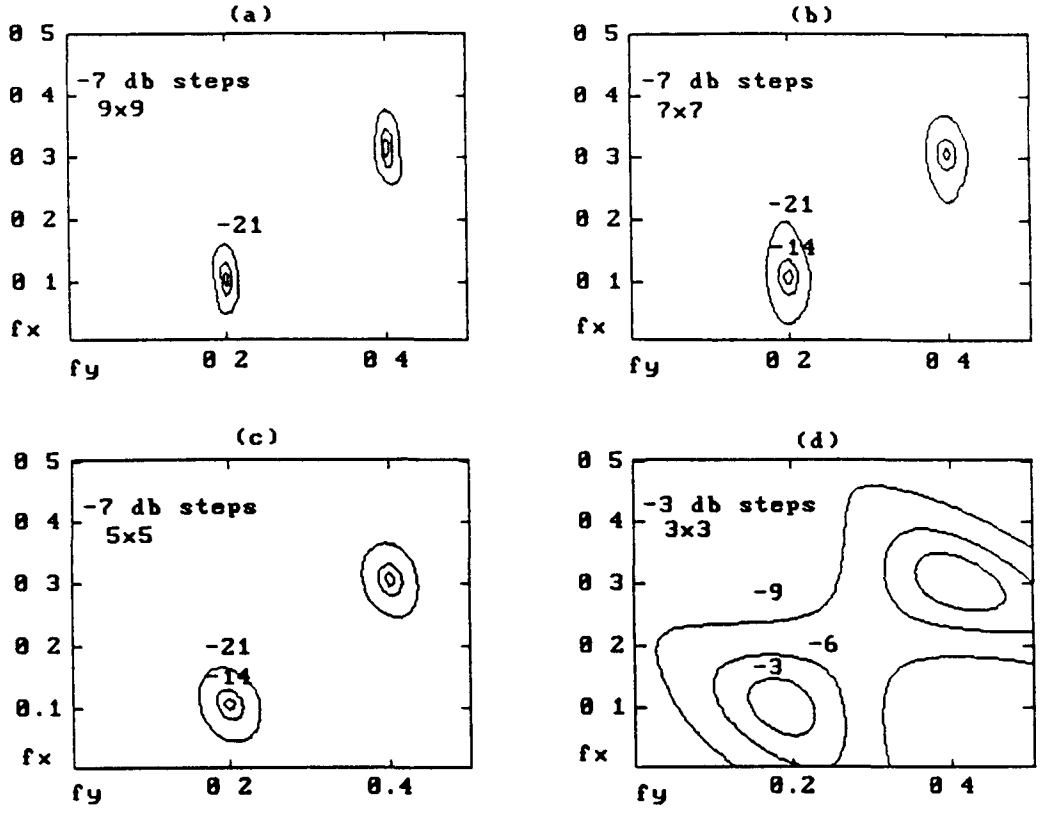

Figure 3 17 MFE spectral estimates of sinusoids at normalised frequencies (0 1, 0 2) and (0 3, 0 4) in white noise at SNR of 0 dB

Contour plot in dB on x and y frequency axes based on (a) model order 9 x 9 at temperature 0 05, (b) model order 7 x 7 at temperature 0 05, (c) model order 5 x 5 at temperature 0 001, and (d) model order 3x 3 at temperature 0 001

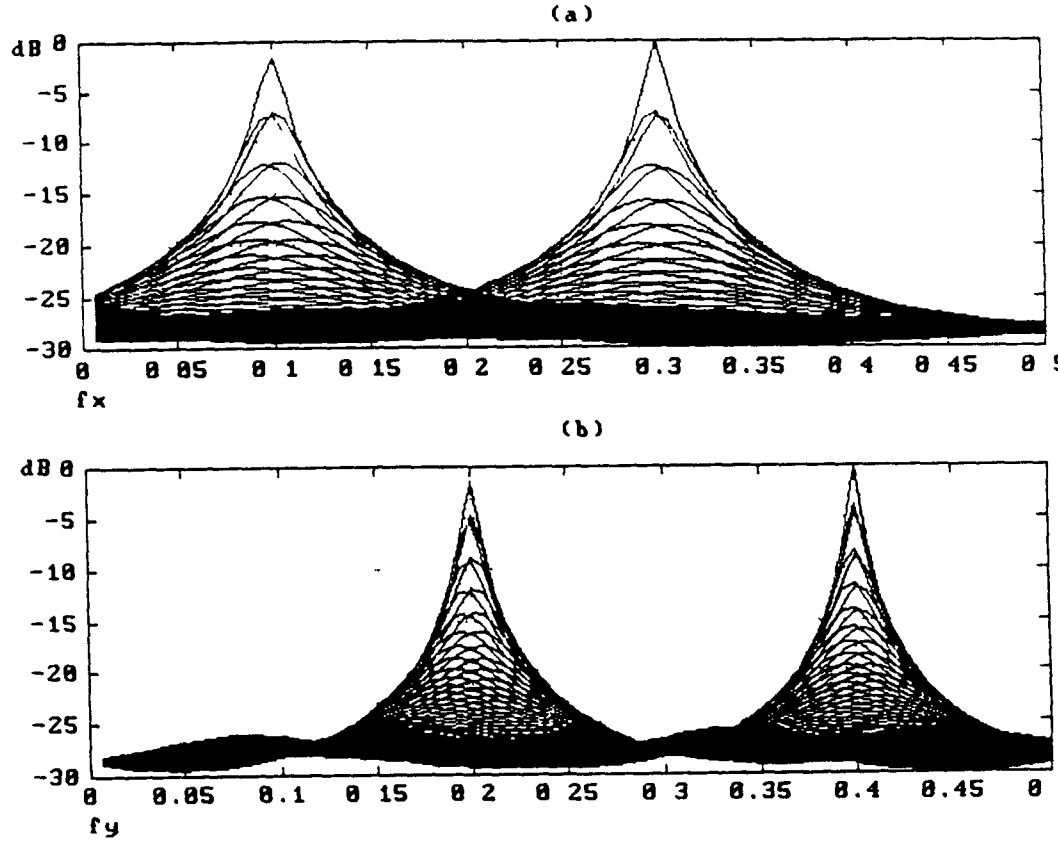

Figure 3 18 MFE model order 5 x 5 spectral estimate of sinusoids at normalised frequencies (0 1, 0 2) and (0 3, 0 4) in white noise at SNR of 0 dB

Log plots of the spectral estimate on (a) the x frequency axis, and (b) the y frequency axis

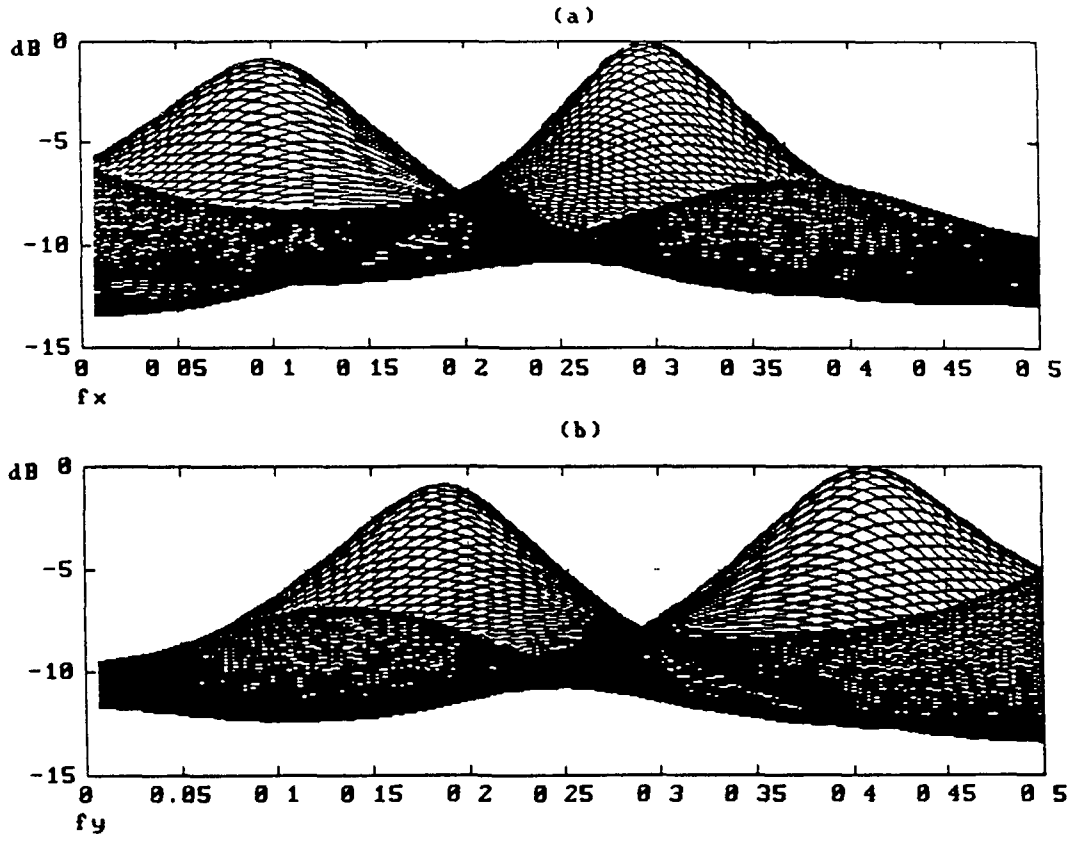

Figure 3 19 MFE model order 3 x 3 spectral estimate of sinusoids at normalised frequencies (0 1, 0 2) and (0 3, 0 4) in white noise at SNR of 0 dB

Log plots of the spectral estimate on (a) the x frequency axis, and (b) the y frequency axis

3.8 Data length

We now examine the effect on MFE spectral estimation of variation of data length at fixed SNR In the first example we took 160 x 160, 80 x 80, 40 x 40 and 20 x 20 point single snapshots of data These snapshots consisted of two equal amplitude sinusoids at spatial frequencies (0 1, 0 2) and (0 3, 0 4) at 6 dB SNR as detailed in Table 3 1 The unbiased estimated autocorrelation was used We carried out 10 trials at each data set size The random number generator used was based on the linear congruential method [53], [62], [19] The same random number generator seed was used to initiate the 10 trials for each data set size This meant that each simulation series of autocorrelations corresponding to each data set size was initiated with the same noise seed and hence used the same set of noise fields The data was subjected to spectral estimation using MFE models of order 5 x 5 All spectral estimates were generated over 160 x 160 points

The 160 x 160, 80 x 80 and 40 x 40 data sets all produced very similar spectral estimates which were accurate to a resolution of $1/160^{th}$ of unity normalised frequency

In the 20 x 20 case five of the spectral estimates were accurate to $1/160^{th}$ of unity normalised frequency The other five estimates show an error of $1/160^{th}$ of unity normalised frequency in one frequency component of one spectral peak Figure 3 20 (a) and (b) shows the log plot on the x frequency axis and the contour plot of the spectral estimate for one of these cases We note that the peak that should occur at $f_x = 0\ 3$ occurs at $f_x = 0\ 3063$ This peak is only 1 5 dB above the value of the spectral estimate at $f_x = 0\ 3$ As the spectral estimates are taken over 160 x 160 points, this represents the smallest possible detectable error If an exact autocorrelation is used instead of the unbiased estimated autocorrelation then no error occurs Hence the error occurs due to the use of the unbiased autocorrelation estimate as opposed to an error in the spectral estimation technique itself

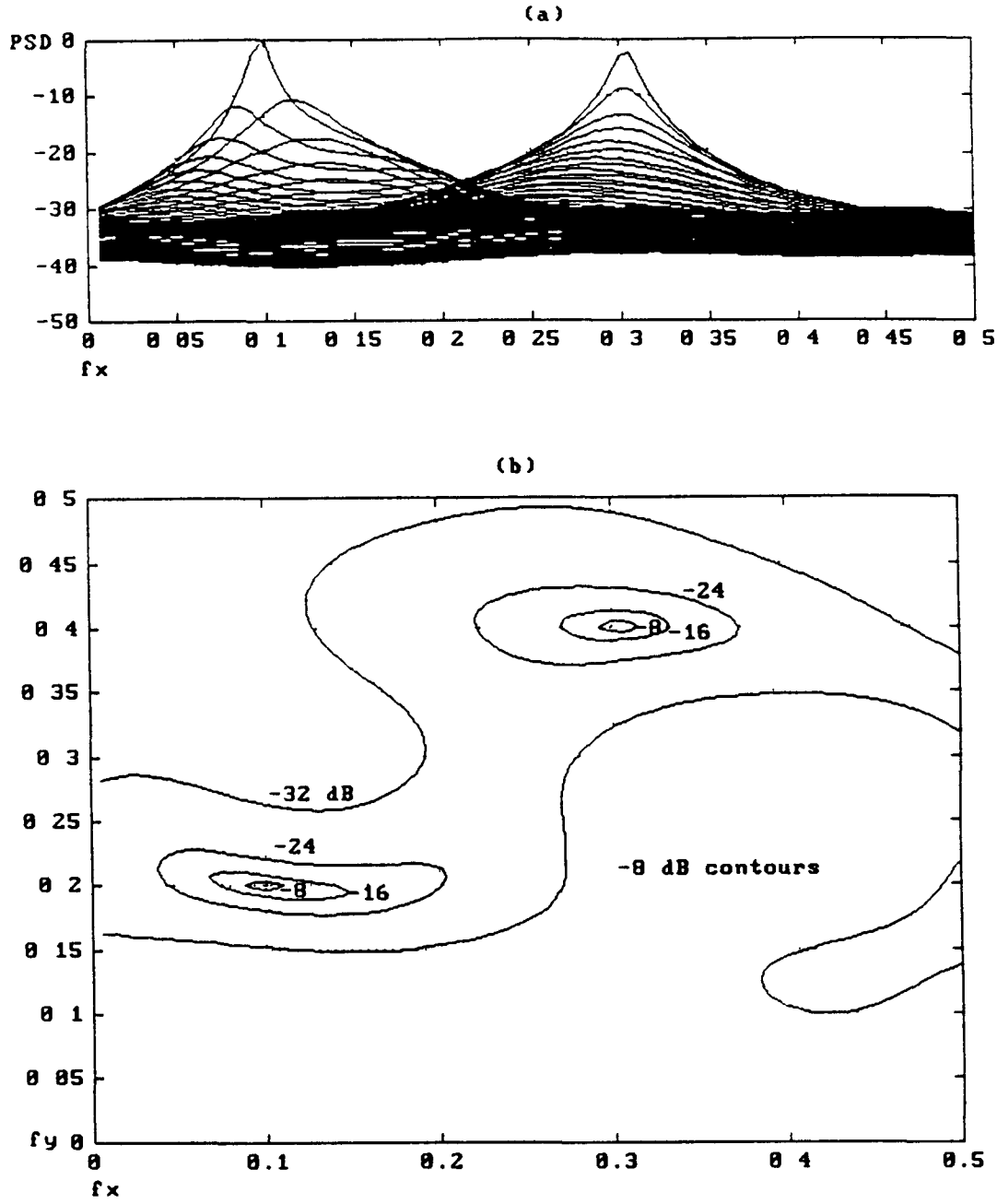

Figure 3 20 MFE 160 x 160 point spectral estimate of sinusoids at normalised frequencies (0 1, 0 2) and (0 3, 0 4) in white noise at SNR of 6 dB and data set size of 20 x 20

(a) Normalised amplitude spectral estimate on the x frequency axis, and (b) Contour plot in dB on x and y frequency axes

The detectable size of the error depends on the resolution of the spectral estimate Figure 3 21 (a) and (b) shows a high resolution 520 x 520 point estimate based on the same model The second frequency peak occurs at $f_x = 0\ 3038$, giving a more accurate reading of the error as 0 0038

Regardless of the data set size employed, the only points in the autocorrelation that are used are those corresponding to the region of support of the model Hence if the exact autocorrelation is used then autocorrelation points used in determining the model are independent of the data set size This means that spectral estimates corresponding to different data set sizes will be the same if the exact autocorrelation is used and if the data set size is larger or equal to the model order Evidence of the independence of spectral estimates to data set size using the exact autocorrelation function is seen in Section 4 3 on conventional transform comparison Hence the spectral estimates for the data set in Table 3 7 for data set size 80 x 80 , 10 x 10 and 5 x 5 are found to be identical For each of these cases the spectral estimate was derived usmg 5 x 5 order MFE models We also show in Section 4 3 that MFE provides reasonably accurate spectral estimates for closely spaced sinusoids at low SNR together with low data set size

Table 3 7 Data set parameters

Number of sinusoids M	White noise power σ^2	Sinusoid power a_i^2	Spatial frequencies
3	6	1 1 1	(0 1, 0 1) (0 3, 0 1) (0 2, 0 2)

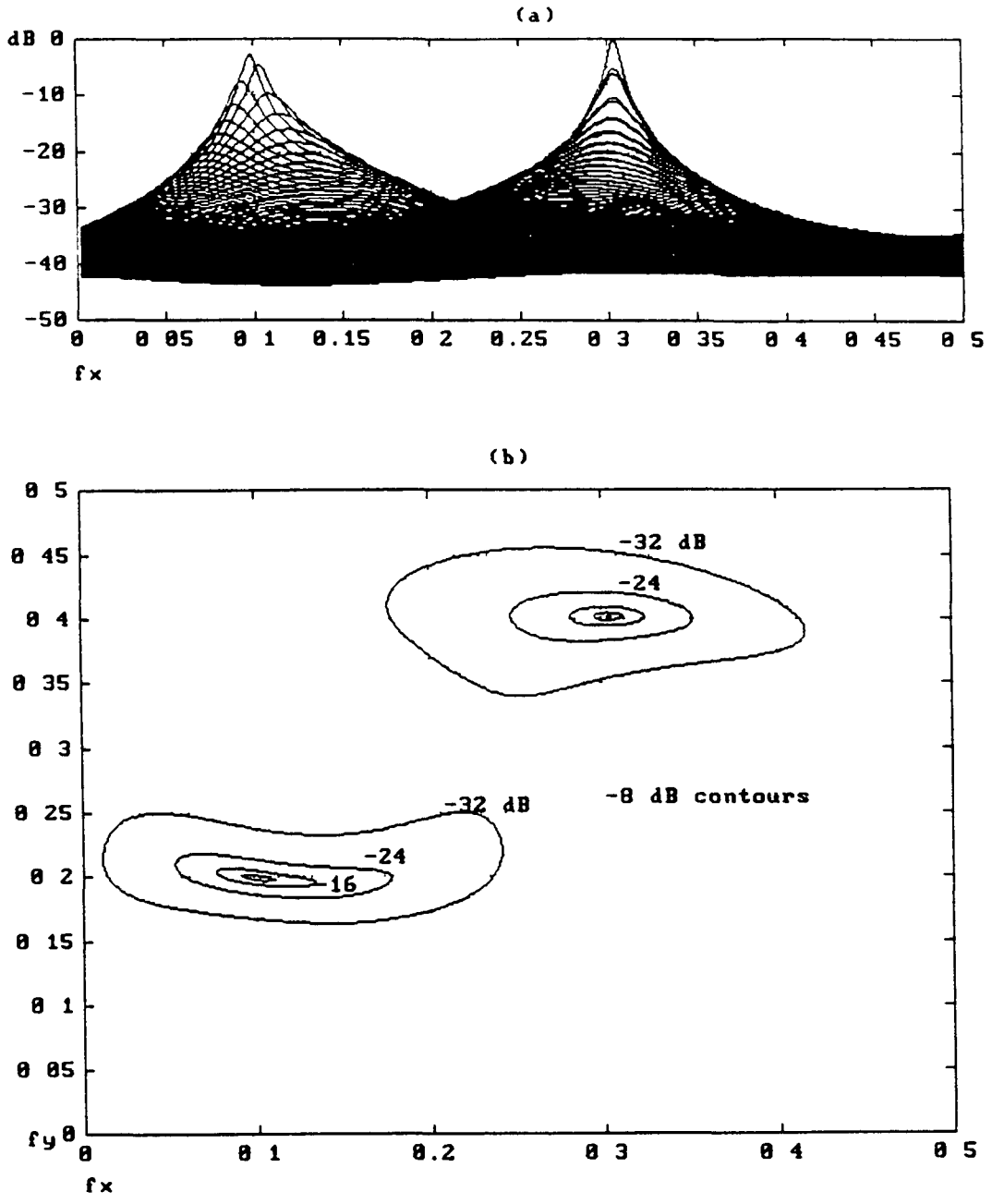

Figure 3 21 MFE 520 x 520 point spectral estimate of sinusoids at normalised frequencies (0 1, 0 2) and (0 3, 0 4) in white noise at SNR of 6 dB and data set size of 20 x 20

(a) Normalised amplitude spectral estimate on the x frequency axis, and (b) Contour plot in dB on x and y frequency axes

3.9 SNR Variation

We investigate the effect on MFE spectral estimates of variation of SNR at fixed data length Temperature emphasises entropy at the expense of error energy Entropy is a measure of the noise in the system, hence there is a direct relationship between the temperature and SNR level Evidence of this is available in the experimental results Extensive experimentation also shows that higher order models with consequent higher temperatures are required at higher SNR Lower order models exhibit instability and produce poor spectral estimates For example, 3 x 3 models can be unstable for synthesis purposes They produce inaccurate spectral estimates for a 160 x 160 data snapshot consisting of two sinusoids at 6 dB SNR as detailed in Table 3 1 However, as shown in Sections 3 4 and 3 6 1, models of order 5 x 5 are stable and produce accurate spectral estimates for the same data set If the SNR for this data set is reduced to 0 dB then as we have seen in Section 3 7 on model order the 3x3 models provide spectral estimates, albeit at low resolution As in 1-D MFE [66] and hybrid MFE [12], the method gives good results at low SNR with appropriate choice of model order

The spectral estimates for the 80 x 80 point data set in Table 3 7 that were derived using MFE 7 x 7 order models at temperature 0 001 are shown in Figure 3 22 (a) The spectral estimate for the data set in Table 3 6 is shown in Figure 3 22 (b) The data sets are identical with the exception that the set in Table 3 7 has a SNR of -3 dB, whereas that in Table 3 6 has a SNR of -6 dB Unbiased autocorrelation estimates are used on both The contour plots in Figure 3 22 (a) and (b) indicate that the higher SNR data set has tighter contours, indicative of sharper peaks, than the lower SNR data set Generally for the same model order and signal processing temperature lower SNR data sets result in broader spectral estimates This agrees with the 1-D case where numerous reported simulations attest to this property [38]

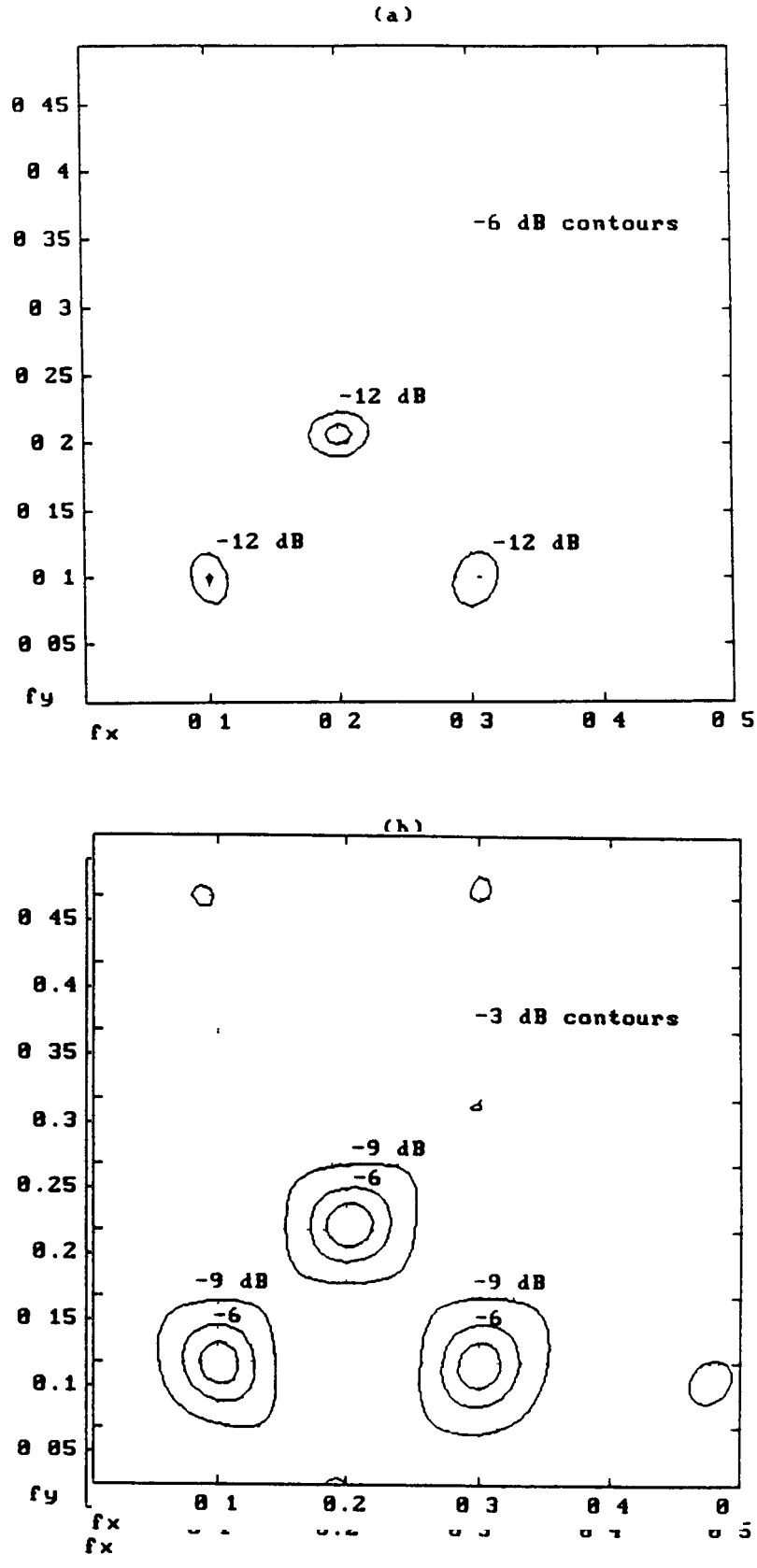

Figure 3 22 MFE temperature 0 001 spectral estimates of sinusoids at normalised frequencies (0 1, 0 1), (0 3, 0 1), and (0 2, 0 2) in white noise

Contour plot in dB on x and y frequency axes at (a) SNR of -3 dB, and (b) SNR of -6 dB

3.10 Spectral resolution

The resolution capability of single quarter plane spectral estimators is dependent on not only the magnitude of the spectral components but also on their relative orientation [86] The combined spectral estimate overcomes to some extent this problem as it takes into account the frequency plane directional selectivity of both quarter plane models Peak splitting and spurious peaks may occur due to interference between spectral components However as they occur along different axis for the different quarter plane model spectra the combined spectrum tends to eliminate them

The resolution capability of spectral estimators also depends on the shape of the region of support for the model Hence it should be noted that any resolution measurement is only an indicator of the relative performance, and should not be considered meaningful as an absolute measure [50] We may also expect some bias in spectral estimates of closely spaced sinusoids due to their fixed relative phases as commented on in the Section 2 5 on autocorrelation type

We examine the results of four tests In the first test we carry out MFE spectral estimation of a data set consisting of two sinusoids in white noise These two sinusoids are very closely spaced in one frequency direction and close in the other In the second and third tests we examine the relative performance of the MCV and MFE methods for two very closely spaced sinusoids In the last test we examine the notion of single peak area (SPA) [86]

In the first test two closely spaced sinusoids at normalised frequencies (0 1, 0 2) and (0 11, 0 38) at 4 6 dB SNR in white noise are used The parameters are given in Table 3 8 We have used a 5 x 5 order MFE model The data set size was 40 x 40 points

Table 3 8 Data set parameters

Number of smusoids M	White noise power σ^2	Sinusoid power a_i^2	Spatial frequencies
2	0 7	1 1	(0 10, 0 20) (0 11, 0 38)

The spectral estimate plotted in Figure 3 23 (a) and (b) was derived using the MFE based AR model of order 5 x 5 at zero temperature The plots in Figure 3 23 (c) and (d) are for temperature 0 5 Figure 3 23 (a) shows the normalised amplitude PSD estimate on the x frequency axis A number of spectral peaks occur However only one of them at $f_x = 0\ 09$ is close to the correct frequency $f_x = 0\ 1$ or $f_x = 0\ 11$ The contour plot in Figure 3 23 (b) shows one peak located near (0 1, 0 2), and several spurious peaks There is no peak at (0 11,0 38) Thus at zero temperature neither of the spectral components at spatial frequencies (0 1, 0 2) nor (0 11, 0 38) are accurately resolved

Figure 3 23 (c) shows the normalised PSD plot at temperature 0 5 on the x frequency axis Spectral peaks at frequencies $f_x = 0\ 1$ and $f_x = 0\ 11$ are clearly visible We can see in Figure 3 23 (d) that the x frequency components at 0 1 and 0 11, and the y frequency components at 0 2 and 0 38 making up the two spatial frequencies (0 1, 0 2) and (0 11, 0 38) are accurately resolved Hence at the non-zero temperature both spectral components at frequencies (0 1, 0 2) and (0 11, 0 38) are accurately resolved We see again that MFE provides accurate spectral estimation where the Levinson algorithm fails

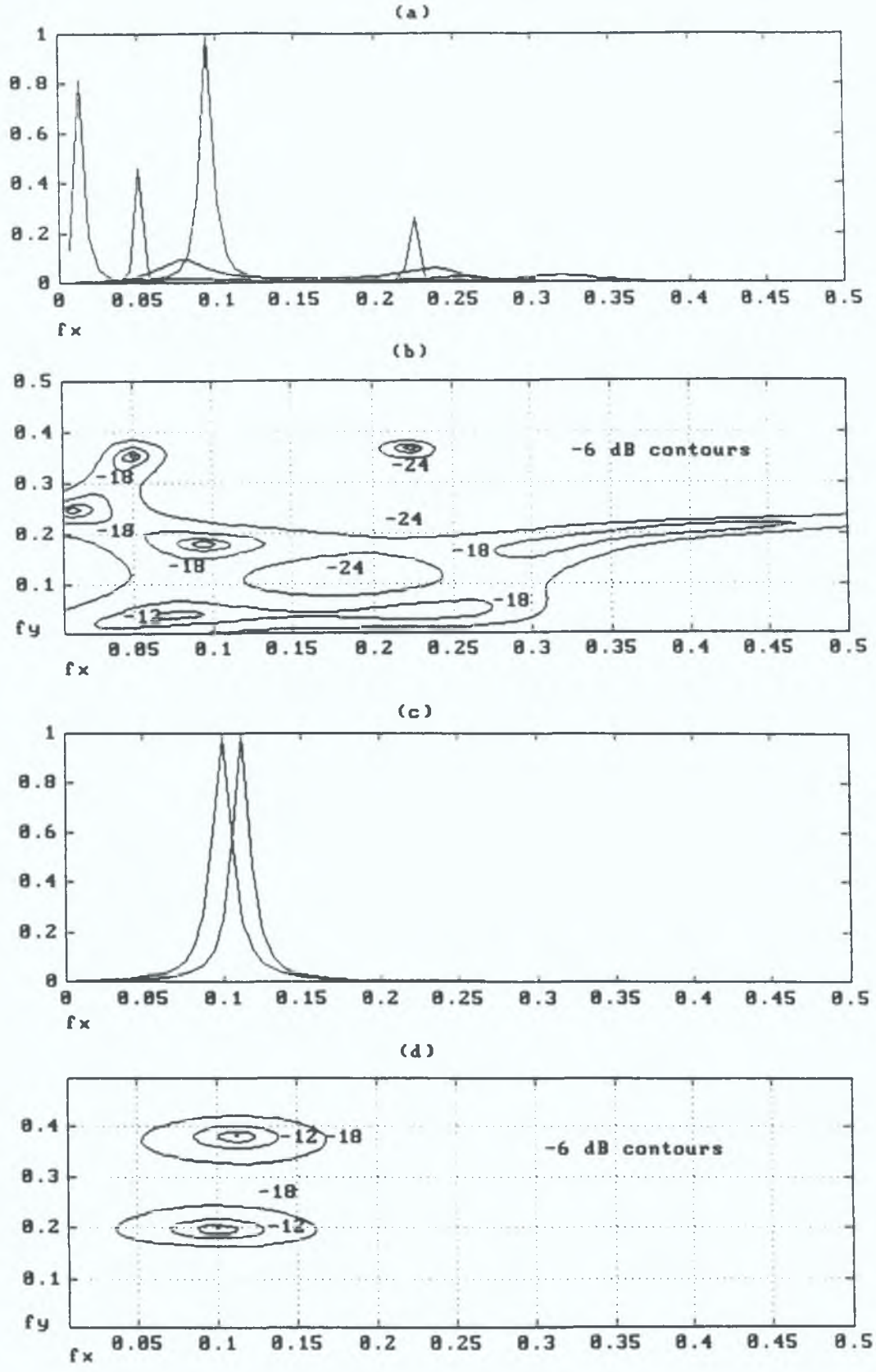

Figure 3.23. MFE spectral estimates of closely spaced sinusoids at normalised frequencies (0.1, 0.2) and (0.11, 0.38) in white noise at SNR of 4.6 dB at temperature (a), (b) zero and (c), (d) 0.5. (a) (c) Normalised amplitude spectral estimate on the x frequency axis, (b) (d) Contour plot..

In the second test on resolution we take a 40 x 40 point data set This data set consists of two very closely spaced sinusoids at frequencies (0 1, 0 3) and (0 15, 0 25) in white noise as detailed in Table 3 9 We performed spectral estimation using MFE at temperature 0 05 using an unbiased autocorrelation We also performed spectral estimation using a modified covariance method (MCV) [38] In both methods we used 7 x 7 order models In Figure 3 24 (a) we see that the MFE spectral estimate displays two distinct peaks at (0 1, 0 3) and (0 15, 0 25) The peak corresponding to (0 1, 0 3) is approximately 2 dB down on the other peak The MCV spectral estimate in Figure 3 24 (b) also displays two distinct peaks at the correct frequencies with the peak at (0 1, 0 3) also approximately 2 dB down on the other peak

MFE and conventional Fourier transform spectral estimation for the very closely spaced sinusoid example described above based on a data set size of only 7 x 7 points is examined in Section 4 3 This Section deals with comparison of MFE and a conventional transform method It is seen that MFE provides reasonably accurate spectral estimation of very closely spaced sinusoids at low SNR and low data set size

Table 3 9 Data set parameters

Number of sinusoids M	White noise power σ^2	Sinusoid power a_i^2	Spatial frequencies
2	4	1 1	(0 1, 0 3) (0 15,0 25)

In the next test we take a 40 x 40 point data set corresponding to the data in Table 3 10 The sinusoids are of equal amplitude at frequencies (0 1, 0 3) and (0 14, 0 26) We perform MFE based spectral estimation at temperature 0 05 based on an unbiased autocorrelation We also performed spectral estimation using MCV In both cases order 7 x 7 models are used The resulting MFE spectral estimate is shown in Figure 3 25 (a) Peaks are located at (0 1, 0 3) and (0 14, 0 28), with the first peak being approximately 2 dB down on the other peak The MCV

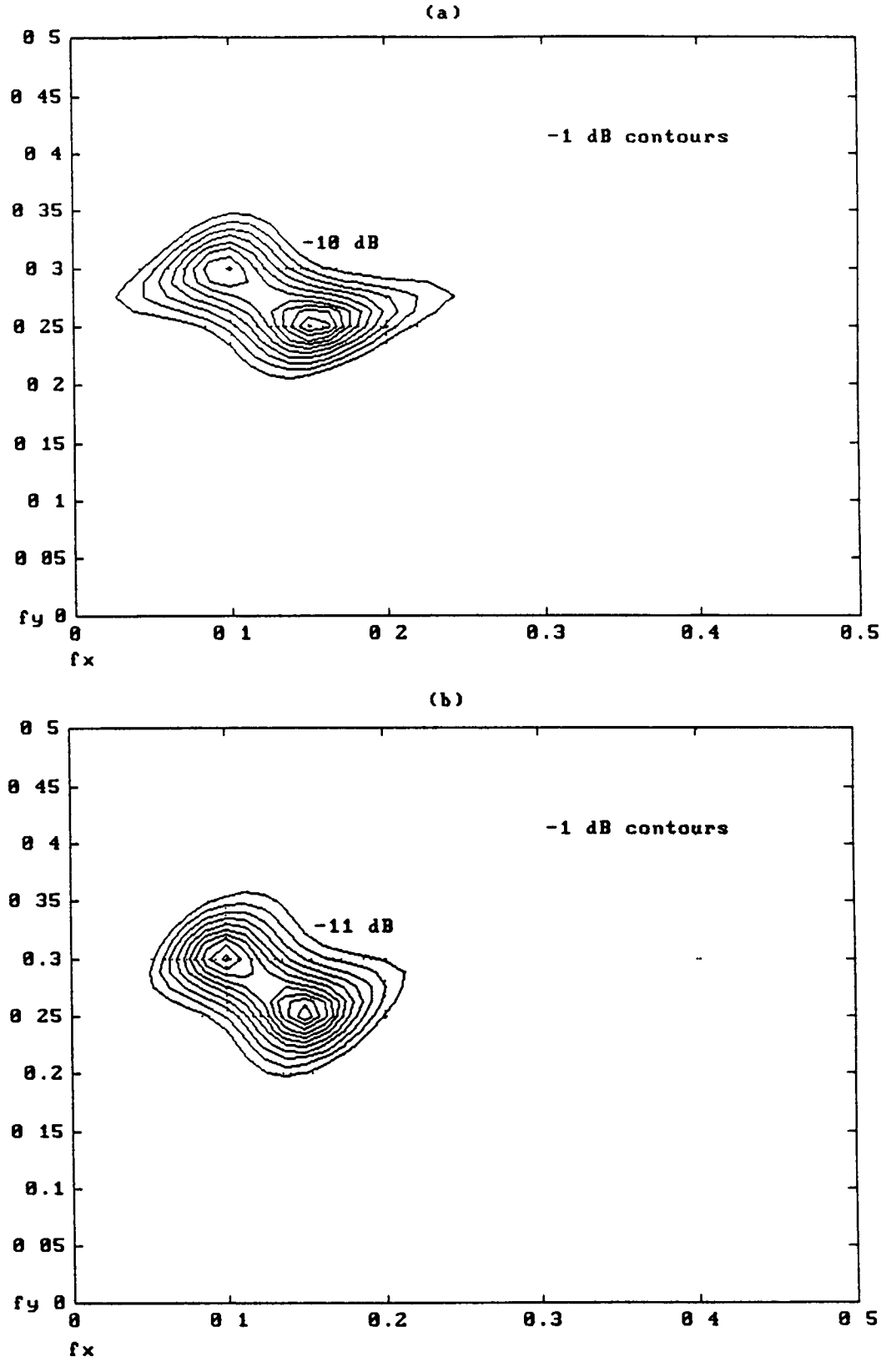

Figure 3 24 MFE and MCV spectral estimates of closely spaced sinusoids at normalised frequencies (0 1, 0 3) and (0 15, 0 25) in white noise at SNR of -3 dB

Contour plot in dB on x and y frequency axes for (a) the MFE estimate at temperature 0 05, and (b) the MCV estimate

spectral estimate, shown in Figure 3 25 (b) also gives two peaks at (0 1, 0 3) and (0 13, 0 27), with the first again 2 dB down on the other peak Clearly reduction of the gap between frequencies results in less accurate spectral estimation for both methods

Table 3 10 Data set parameters

Number of sinusoids M	White noise power σ^2	Sinusoid power a_i^2	Spatial frequencies
2	4	1 1	(0 1, 0 3) (0 14,0 26)

When the frequency separation between two sinusoidal components is small then a spectral estimate may exhibit only one peak Zou and Liu [86] introduce the notion of SPA When the frequency separation of two sinusoids of equal power is within the SPA then a single peak is observed, hence a smaller SPA for a spectral estimator implies better resolution For our last test on spectral resolution we examine the MFE spectral estimation of two very closely spaced sinusoids at normalised frequencies (0 1, 0 275) and (0 125, 0 25) in white Gaussian noise at -3 dB SNR The 20 x 20 data set is detailed in Table 3 11 Figure 3 26 (a) shows the spectral estimate for the two sinusoids using an MFE 7 x 7 order model derived at temperature 0 05 Only one peak is visible at (0 11, 0 26) However increasing the model order overcomes this effect The spectral estimate for the case where the model order is marginally increased to 9 x 9 is shown in Figure 3 26 (b) Two distinct peaks are seen to emerge If the model order is increased further to 12 x 12 then the peaks become more distinct again, as seen in Figure 3 26 (c)

Table 3 11 Data set parameters

Number of sinusoids M	White noise power σ^2	Sinusoid power a_i^2	Spatial frequencies
2	4	1 1	(0 1, 0 275) (0 125,0 25)

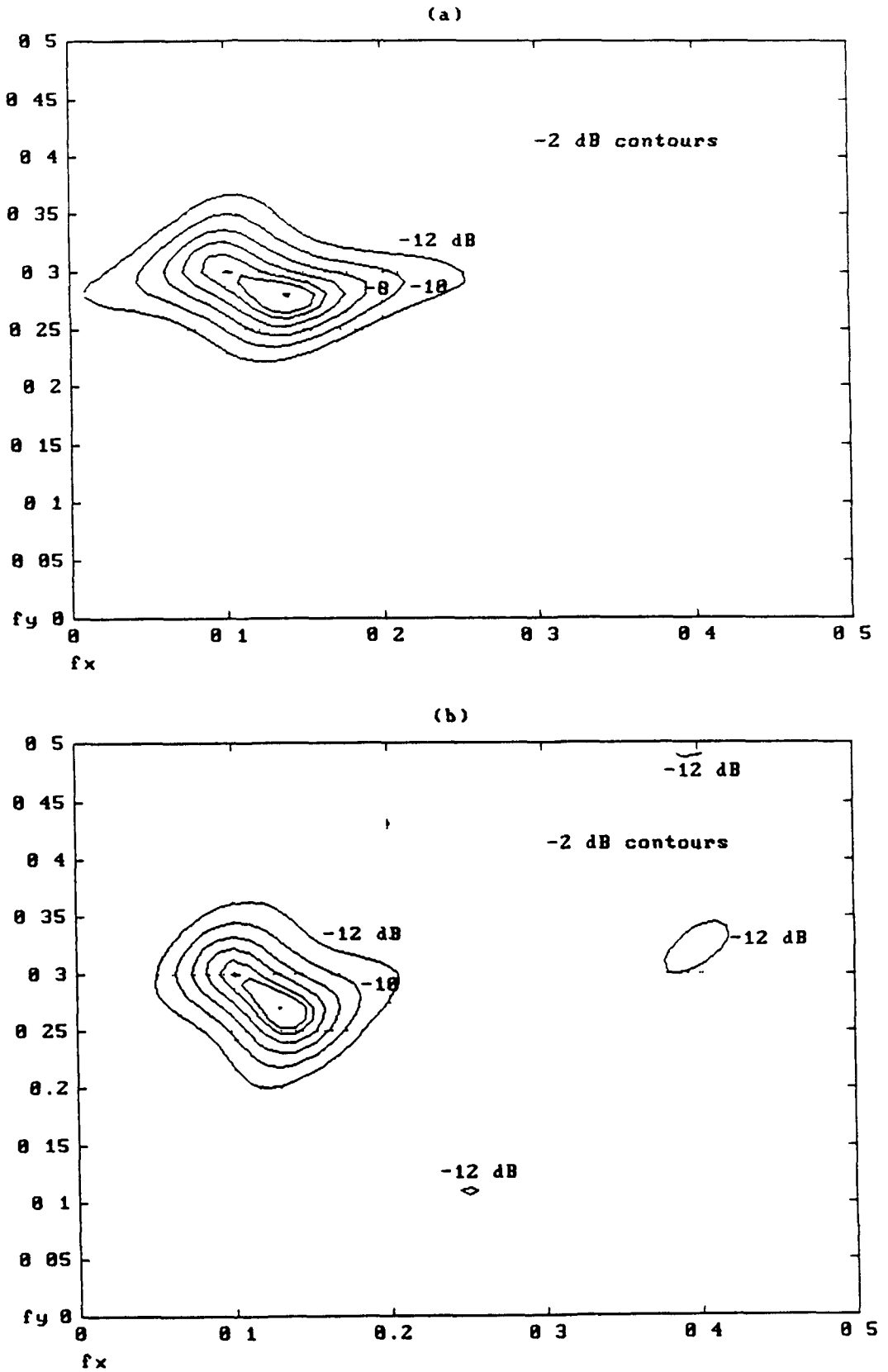

Figure 3 25 MFE and MCV spectral estimates of closely spaced sinusoids at normalised frequencies (0 1,0 3) and (0 14,0 26) in white noise at SNR of -3 dB

Contour plot in dB on x and y frequency axes for (a) the MFE estimate at temperature 0 05, and (b) the MCV estimate

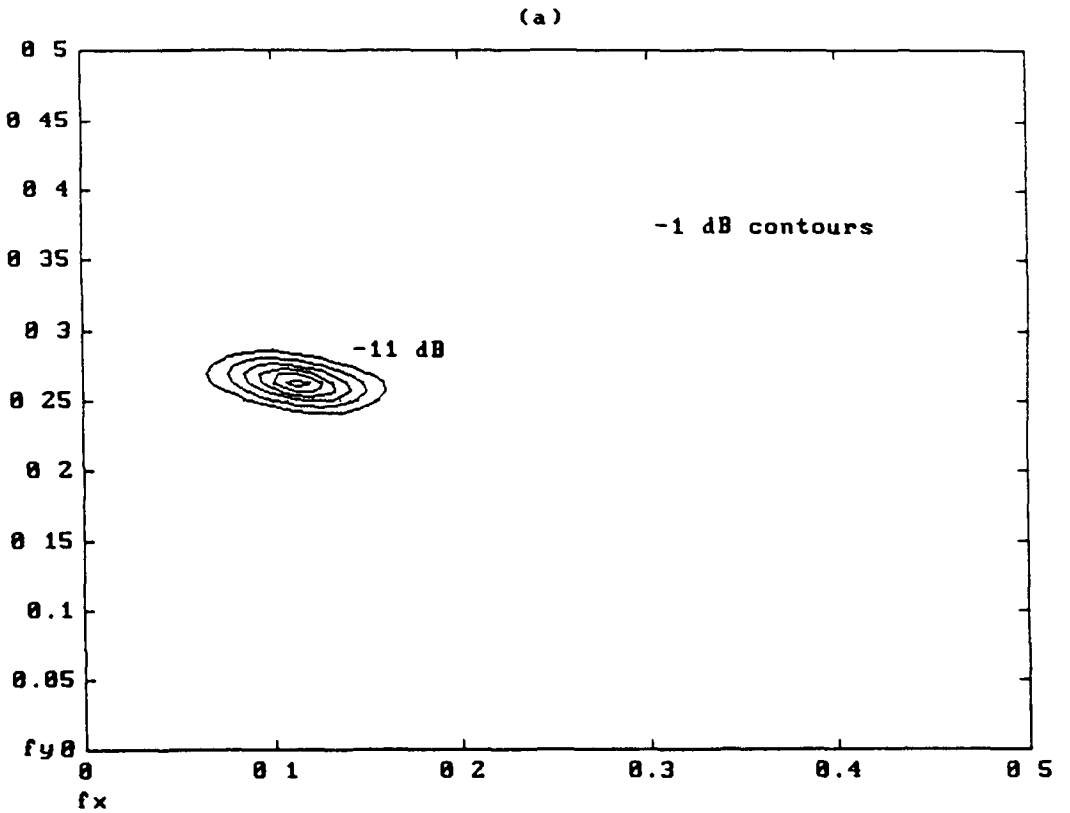
(a)
0 5
0 45
0 4
0 35
0 3
0 25
0 2
0 15
0.1
0.05
fy 0
0
0 1
0 2
0.3
0.4
0 5
fx
-1 dB contours
-11 dB

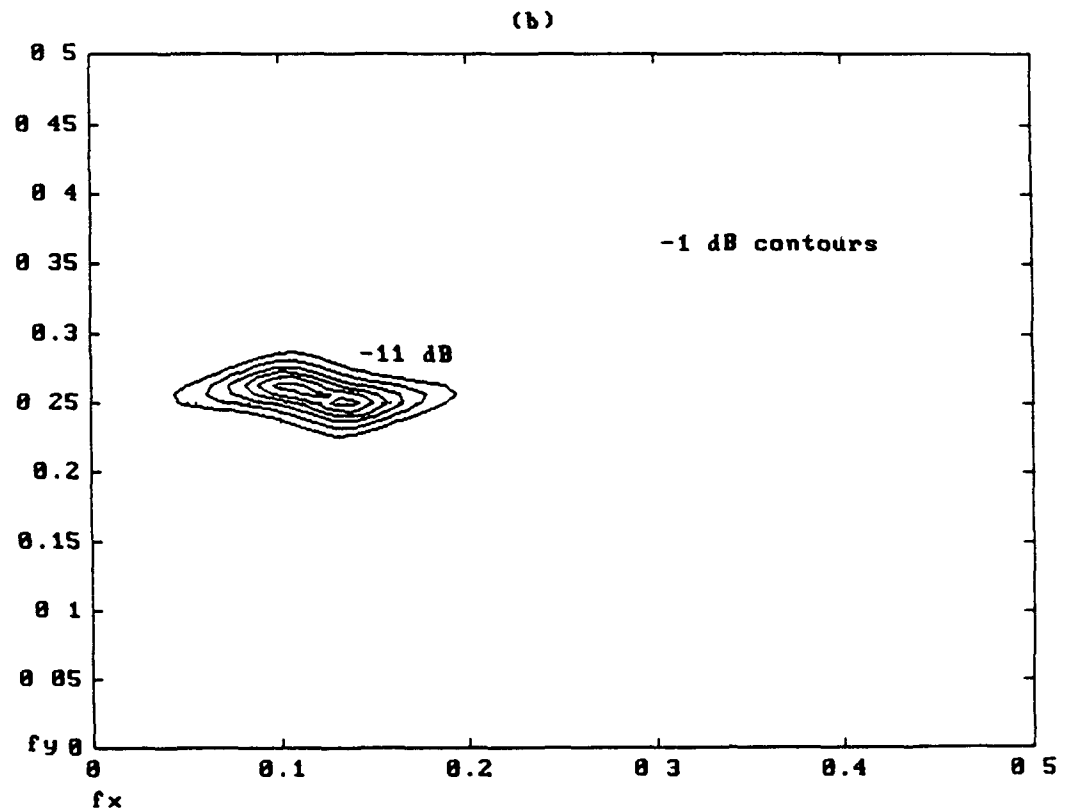
(b)
0 5
0 45
0 4
0 35
0.3
0 25
0.2
0.15
0 1
0 05
fy 0
0
0.1
0.2
0 3
0.4
0 5
fx
-1 dB contours
-11 dB

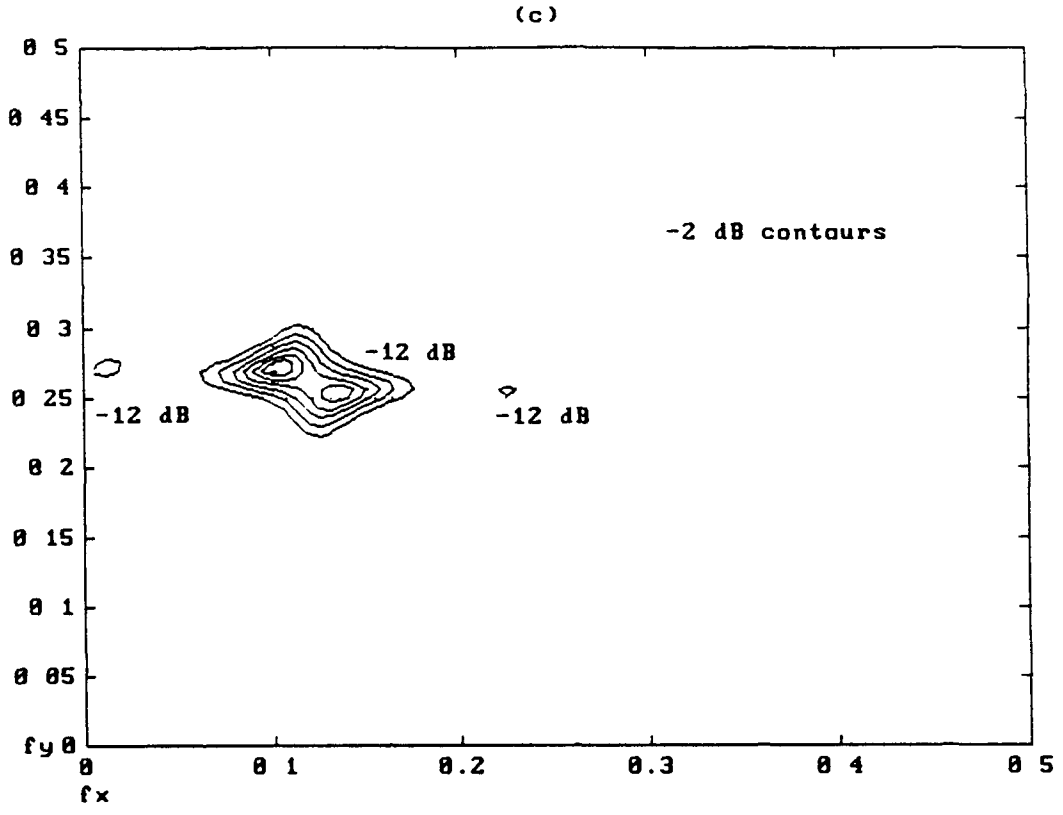

Figure 3 26 MFE spectral estimates of very closely spaced sinusoids at normalised frequencies (0 1, 0 275) and (0 125, 0 25) in white noise at SNR of -3 dB and data set size 20 x 20

Contour plot in dB on x and y frequency axes for (a) 7 x 7 model order estimate, (b) 9 x 9 model order estimate, and (c) 12 x 12 model order estimate

3.11 Dynamic range difference

In MFE as in other 2-D and 1-D AR parametric spectral estimation schemes the peak of the power spectral density is proportional to the square of the power of each sinusoid This is unlike Fourier transform techniques where the peak is proportional to the sinusoid power It can result in lower level sinusoids being masked by the higher level ones [38] We take an example of two sinusoids at normalised frequencies (0 3333, 0 2) and (0 1, 0 22) in white noise, the parameters for which are given in Table 3 5 The amplitude ratio of the sinusoids is $\sqrt{2}$ 1, giving a sinusoid power ratio of 2 1 or 1 0 5 In Section 3 3 on autocorrelation type we derived 6 x 6 models at temperature 0 5 for this example using exact, biased and unbiased autocorrelation functions The spectral estimate in the exact autocorrelation case gives the square of the power ratio as 1 0 25 preserving the power ratio as 1 0 5 or 2 1 and the amplitude ratio as 1 4142 1 In the unbiased autocorrelation case the spectral estimate gives the square of the power ratio as 1 0 185 resulting in the power ratio 1 0 43 and amplitude ratio 1 523 1 In the biased autocorrelation case the spectral estimate gives the square of the power ratio as 1 0 14 resulting in the power ratio 1 0 374 and amplitude ratio 1 635 1 The errors in amplitude ratio are due to the process of autocorrelation estimation

3.12 Models with non-symmetric region of support

We took a 40 x 40 point data snapshot consisting of sinusoids at arbitrary unity normalised frequencies (0 1, 0 2) and (0 3, 0 4) The sinusoids are of equal amplitude at SNR of 0 dB in uncorrelated white Gaussian noise The parameters are given in Table 3 4 above Figure 3 27 (a) shows the contour plot for the MFE spectral estimate at temperature 0 001 of the two sinusoids in noise A 5 x 5 order model was used The contours of constant PSD level are slightly elliptical in shape The ratio of x to y frequency bandwidth of the spectral peaks at the -18 dB contour is given in Table 3 12 The eccentricity of the spectral peaks at the -18 dB contour is also given The -18 dB contour is chosen arbitrarily as the figures are reasonably constant over a wide

dynamic range up to at least -6 dB These figures indicate a resolution bias in the y frequency direction This is portrayed by a slight bias in the variance statistics in a statistical test which is discussed later in Section 4 4 3 As discussed in Section 3 4, AR spectral estimators may exhibit directional dependent resolution capabilities depending on the location of sinusoids in the data set under test Hence whether directional dependency occurs or not depends on the particular data set The accuracy of AR model based spectral estimates also depends on the size and shape of the model used [50] We show that this slight bias may be overcome by using a model with non-symmetric region of support Figure 3 27 (b) shows the contour plot for the MFE spectral estimates at temperature 0 001 using a 7 x 5 order model The same unbiased autocorrelation data was used as in the 5 x 5 case The directional bias is less pronounced This is reflected in the x to y frequency bandwidth ratio and eccentricity figures in Table 3 12 Hence the spectral peaks are less elliptical than those at model order 5 x 5 Figure 3 27 (c) shows the MFE spectral estimates at temperature 0 001 using a 9 x 5 order model The same unbiased autocorrelation data was used as in the 5 x 5 and 7 x 5 cases above The directional bias is reduced even further This is reflected in the f_x to f_y maximum width ratio and eccentricity figures in Table 3 12

Table 3 12 Ratio of f_x to f_y bandwidth and eccentricity of spectral peaks at (0 1, 0 2) and (0 3, 0 4) at 0 dB SNR Figures are for the -18 dB contour for spectral estimates derived using MFE models of order 5 x 5, 7 x 5 and 9 x 5

	Spectral Peaks			
	(0 1, 0 2)		(0 3, 0 4)	
Model order	f_x/f_y Width Ratio	Eccentricity	f_x/f_y Width Ratio	Eccentricity
5 x 5	1 72	0 814	1 42	0 711
7 x 5	1 41	0 704	1 20	0 553
9 x 5	1 12	0 458	1 05	0 300

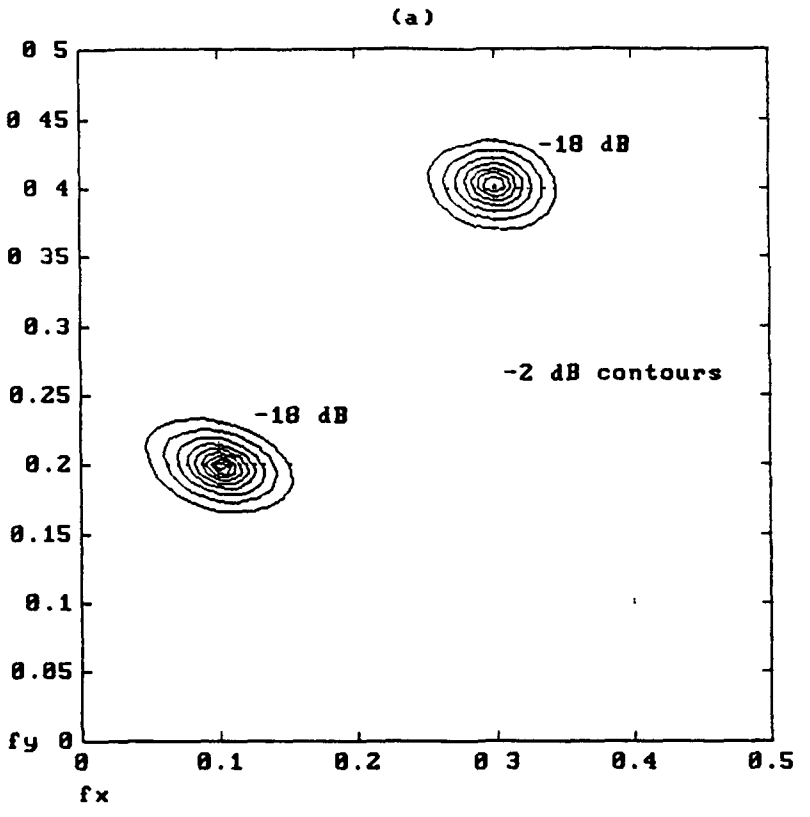
(a)
0 5
0 45
0 4
0 35
0.3
0.25
0.2
0.15
0.1
0.05
fy 0
0
0.1
0.2
0 3
0.4
0.5
fx
-18 dB
-2 dB contours
-18 dB

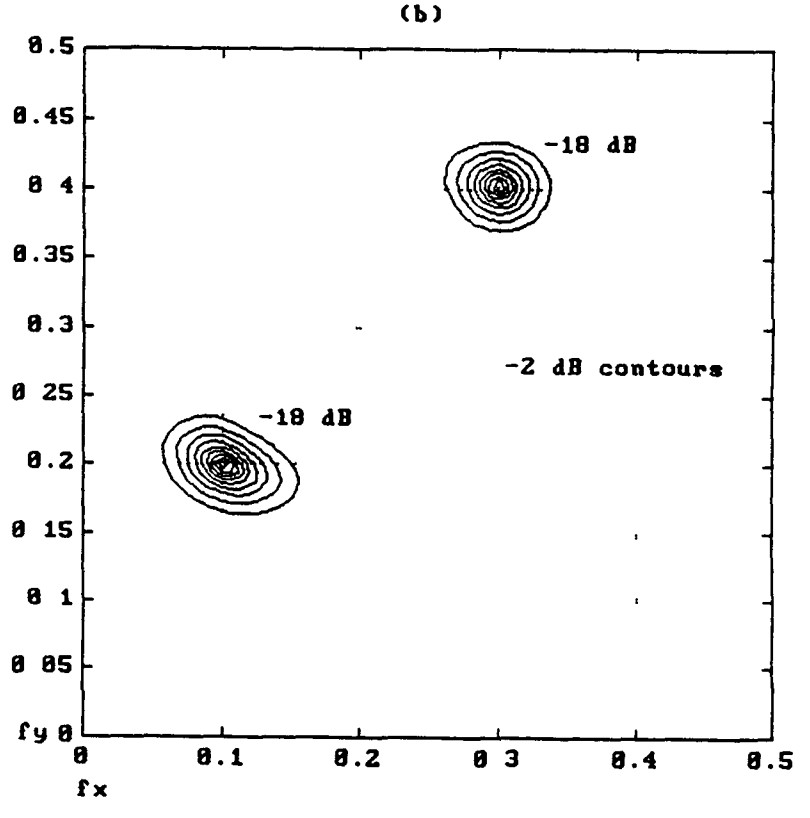
(b)
0.5
0.45
0 4
0.35
0.3
0 25
0.2
0 15
0 1
0 05
fy 0
0
0.1
0.2
0 3
0.4
0.5
fx
-18 dB
-2 dB contours
-18 dB

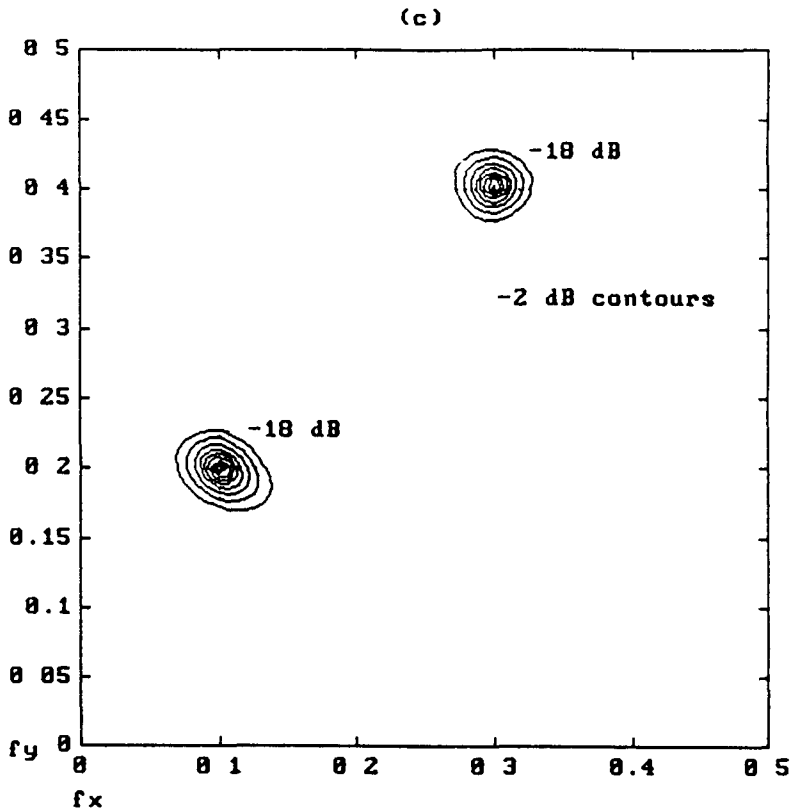

Figure 3 27 MFE spectral estimates of sinusoids at normalised frequencies (0 1, 0 2) and (0 3, 0 4) in white noise at SNR of 0 dB

Contour plot in dB for (a) 5 x 5 model order estimate, (b) 7 x 5 model order estimate, and (c) 9 x 5 model order estimate

In the second test on non-symmetric regions of support we took the same set of sinusoids as above at an SNR of 6 dB In Section 3 4 we have seen that the effect on the resolution caused by relative position dependency of sinusoids to each other may be due to interference that occurs between these sinusoids We have seen in the last simulation that the location of the sinusoids at (0 1, 0 2) and (0 3, 0 4) gives rise to a small bias in the resolution Increasing the SNR increases the sinusoidal power and emphasises this effect This results in a resolution bias in the y frequency direction for both MFE and MCV spectral estimates It may also result in peak splitting as discussed in Section 3 4 An example of peak splitting for a snapshot data set is shown in the x axis log plot in Figure 3 28

Figure 3 29 (a) shows the contour plot for the MFE spectral estimates at temperature 0 05 of the two sinusoids in noise A 5 x 5 order model was used We note that the estimates are elliptical in shape The ratio of x frequency to y frequency bandwidth and eccentricity of the spectral peaks at the -18 dB contour is given in Table 3 13 The figures for the 5 x 5 model case indicate a resolution bias in the y frequency direction Figure 3 29 (b) shows the contour plot for the MFE spectral estimates at temperature 0 05 using a 15 x 5 order model The same unbiased autocorrelation data as in the 5 x 5 case was used The directional bias is eliminated This is reflected in the x to y frequency bandwidth ratio and eccentricity figures in Table 3 13

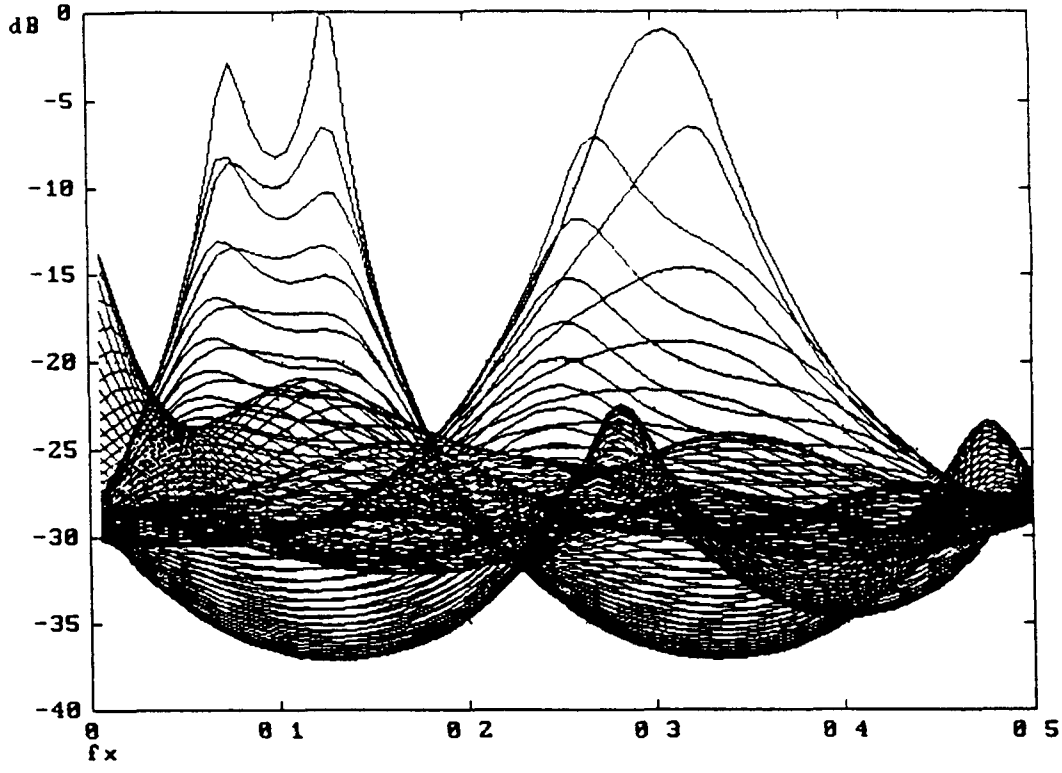

Figure 3 28 Log plot of the MFE spectral estimate on the x frequency axis of sinusoids at normalised frequencies (0 1, 0 2) and (0 3, 0 4) in white noise at SNR of 6 dB

Table 3 13 Ratio of f_x to f_y bandwidth and eccentricity of spectral peaks at (0 1, 0 2) and (0 3, 0 4) at 6 dB SNR Figures are for the -18 dB contour for spectral estimates derived using MFE models of order 5 x 5 and 15 x 5

	Spectral Peaks			
	(0 1, 0 2)		(0 3, 0 4)	
Model order	f_x/f_y Width Ratio	Eccentricity	f_x/f_y Width Ratio	Eccentricity
5 x 5	2 75	0 932	2 64	0 926
15 x 5	1 11	0 434	0 94	0 341

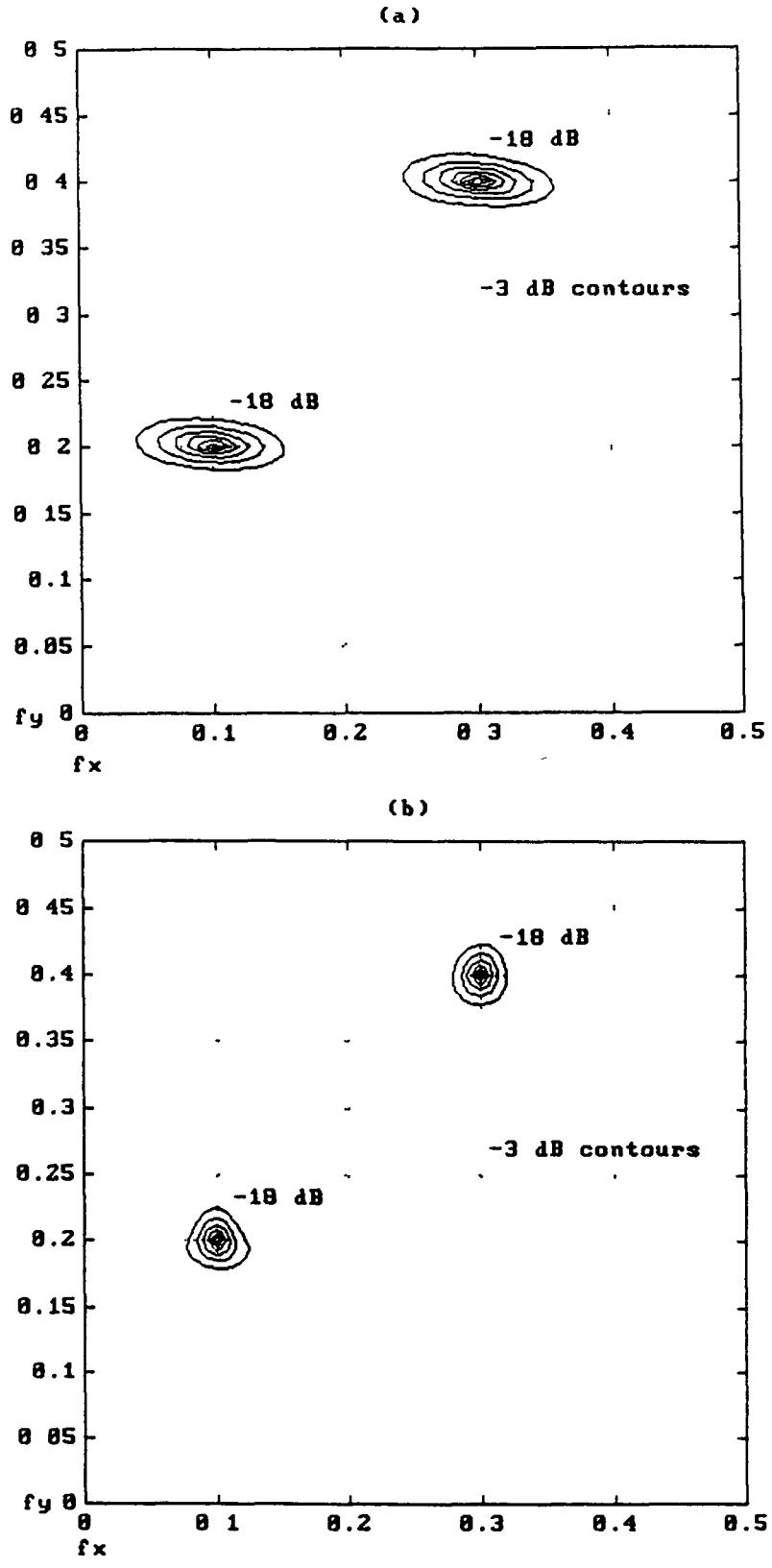

Figure 3 29 MFE spectral estimates of sinusoids at normalised frequencies (0 1, 0 2) and (0 3, 0 4) in white noise at SNR of 6 dB

Contour plot in dB for (a) 5 x 5 model order estimate, and (b) 15 x 5 model order estimate

Chapter 4. Comparisons with Other Methods

4.1 Introduction

In this Chapter we compare the performance of MFE spectral estimation with that of other methods These methods include MCV [38], the multidimensional Levinson method [52], the hybrid approach of Kimura and Honoki [47], the maximum entropy method of Lim and Malik [51], and a conventional transform technique [53] In addition we briefly revise the relevant results presented in Chapter 3 where comparisons with some of the techniques above have already been made

The first comparison is with zero temperature MFE or the multidimensional Levinson method We then compare the MFE spectral estimates with that produced by conventional transform based methods for examples with very low data set size Comparisons are made of the

computational expense, model stability and accuracy of spectral estimates with that of multidimensional Levinson, maximum likelihood estimation (MLE) [33], and MCV methods Finally, using the same examples as employed by Kimura and Honoki [47], and Lim and Malik [51] we compare their results with MFE spectral estimates

As in Chapter 3 all spectral estimates are calculated over 160 x 160 points unless otherwise stated Spectral estimates are plotted as normalised amplitude PSD plots or as log plots on the x frequency axis $psd(f_x,0)\ 0 \le f_x \le 0.5$ and on the y frequency axis $psd(0,f_y)\ 0 \le f_y \le 0.5$ Contour plots are also used as in Chapter 3

4.2 Multidimensional Levinson comparison

An advantage of MFE over the zero temperature Levinson approach is that it provides stable models by appropriate selection of temperature range in cases where the multidimensional Levinson algorithm does not

Sections 3 2, 3 3 and 3 6 give examples of cases where the MFE method outperforms the multidimensional Levinson algorithm The MFE method extends the range of the Levinson algorithm by virtue of the entropy term In Section 3 10 MFE provides accurate spectral estimates and outperforms the Levinson algorithm for very closely spaced sinusoids

4.3 Conventional transform comparison

The comparison of results from the MFE method with those from a Fourier transform method is particularly of interest at low data set size This illustrates the high resolution performance of the MFE method over classical transform methods We take a 5 x 5 point data set generated from 3 sinusoids in white noise at SNR of -3 dB with parameters as in Table 3 7 above An exact autocorrelation is used

We generate a conventional estimate by performing a fast Fourier transform of the exact autocorrelation of the 5 x 5 data set The resulting spectral estimate is shown in Figures 4 1 (a)

on the x frequency axis and 4 2 (a) on the y frequency axis We also generate a spectral estimate using a 5 x 5 order MFE model at temperature 0 05 The spectral estimates generated by this model for data set size 80 x 80, 10 x 10 and 5 x 5 are found to be identical The 5 x 5 case is shown in Figures 4 1 (b) and 4 2 (b) on the x frequency and y frequency axis respectively Evidently MFE provides higher resolution estimates than the conventional method It is also advantageous that the usual sidelobe structure [38] associated with conventional methods does not appear in the MFE estimate Reduction of the sidelobes in the conventional estimate may be effected by windowing the data However this results in reduction in the resolution of the estimate

The search for high resolution spectral estimators which may be used for low data set size and low SNR continues to be a motivating force behind research into multidimensional spectral estimation This has been highlighted in Chapter 1 We now compare conventional Fourier transform and MFE spectral estimates of a 9 x 9 point data set consisting of three sinusoids in -6 dB noise The data set details are given in Table 3 6 above Figure 4 3 (a) and (b) shows the MFE spectral estimate at temperature 0 5 and the conventional estimate Both are based on the exact autocorrelation The MFE estimate exhibits very close 1 dB contours running from -12 dB upwards to a peak The contours of the conventional estimate are much more widely spaced For approximately the same frequency plane area they run from -5 dB to a flat plateau Evidently the MFE estimate possesses far sharper peaks that are better resolved than those of the conventional estimate We also see from this test that MFE is capable of performing accurate spectral estimation at low SNR and low data set size

The third example in this section is for two very closely spaced sinusoids at low SNR with low data set size We take a 7 x 7 point data set for two sinusoids at frequencies (0 1, 0 3) and (0 15, 0 25) as detailed in Table 3 9 The SNR is -3 dB We performed MFE spectral estimation at temperature 0 5 using the exact autocorrelation We also performed spectral

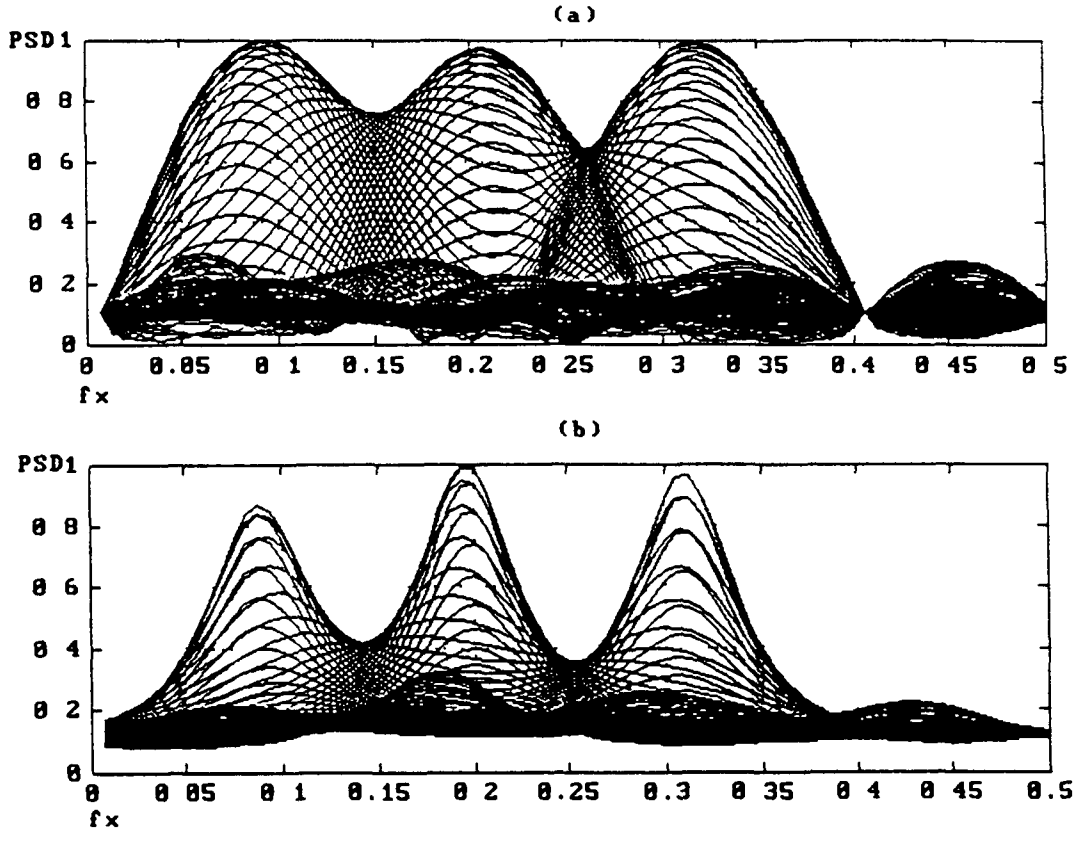

Figure 4 1 Conventional Fourier transform and MFE spectral estimates of sinusoids at normalised frequencies (0 1, 0 1), (0 3, 0 1) and (0 2, 0 2) in white noise at SNR of -3 dB and data set size 5 x 5

Log plots of spectral estimates on the x frequency axis derived using (a) conventional Fourier method, and (b) MFE at temperature 0 05

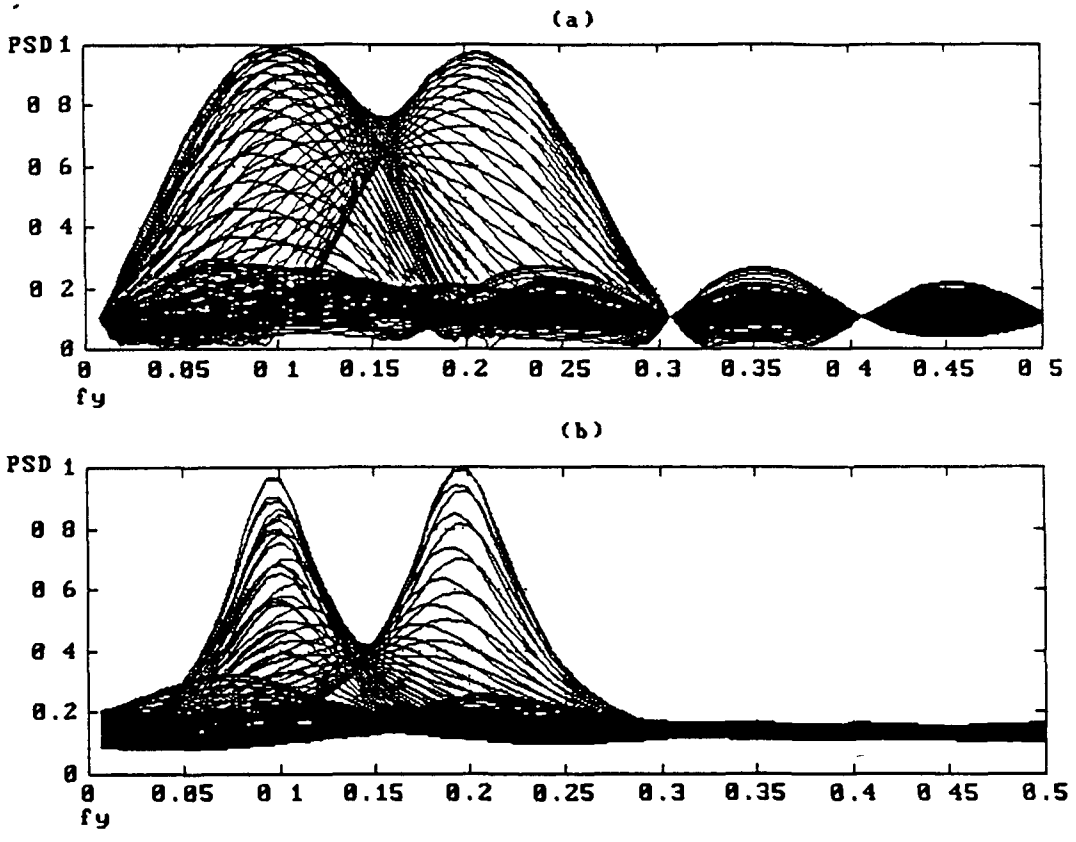

Figure 4 2 Conventional Fourier transform and MFE spectral estimates of sinusoids at normalised frequencies (0 1, 0 1), (0 3, 0 1) and (0 2, 0 2) in white noise at SNR of -3 dB and data set size 5 x 5

Log plots of spectral estimates on the y frequency axis derived using (a) conventional Fourier method, and (b) MFE at temperature 0 05

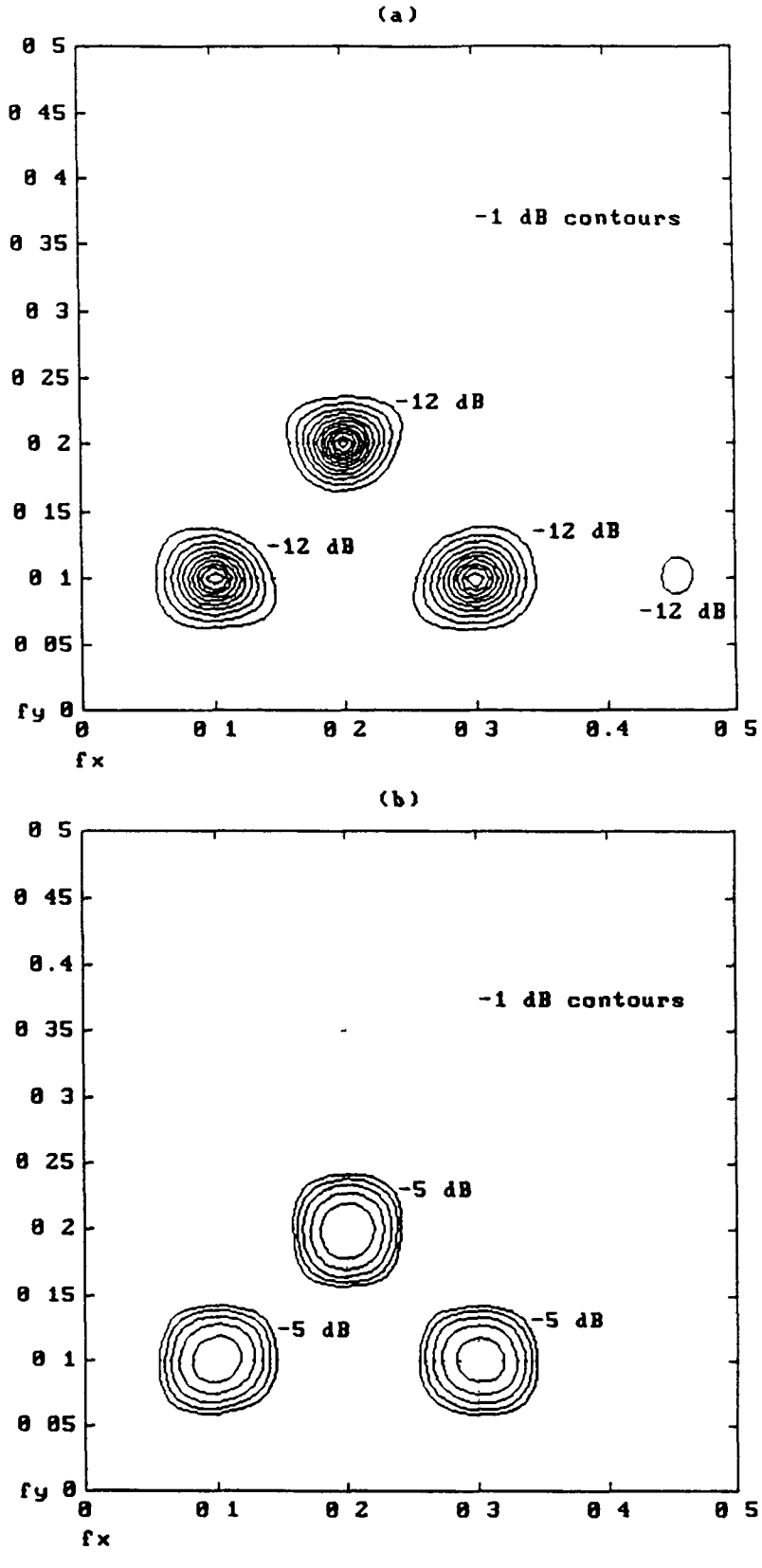

Figure 4 3 MFE and conventional Fourier transform spectral estimates of sinusoids at normalised frequencies (0 1, 0 1), (0 3, 0 1) and (0 2, 0 2) in white noise at SNR of -6 dB and data set size 9 x 9

Contour plot in dB using (a) MFE at temperature 0 5, and (b) conventional Fourier method

estimation by applymg a fast Fourier transform on the same autocorrelation data In Figure 4 4 (a) and (b) we see that the MFE spectral estimate displays two distinct peaks on the x and y frequency axes The peaks are located at (0 0942, 0 3) and (0 1558, 0 25) The peak corresponding to (0 0942, 0 3) is approximately 0 5 dB down on the second peak The conventional transform spectral estimate in Figure 4 5 (a) and (b) displays a single broadly resolved flat spectral peak across the region of interest on the x and y frequency axes The contour plot of Figure 4 6 (a) again shows two distinct MFE spectral peaks The poorly resolved conventional estimate in Figure 4 6 (b) has a plateau at 1 dB that lies over a wide spectral area MFE outperforms the conventional estimate for closely spaced sinusoids at low SNR with low data set size

4.4 Modified covariance comparison

We first compare the computational expense and model stability of MLE [33], MCV [38] and our MFE method, where the MLE method is based on the Fourier transform of the observed data set We then compare the bias and standard deviation of spectral estimates obtained by MCV and MFE techniques over a number of independent simulation trials We have seen in Section 3 10 that MFE performs as well as MCV in terms of spectral resolution for data snapshot examples

4.4.1 MCV comparison - Computational expense

The data set size is taken as M x N and model order as p_1 x p_2, where $M >> p_1$ and $N >> p_2$ The cost functions in MFE, MCV and MLE are minimised at $O((p_1\text{-}1)(2p_2^4))$, $O(2(M\text{-}p_1)(N\text{-}p_2)p_1p_2)$, and $O(MNp_1p_2)$ multiplies per iteration In MLE one of the elements is a trigonometric function It is evident therefore that MFE is computationally less expensive We have found that MFE performs spectral estimation 8 times faster than MLE and 12 times faster than MCV for any data snapshot in the comparative variance test discussed below

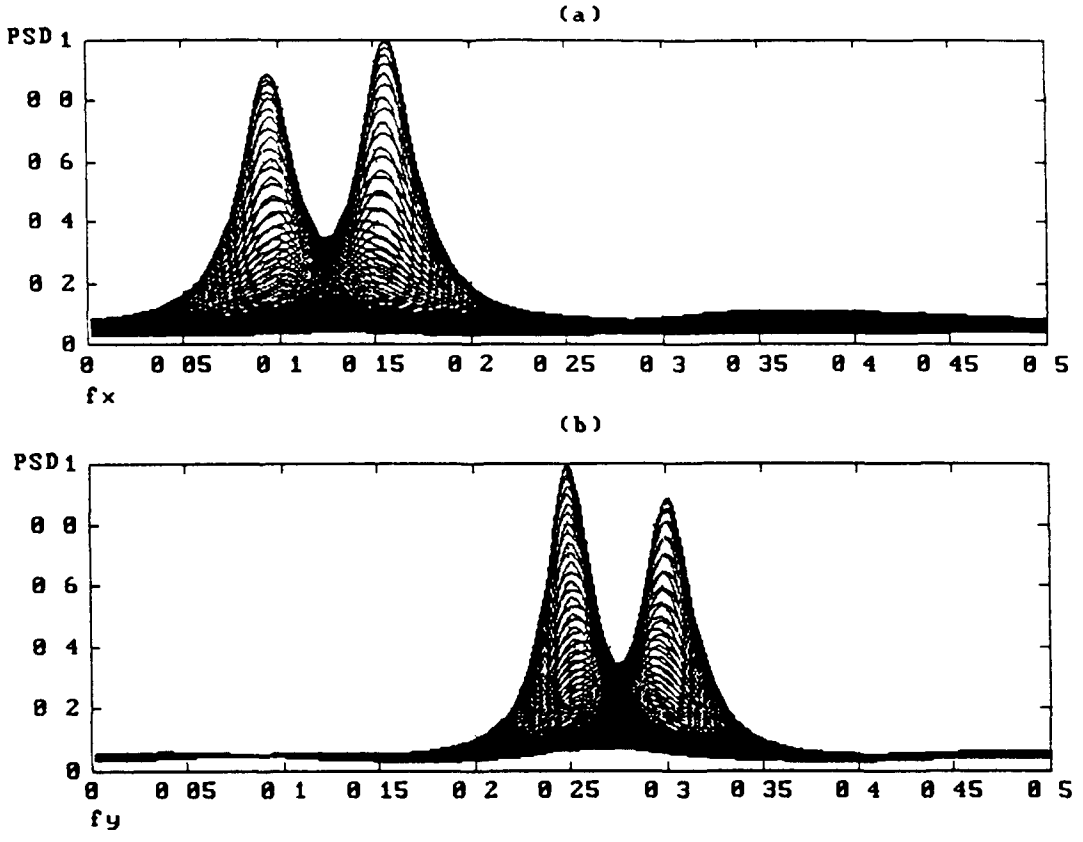

Figure 4 4 MFE spectral estimate of closely spaced sinusoids at normalised frequencies (0 1, 0 3) and (0 15, 0 25) in white noise at SNR of -3 dB and data set size 7 x 7

Normalised amplitude spectral estimate on (a) the x frequency axis, and (b) the y frequency axis

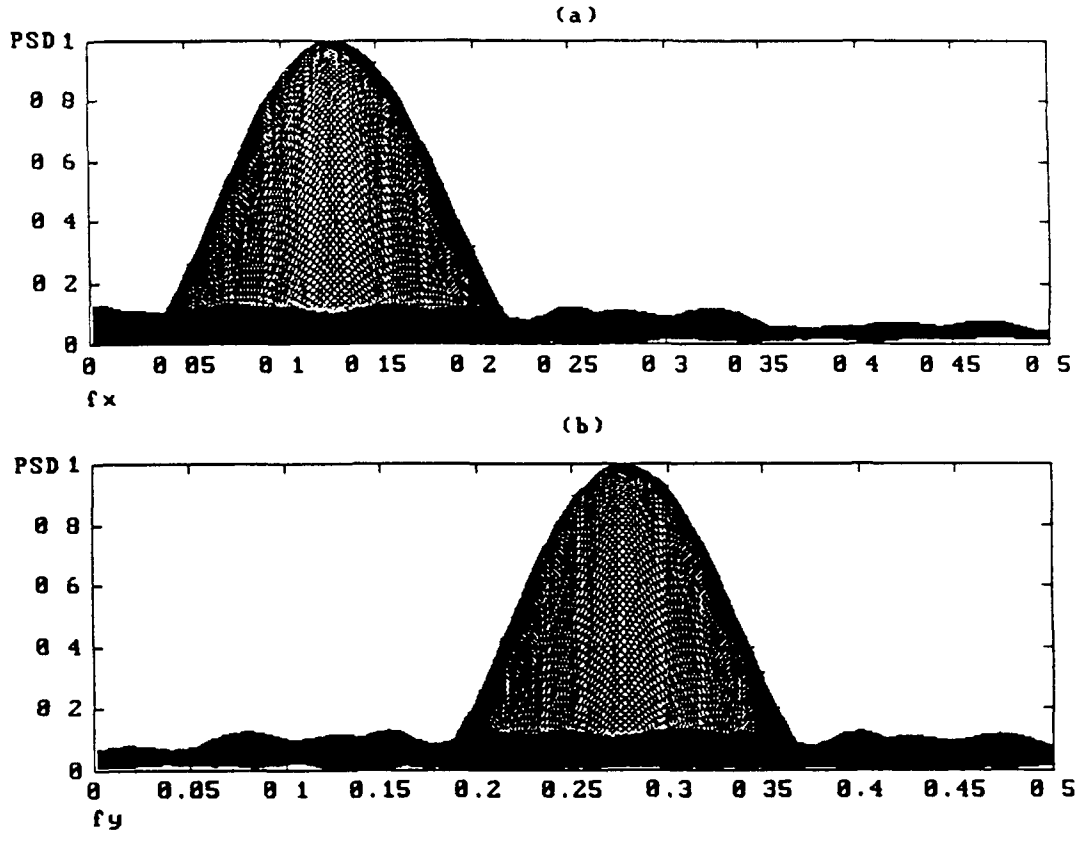

Figure 4 5 Conventional transform spectral estimate of closely spaced sinusoids at normalised frequencies (0 1, 0 3) and (0 15, 0 25) in white noise at SNR of -3 dB

Normalised amplitude spectral estimate on (a) the x frequency axis, and (b) the y frequency axis

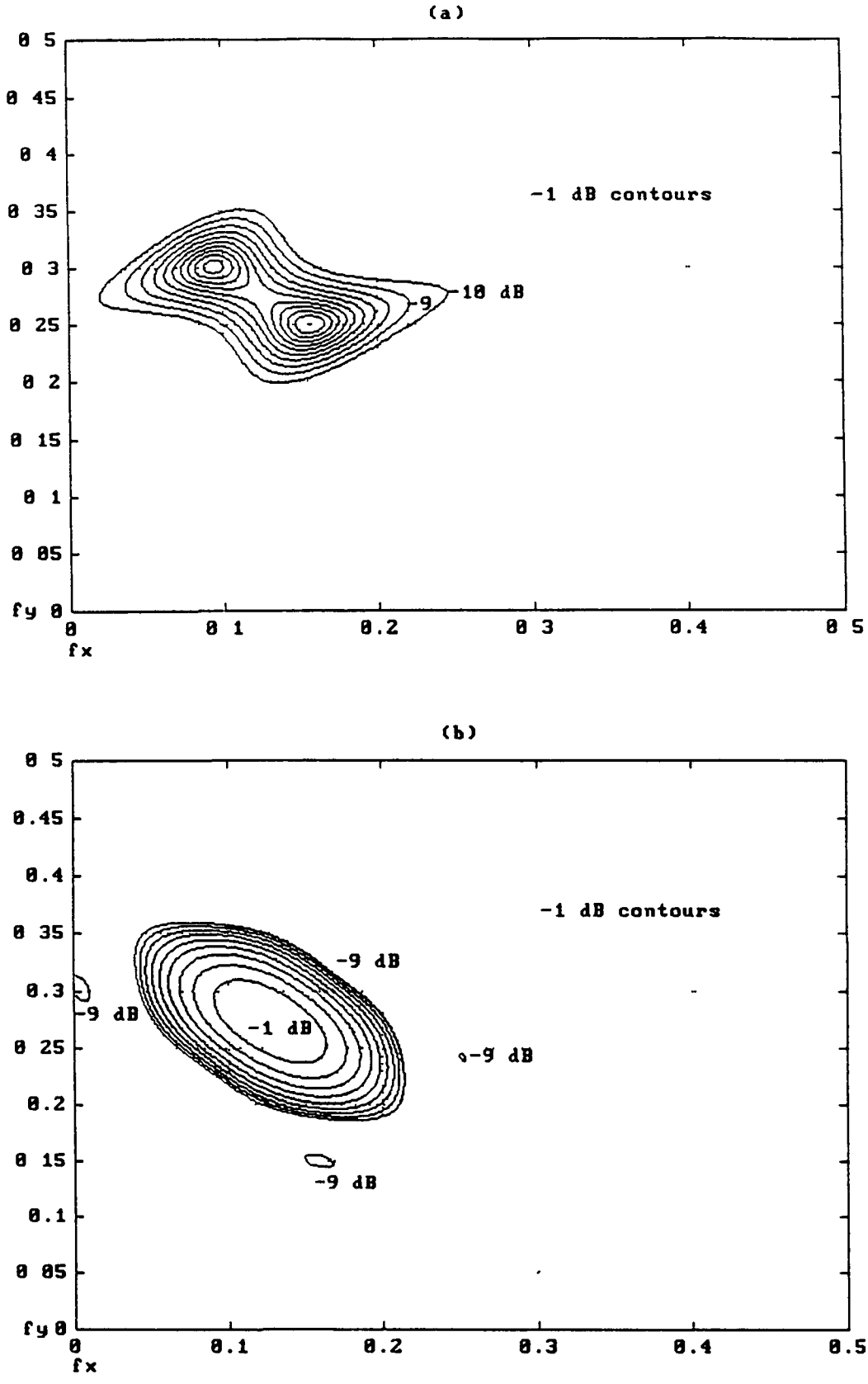

Figure 4 6 MFE and Conventional transform spectral estimates of very closely spaced sinusoids at normalised frequencies (0 1, 0 3) and (0 15, 0 25) in white noise at SNR of -3 dB and data set size 7 x 7

Contour plot using (a) MFE at temperature 0 5, and (b) the conventional transform method

4.4.2 MCV comparison - Stability

In addition to computational expense an important issue for comparison is that of model stability A recursively computable and stable system is important if field synthesis or correlation extension is envisaged A stable system is marked by unity bounded AR model parameters and positive white noise variance MLE provides stable models whereas MCV does not necessarily provide stable models MFE provides stable models by appropriate selection of temperature range This is because the magnitude of reflection coefficients in the reflection matrices within the algorithm are a function of the temperature

4.4.3 MCV comparison - Statistical accuracy of spectral estimates.

We statistically compare spectral estimates produced by the MFE and MCV methods We implemented both algorithms and made 24 simulation trials on each We note that the bias and variance of the spectral estimates vary only to a very small extent with the number of trials This is also seen to be the case in 1-D MFE [75], where 10 independent trials were used All trials used a single snapshot of data consisting of sinusoids at arbitrary unity normalised frequencies (0 1, 0 2) and (0 3, 0 4) The sinusoids were of equal amplitude at arbitrary SNR of 0 dB in uncorrelated white Gaussian noise The data set is detailed in Table 3 4 To ensure a fair comparison, the same random number generator seed was used to initiate the 24 trials for both algorithms so that each simulation series contained an identical sequence of noise spectra This meant that the same set of 24 uncorrelated and independent noise fields were used for both algorithms The size of the sinusoid and white noise data fields were 40 x 40 pomts The model size used was 5 x 5, indicating a 5 x 5 region of correlation support The unbiased autocorrelation estimate was used for MFE The MFE signal processing temperature was set at 0 001 This temperature was arbitrarily chosen from within a wide band of temperature which previous tests have indicated provides accurate spectral estimation Table 4 1 shows the bias and standard deviation of spectral estimates for both frequencies for each method The PSDs were calculated over 520 x 520 points and therefore the resolution of each estimate is to 0 001 92 of

unity normalised frequency The bias figures for MFE and MCV spectral estimates are comparable The variance figures for MFE spectral estimates are on average 1 65 times those achievable by MCV The statistics show that MFE provides accurate spectral estimation

Table 4 1 Bias and standard deviation of MFE and MCV spectral estimates for sinusoids at normalised frequencies (0 1,0 2) and (0 3,0 4) in white noise

	MFE		MCV	
f_x	Bias x 10^{-3}	Var x 10^{-6}	Bias x 10^{-3}	Var x 10^{-6}
0 1	-0 079	4 15	-0 079	1 69
0 3	-0 563	2 31	-0 400	1 84
f_y	Bias x 10^{-3}	Var x 10^{-6}	Bias x 10^{-3}	Var x 10^{-6}
0 2	-0 158	2 44	0 242	1 95
0 4	0 400	1 84	0 321	1 13

The variance figures for the MFE case are slightly better in the y frequency direction than in the x frequency direction for each sinusoid This indicates a slight resolution directional bias for the particular example given As discussed in Sections 3 4 and 3 12, AR spectral estimators may exhibit directional dependent resolution capabilities, depending on the location of sinusoids in the data set under test The accuracy of AR model based spectral estimates also depends on the size and shape of the model used This slight directional bias may be eliminated by using a MFE model with non-symmetric region of support as seen in Section 3 12

Spectral estimates were determined over 160 x 160 points using the MFE models from the variance test above Figure 4 7 (a) and (b) shows the overlaid PSD log plots of the spectral estimates on the x and y frequency axes This indicates the statistical variability of the estimator

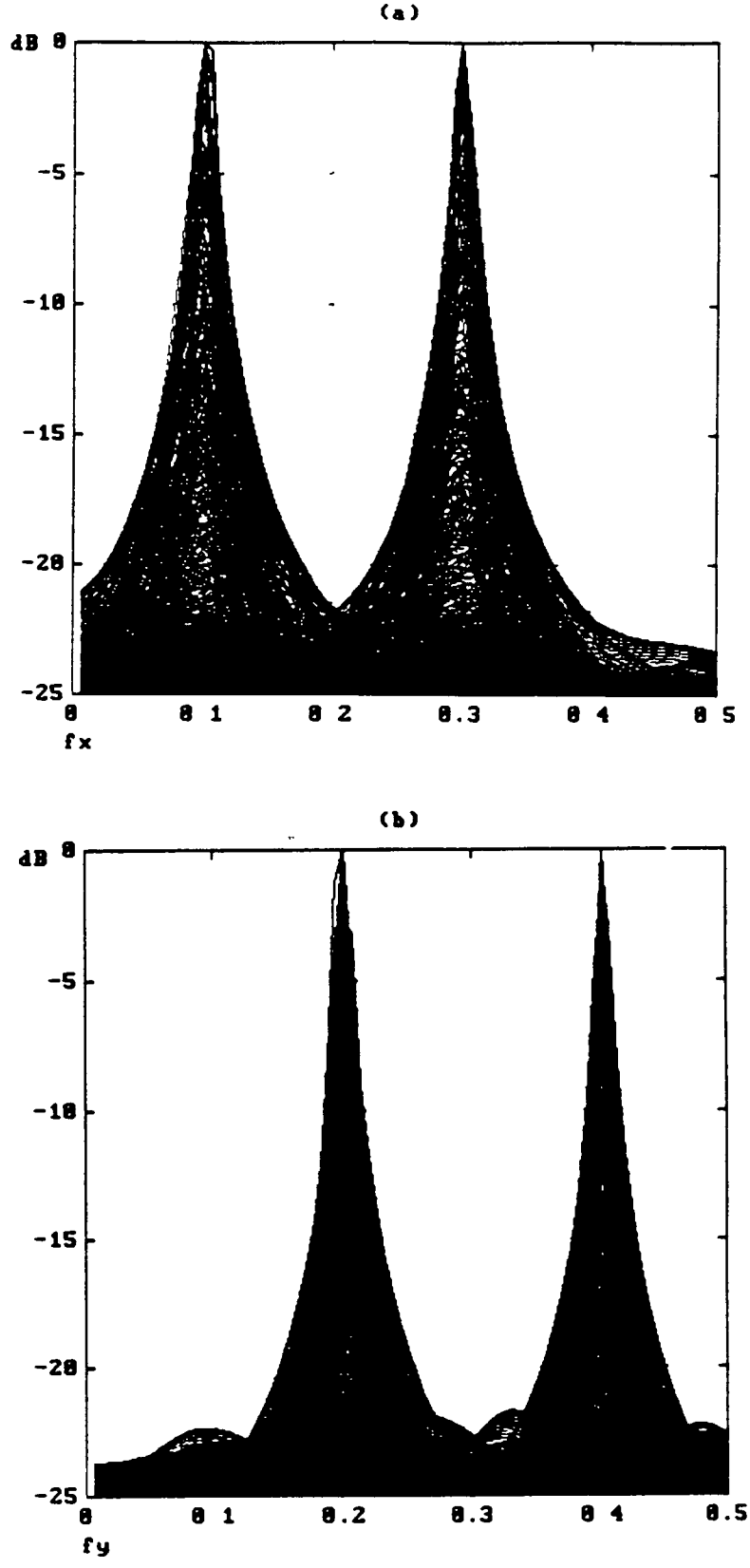

Figure 4 7 Overlaid MFE spectral estimates of sinusoids at normalised frequencies (0 1, 0 2) and (0 3, 0 4) in white noise at SNR of 0 dB

Log plots of MFE spectral estimates on (a) the x frequency axis, and (b) the y frequency axis

4.5 Hybrid method and maximum entropy method comparison

We compare our results with those from the hybrid dual 1-D method of Kimura and Honoki [47], and the maximum entropy method of Lim and Malik [51] We take two snapshot data set examples from their papers, the parameters of which are as given in Tables 3 5 and 3 6 above Both Kimura and Honoki and Lim and Malik use exact autocorrelation data

For the data set in Table 3 5, the contour plots of the spectral estimates in Figures 4 8 (a) and (b) are from [47] and that in Figure 4 8 (c) is from [51] The spectral estimate derived using a 6 x 6 order MFE model at temperature 0 5 based on the exact autocorrelation is shown in Figure 4 9 The MFE spectral estimate provides two distinct peaks from the -18 dB level upwards The peaks are accurately estimated This estimate is superior to that produced by the hybrid method at 5 x 5 covariance support which is shown in Figure 4 8 (a) The hybrid method at 7 x 7 covariance support is shown in Figure 4 8 (b) It possesses tighter contours than the MFE method However it is not possible to determine the dB level at which the peaks occur for the frequencies (0 333, 0 2) and (0 1, 0 22) This is because the highest contour provided for the (0 1, 0 22) peak is at -24 dB and for the (0 333, 0 2) is at -12 dB The spectral estimate due to the maximum entropy method is shown in Figure 4 8 (c) It displays tighter contours than the MFE estimate However the contours stop at -24 dB for the (0 1, 0 22) peak The location of this contour shows inaccurate spectral estimation for the (0 1, 0 22) frequency, whereas it is accurate for the MFE case

For the data set in Table 3 7, the contour plots of the spectral estimates in Figures 4 10 (a) and (b) are from [47] and that in Figure 4 10 (c) is from [51] The spectral estimate in Figure 4 11 is derived using an order 7 x 7 MFE model at temperature 0 001 based on an exact autocorrelation The MFE estimate is superior to that of the hybrid method at 7 x 7 covariance support which is shown in Figure 4 10 (a) The MFE estimate shows tighter contours and therefore sharper peaks than the hybrid method at 9 x 9 covariance support which is shown in Figure 4 10 (b) The exact

location of the hybrid method peaks is not given The maximum entropy method provides the estimate in Figure 4 11 (c) The peaks are distinct only above the -6 and -3 dB levels and are inaccurate The MFE estimate is superior in terms of sharpness and location of the peaks

(a)

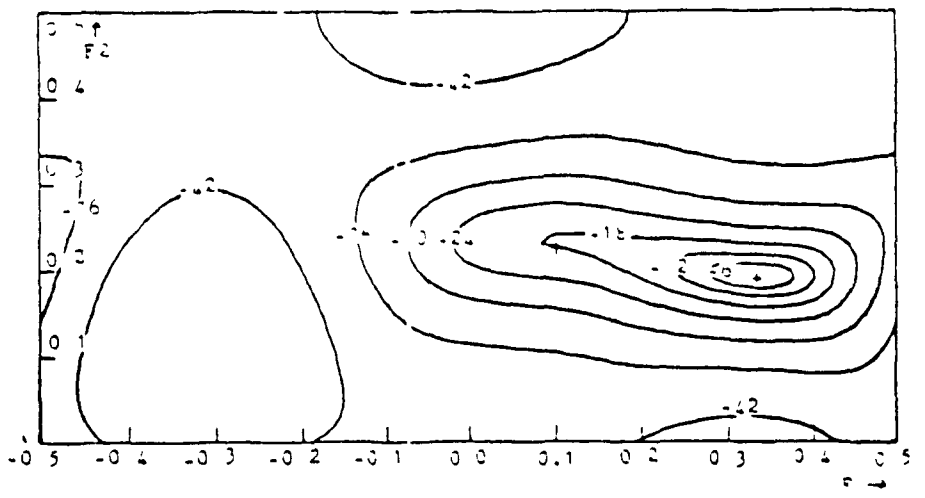

(b)

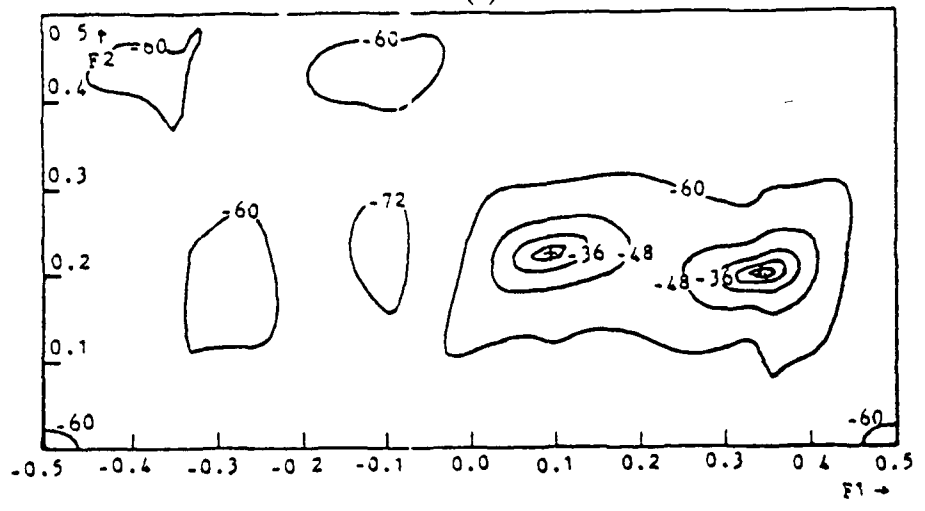

(c)

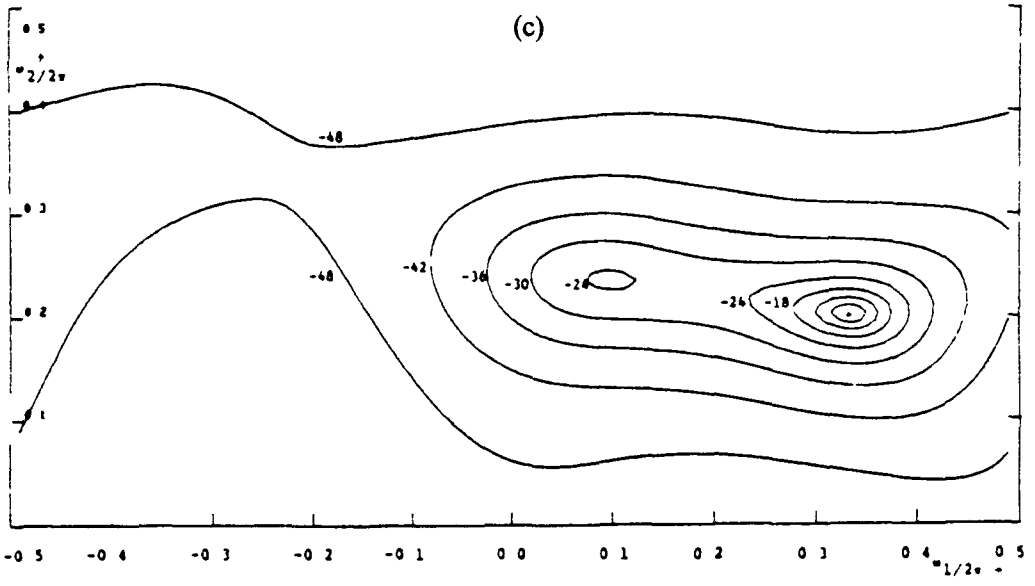

Figure 4 8 Spectral estimates of sinusoids at normalised frequencies (0 333, 0 2) and (0 1, 0 22) in white noise Contour plots (a), (b) from Kimura and Honoki [47], and (c) from Lim and Malik [51]

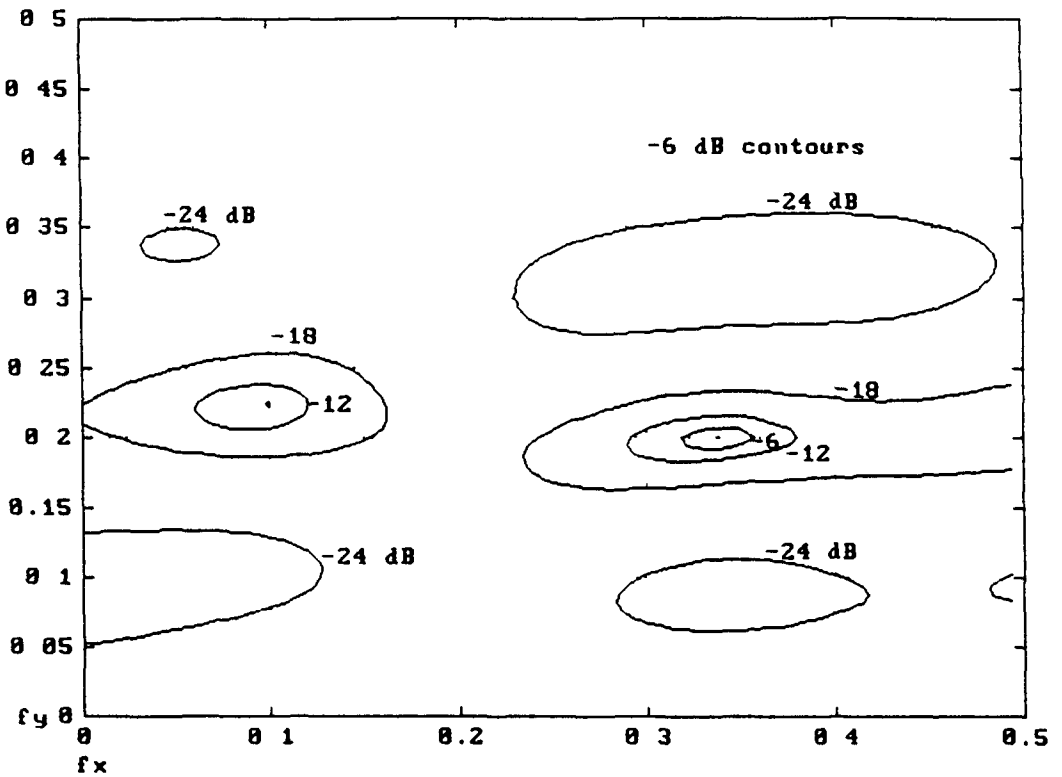

Figure 4 9 Contour plot in dB on x and y frequency axes of MFE spectral estimate of sinusoids at normalised frequencies (0 333, 0 2) and (0 1, 0 22) in white noise at SNR of 1 77 dB based on the exact autocorrelation

(a)

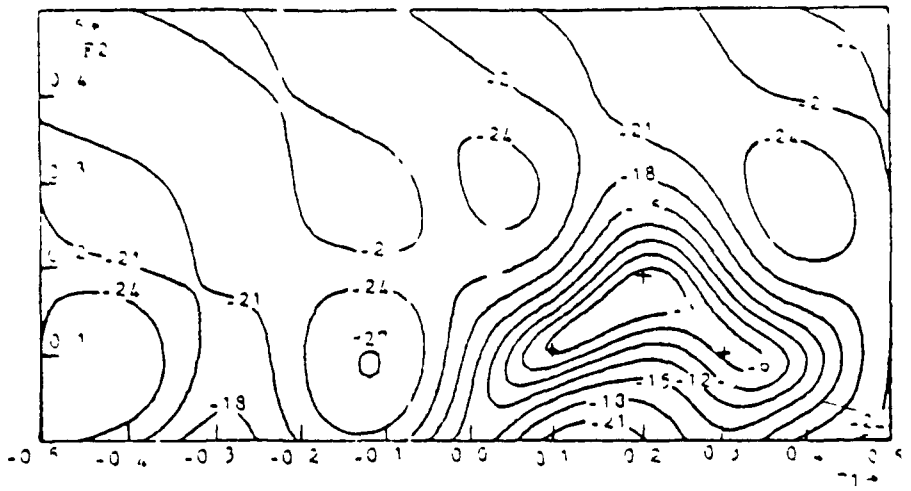

(b)

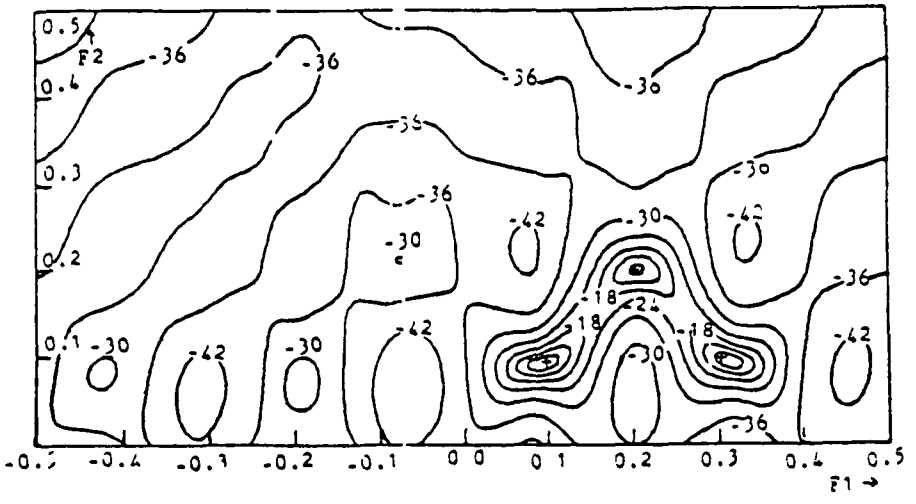

(c)

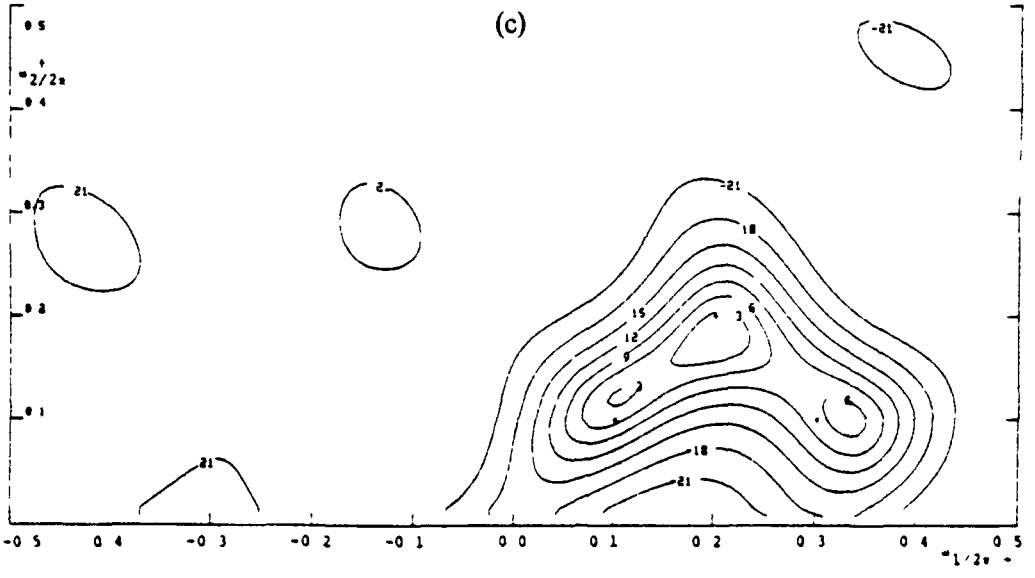

Figure 4 10 Spectral estimates of sinusoids at normalised frequencies (0 1, 0 1), (0 3, 0 1) and (0 2, 0 2) in white noise Contour plots (a), (b) from Kimura and Honoki [47], and (c) from Lim and Malik [51]

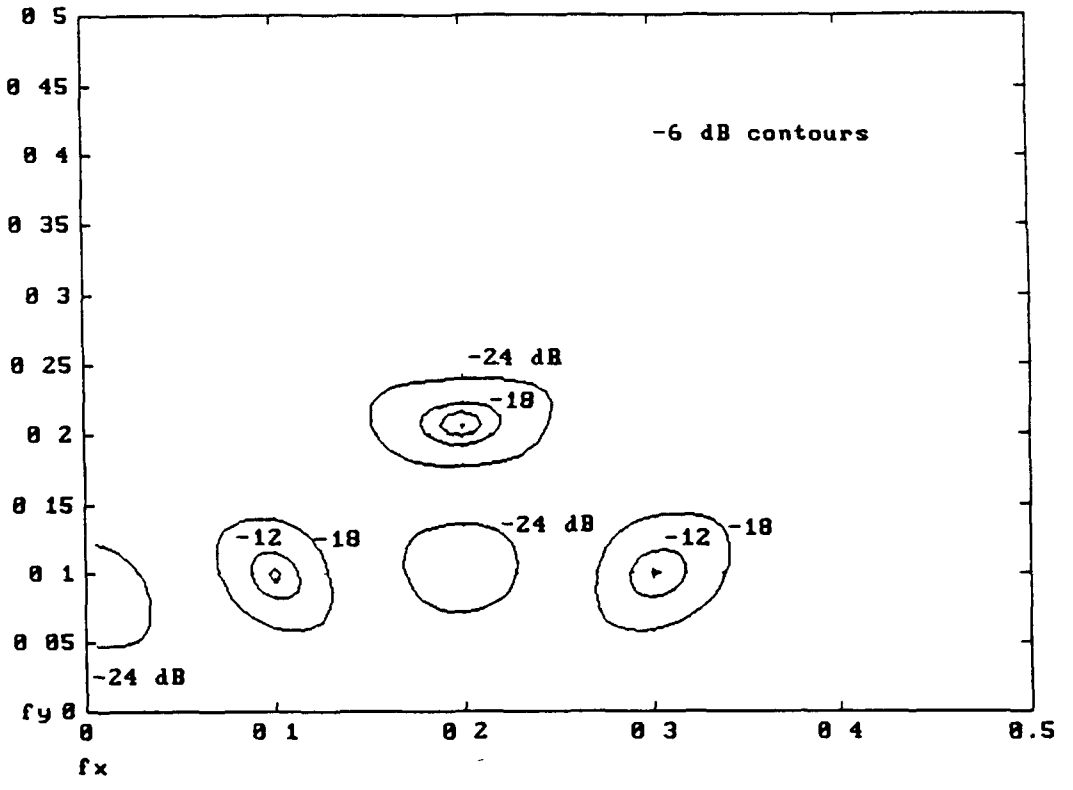

Figure 4 11 Contour plot in dB on x and y frequency axes of MFE spectral estimate of sinusoids at normalised frequencies (0 1, 0 1), (0 3, 0 1) and (0 2, 0 2) in white noise at SNR of -3 dB based on the exact autocorrelation

Chapter 5. Conclusions

5.1 Introduction

We draw conclusions regarding the performance of the 2-D MFE spectral estimation method based on the various tests and numerical simulations detailed in Chapter 3 We also furnish our findings on the merit of MFE compared to other methods based on the comparative experimental tests that are outlined in Chapter 4

5.2 Conclusions - The 2-D MFE method

We have proposed a 2-D extension of the MFE parameter estimation technique We have demonstrated the performance of the technique by executing a wide variety of tests involving MFE AR modelling and spectral estimation of various data sets consisting of sinusoids in white Gaussian noise These data sets include single and multiple sinusoids at various power levels, SNR and respective locations in the frequency plane

Experimental findings have been presented These findings are based on tests in spectral resolution, estimator bias and variance, autocorrelation function type, and dynamic range

difference They are also based on tests of dependency on signal processing temperature, and the effects of SNR, data length, and model shape and size on spectral estimates The directional resolution capability of single and combined quarter plane spectral estimators has been examined

We conclude that MFE can be used to provide accurate spectral estimation of single and multiple sinusoids in noise at various SNR, power levels and frequency separation We have seen accurate spectral estimation for various data sets ranging from a single sinusoid at 27 dB SNR to three sinusoids at -6 dB SNR

MFE provides stable models and accurate spectral estimation over broad temperature ranges which are typically of order ($\sim 10^2$) Hence determination of specific critical temperatures is unnecessary The optimal temperature range depends on the SNR and model size This temperature range may be determined empirically As seen in Section 3 6 1 the spectral estimate obtained at a temperature above the optimal temperature range is excessively smoothed This is due to over-emphasis of the entropy term in the free energy Below the optimal temperature range poor spectral estimation occurs The upper temperature range limit can be determined by selecting a high temperature and reducing the temperature until adequate spectral resolution is achieved The Q-factor described in Section 3 7 on model order can be used as the measure of resolution The lower temperature range limit can be set by determining the temperature at which poor spectral estimation occurs This is accompanied by negative driving noise variance or non-unity bounded autoregressive model parameters Such models are unstable for synthesis purposes The optimal temperature range may also be determined by increasing the temperature from zero, with the lower and upper temperature limits determined as above

The temperature range may also be determined through monitoring the cost function order difference or the state of reflection matrices within the algorithm The MFE method produces superior spectral estimates to those possible at zero temperature, even for very closely spaced sinusoids

The quality of spectral estimates in terms of peak amplitude and peak width improves with model order Higher model orders are also required as the separation between sinusoids on the frequency plane becomes very small We have seen that the accuracy of peak location for very closely spaced sinusoids increases with model order The SPA criterion for sinusoids that are very closely spaced in both frequency directions may be overcome by increasing the model order The minimum temperature corresponding to the lower end of the optimal temperature range increases with model order Data sets with higher SNR demand higher model orders with consequent higher temperatures

Single QP spectral estimators may exhibit a resolution bias in one direction on the frequency plane This bias may be resolved by using a combined QP MFE spectral estimate In some cases, depending on the power and location of the sinusoids on the frequency plane there may still be a resolution bias in some direction This may be eliminated using models with non-symmetric regions of support Spurious noise spikes may also occur for single QP MFE spectral estimates These noise elements may be very effectively removed by use of the combined QP MFE spectral estimate

We conclude that if the exact autocorrelation is used then the resulting spectral estimate is independent of data set size Additionally, in Section 4 3 we have seen that MFE estimates, with reasonable accuracy, multiple sinusoids with low SNR at low data set size using the exact autocorrelation The MFE method of spectral estimation may also use autocorrelation estimates that are unbiased or biased As seen in Section 2 5 the biased estimate suffers from nonequitable weighting of the correlation lag terms The long correlation lag terms are responsible for resolving spectral fine structure, hence the biased form can result in loss of resolution The unbiased form has equitable weighting of the lag terms are therefore provides higher resolution At low data set size there may be an error in the spectral estimates due to the autocorrelation estimation process This may be overcome by increasing the data set size

The sinusoids in a data set may have different dynamic ranges or power levels For the examples tested the ratio of these power levels is preserved if the exact autocorrelation is used If an estimated autocorrelation is used there may be some error due to the autocorrelation estimation process The MFE spectral estimation technique produces estimates with some very small variance in power levels just as there is variance in the location of spectral peaks

In many applications one of the major performance criteria is high resolution [47] This is reiterated by Nikias and Raghuveer [60] They state 'Important requirements to be satisfied by the spectrum estimation method are high resolution/good spectrum matching, and tolerance towards inhomogeneities in the data field while making use of small sized data set' We have seen that the MFE technique performs well for closely spaced sinusoids at low SNR even at low data set size This highlights the high resolution capability of the method

Overall, the numerical simulations of Chapter 3 illustrate that MFE provides low model order accurate spectral estimation over a range of input data sets and operating conditions

5.3 Conclusions - Comparisons with other methods

We have shown for a variety of data set examples that superior spectral estimation may be performed at non-zero temperature than at zero temperature with equivalent computational burden We see that the MFE method outperforms the multidimensional Levinson method At zero temperature our algorithm reverts to the multidimensional Levinson algorithm or Burg type technique Furthermore MFE provides stable models where the Levinson technique may not Hence the MFE method extends the range of the multidimensional Levinson algorithm

We have compared MFE spectral estimates to results obtained by a conventional Fourier transform technique The MFE method does not suffer from the sidelobe structure associated with conventional transform based methods The resolution of MFE spectral estimates is far superior to that produced by conventional techniques at low data set size This highlights the high resolution capability of the MFE spectral estimator

The MFE method has been compared to a hybrid dual 1-D method [47] and a maximum entropy method [51] For a case involving three sinusoids the MFE method outperforms both of these methods in terms of location and sharpness of spectral peaks For a case involving two sinusoids the MFE method at 6 x 6 region of correlation support is superior to the 5 x 5 hybrid method The maximum entropy estimate exhibits sharper peaks However the MFE estimate is more accurate in terms of peak location Overall we conclude from our tests that MFE method is as good as if not better than these two techniques

In terms of spectral resolution we conclude that the MFE method using an unbiased autocorrelation performs just as well as the MCV method for snapshot data consisting of closely spaced sinusoids in white noise We have also compared MFE to a modified covariance technique over a number of simulation trials The bias and variance statistics for MFE are comparable to those for the MCV method The results show that MFE provides accurate spectral estimation

over a series of independent trials MFE is significantly faster than the MCV or MLE method The temperature parameter in MFE allows for the generation of models with unity bounded AR parameters and positive white noise variance, thus ensuring model stability The MCV method does not necessarily produce stable models

Chapter 6. Directions for Future Research

6.1 Introduction

Extensions to the MFE method of AR parameter estimation presented above are possible These include techniques for the improvement in computational efficiency of the method and extension to the complex case The complex case involves spectral estimation of damped exponential signals in noise Other important issues that could be addressed include a priori temperature determination and characterisation of the performance of the technique for other types of signals

6.2 Computational efficiency

The computational efficiency of modern spectral estimation techniques is an important issue This issue needs to be addressed particularly if real time implementation is to be envisaged In 2-D MFE we have implemented a non-linear unconstrained minimisation of the multivariate matrix function given in expression (50) Depending on the model order the direct search Nedler-Mead simplex [14], [53] or the Newton gradient [15], [53] methods have been used to perform the

minimisation The computational efficiency of the method is directly influenced by this optimisation Improvement of the computational efficiency may be obtained with faster optimisation algorithms

Alternatively, we may seek a simplified form of the algorithm Silverstein [74] shows how the ACS form of 1-D MFE may be simplified by linearisation, with consequent substantial computational benefit It remains an open question whether a simplified form of 2-D MFE can be found Such a form should preserve the essence of the full version while providing for faster execution with little loss of performance

6.3 Complex fields

It is of interest to extend our algorithm to the case of damped exponential signals m noise An application of the use of such signals is m direction finding or beamforming [38] This extension of 2-D MFE involves matrix differentiation with respect to a complex matrix and the development of associated cost functions We may then compare the results from the application of such an extension to that from the Hua matrix enhancement and matrix pencil method [28] We may also compare the results to that from the two-step 1-D Prony model technique of Sacchini, Steedly and Moses [72]

The Cramer-Rao bound (CRB) [79] is used to lower bound the variance performance of an unbiased estimator of a scalar parameter It would be of interest to compare the variance of MFE estimates of the magnitude and the x and y pole frequencies of an undamped or damped exponential data model with the CRB at various SNR As the estimator must be unbiased this would require swappmg estimator bias for variance In 1-D this is achieved by appropriate choice of model order as higher model order decreases bias at the expense of increased variance

6.4 A priori temperature determination

We have seen in Chapter 3 that a method of identification of the best temperature range before or within the MFE parameter estimation algorithm should provide a computational advantage

especially for high order models However there exists no fundamental theory for a priori temperature determination Hence, a priori temperature determination remains an open and unsolved question for both 1-D and 2-D MFE

Gibbs random field (GRF) and Markov random field (MRF) models [16], [13], [46] have been used for the characterisation of homogeneous random fields with mixed spectra The relationship between SAR and conditional Markov models is discussed in [10], [11] Pickard [63], [64] stresses the importance of temperature effects in GRF and MRF model parameter estimation In particular he examines the important property of phase transition and shows that it is possible to isolate and measure the temperature at which data phase changes occur In statistical physics a phase transition is where the free energy of one physical state is discontinuously lower than another For example, at some temperature, in the liquid to solid phase transition, the solid phase may have discontinuously lower free energy than the liquid state These special temperatures are known as critical temperatures In signal processing these critical temperatures indicate a phase change in the data field [63]

Silverstein and Pimbley [76] do not propose any relevance of physical phase transitions to problems in signal analysis However it still remains an open question whether the critical temperatures and phase changes used in image modelling by Pickard may in some way be related to MFE AR models

There are other initiatives that may lead to a solution of the question of a priori temperature determination 'With some adaptations, Gull [27] and Sibisi [73] each present more objective approaches for choosing alpha ' [12] Gull uses Bayesian analysis to determine a value of signal processing temperature in an image reconstruction context

Sibisi determines the optimal Bayesian estimate for the signal processing temperature for the regularisation process The regularisation process constructs an estimate of an autocorrelation matrix with equitable lag weighting and positive definiteness This is achieved by multiplying the

identity matrix by a positive constant and adding the result to the unbiased Toeplitz form of the autocorrelation matrix In 1-D the regularisation process corresponds to the additional cost element in MFE 'MFE-ACS estimation intrinsically provides the desired regularization function of stabilizing potentially ill-conditioned solutions as well as simultaneously compensating for noise' [77] The Shannon entropy term in maximum entropy image reconstruction can also be closely approximated by the regularisation function [82]

Finally, the investigation of the relationship between the reflection coefficient matrices in 2-D MFE and optimal signal processing temperature gives us an early indication of temperature range suitability Another method of early indication is the minimisation of the order of magnitude difference between cost functions associated with expression (50) These issues are discussed in Sections 2 6 on optimisation and cost functions, in Section 3 6 2 on temperature determination, and Section 6 5 below

6.5 Other signal types - Mixed and Wideband spectra

Generally we have concentrated on spectral estimation of narrowband signals with low SNR However it is also of interest to determine the performance of spectral estimation techniques including the MFE technique for wideband spectra matching 'More effort needs to be directed towards spectral analysis of wideband signals and signals buried deeper in noise' [52]

An application in which wideband and mixed spectra have considerable use is in texture modelling [46] It is not possible to characterise an entire texture by use of AR models alone 'Since in general, a homogeneous random field is characterised by a mixed spectral distribution, parameter estimation techniques which are solely based on spectral density estimators are not adequate' [20] Typically in texture spectral estimation and synthesis the texture is decomposed into a deterministic and an indeterministic field The deterministic field is further decomposed into a harmonic field for the periodic features and evanescent field for the global directional features [20], [24] 'The harmonic random field is the sum of 2-D sine waves of random amplitude and

phase, while the generalized evanescent field consists of a countable number of wave systems' [23] AR spectral estimators may be used to model the indeterministic field This field is typically wideband It is possible to determine AR models that produce power spectral densities approximating that of the indeterministic field A first step in the application of the MFE method to this area would be to produce a simulated wideband field using a test parametric AR process Subsequently MFE may be used to determine the MFE AR parameters and an estimated PSD The estimated PSD may then be compared to the original PSD The best temperature range for spectral matching can be determined by calculating the mean square difference or error between the original and the synthesised texture PSD Another method of determination of the best temperature range is to monitor the order of magnitude difference between cost functions associated with expression (50)

Another method [22] for texture characterisation decomposes the texture into a periodic or global structural components field, a singularities or local structural components field, and a stochastic field Figures 6 1 and 6 2 [44] show constituent fields for the Brodatz [6] D93 'hair' texture and D100 'ice crystals on an automobile' texture The periodic field is merely a set of sinusoids at various power levels and spatial frequencies A Fourier transform method [22] is generally used AR spectral estimators, including MFE, may be also used to determine a parametric model for this field The ability of MFE parametric model determination methods to parameterize the periodic component of texture spectra is dependent on its ability to effectively resolve simpler spectra consisting of a number of sinusoids in white noise

The stochastic or homogeneous random field is generally modelled by an AR process A Levinson type algorithm is used in [21] In [44] we used a MLE method to derive models with various model regions of support including single QP In [45] we proposed the use of cepstral stabilized ARMA models and compared the results with other model types including single QP AR models In both [44] and [45] we generated spectral estimates and synthesised the homogeneous random constituent of texture using the various models A MFE AR model may be also used to model the

homogeneous random constituent of texture The best temperature range for spectral matching of such wideband fields can be determined as above by calculating the mean square error between the original and estimated PSD

Preliminary investigation has shown that further decomposition of constituent texture fields to multiple fields may yield results for the parametric modelling of mixed spectra This may be achieved by thresholding the constituent field at various power levels in the spatial frequency domain Subsequently MFE parametric models may be derived for each of the resultant fields

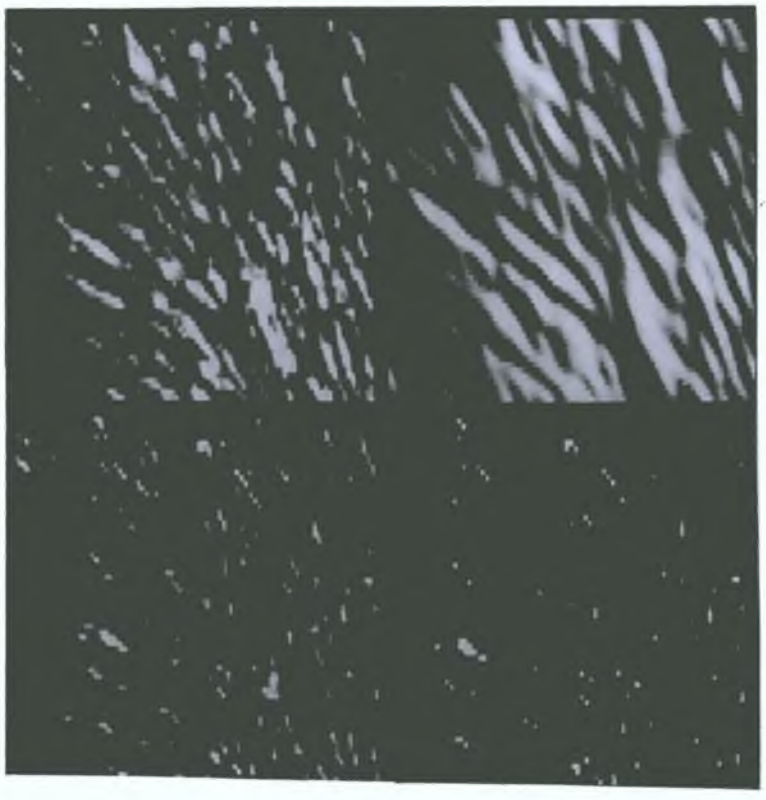

Figure 6.1 D93 texture constituent fields.

(1,1) original texture, (1,2) periodic field, (2,1) random field, and (2,2) singularities field.

Figure 6.2 D100 texture constituent fields.

(1,1) original texture, (1,2) random field, and (1,3) periodic field.

6.6 Higher order statistics

The autocorrelation function and power spectral density do not provide phase information They are sufficient for a complete statistical description of a Gaussian signal However, multidimensional signals may be non-Gaussian, may be rich in phase information, and may have additive coloured Gaussian noise of unknown power spectrum The absence of phase information and the Gaussianity restriction has limited the utility of second order statistical techniques This has prompted much recent interest in higher order statistics and polyspectra [58], [59], [80] An interesting area of research is the extension of parametric estimation techniques to third and fourth order statistics For 2-D MFE an appropriate starting point is at the solution of extended Yule-Walker type equations involving higher order cumulants for AR parameter estimation Alternatively, second order statistics may be estimated from higher order statistics [25] and used in autocorrelation based methods such as 2-D MFE Slices of fourth order cumulants may also be used in place of correlation quantities in correlation based techniques where the data set has white Gaussian noise or coloured Gaussian noise of unknown spectral density [58]

References

[1] Aizenberg I A and Yuzhakov A P , Integral Representations and Residues in Multidimensional Complex Analysis, Providence, RI American Mathematical Society, vol 59, 1980

[2] Bose N K , Multidimensional Digital Signal Processing Problems, Progress, and Future Scopes, Proceedings of the IEEE, vol 78, no 4, April 1990

[3] Bose N K , Applied Multidimensional Systems Theory, Van Nostrand Reinhold Company, 1982

[4] Bose N K , Problems and Progress in Multidimensional Systems Theory, Proceedings of the IEEE, vol 65, no 6, pp 824-840, June 1977

[5] Box G E P and Jenkins G M , Time Series Analysis Forecasting and Control, Holden-Day, CA, 1976

[6] Brodatz P , Textures A Photographic Album for Artists and Designers, Dover, New York, 1966

[7] Cadzow J A and Ogino K , Two-Dimensional Spectral Estimation, IEEE Transactions on Acoustics, Speech and Signal Processing, vol ASSP-29, no 3, pp 396-401, June 1981

[8] Capon J , High Resolution Frequency-Wavenumber Spectrum Analysis, Proc IEEE, vol 57, pp 1408-1418, Aug 1969

[9] Carrier G F , Krook M and Pearson C E , Functions of a complex variable theory and technique, Hod Books, NY, 1983

[10] Chellappa R and Kashyap R L , Synthetic Generation and Estimation in Random Field Models of Images, Proc IEEE Comput Soc Conf Pattern Recog Image Proc Dallas, TX . pp 577-582, Aug 1981

[11] Chellappa R and Kashyap R L , On the Correlation Structure of Random Field Models of Images and Textures, Proc IEEE Comput Soc Conf Pattern Recog Image Proc Dallas, TX , pp 574-576 Aug 1981

[12] Cooper D K and Pimbley J M , A Minimum Free-Energy Hybrid Algorithm for 2-D Spectral Estimation, IEEE Trans on Signal Processing, vol 42, no 3, pp 698-702, March 1994

[13] Cross G R and Jam A K , Markov Random Field Texture Models, IEEE Transactions on Pattern Analysis and Machine Intelligence, vol 5, no 1, pp 25-39, Jan 1983

[14] Dennis Jr, J E and Woods D J , Optimization on Microcomputers The Nedler-Mead Simplex Algorithm, New Computing Environments Microcomputers in Large-Scale Computing, A Wouk Ed , SIAM, pp 116-122, 1987

[15] Dennis Jr, J E and Schnabel R B , Numerical Methods for Unconstrained Optimization and Nonlinear Equations, Prentice-Hall, 1983

[16] Dubes R C and Jain A K , Random field models in image analysis, Journal of Applied Statistics, vol 16, pp 131-164, 1989

[17] Dudgeon D E and Mersereau R M , Multidimensional Digital Signal Processing, Prentice-Hall, Signal Processing series, Englewood Cliffs, NJ, 1984

[18] Edward J A and Fitelson M M , Notes on Maximum Entropy Processing, IEEE Trans on Information Theory, vol 19, pp 232-4, March 1973

[19] Forsythe G E , Malcolm M A and Moler C B , Computer Methods for Mathematical Computations, Prentice-Hall, 1977

[20] Francos J M , de Garrido D P and Woods J W , On the parameter estimation of the harmonic, evanescent and purely indeterministic components of homogeneous random fields, IEEE Intl Conf on Acoustics, Speech and Signal Proc , ICASSP-92, vol 3, pp 41-44, March 1992, San Francisco, USA

[21] Francos J M , Meiri A Z , A 2-D Autoregressive, Finite Support, Causal Model for Texture Analysis and Synthesis, 1989 IEEE Intl , Conf on Acoustics, Speech and Signal Proc, ICASSP-89, vol 3, pp 1552-5, 1989

[22] Francos J M , Meiri A Z , A Unified Structural-Stochastic Model for Texture Analysis and Synthesis, 9th Int Conf on Pattern Recognition, Nov 14-17, 1988, pp 41-45, Rome, Italy

[23] Francos J M , Meiri A Z and Porat B , A Unified Texture Model Based on a 2-D Wold-Like Decomposition, IEEE Transactions on Signal processing, vol 41, no 8, pp 2665- 2677, August 1993

[24] Francos J M , Meiri A Z and Porat B , Modeling of the texture structural components using 2-D deterministic random fields, Proceedings of the SPIE - The International Society for Optical Engineering, vol 1606, pt 1, pp 553 - 565, 1991

[25] Giannakis G B and Delopoulos A , Non-parametric estimation of autocorrelation and spectra usmg cumulants and polyspectra, The International Society for Optical Engineering, vol 1348, Advanced Signal-Processing Algorithms, Architectures and Implementations, pp 503-517, 1990

[26] Graham A , Kronecker Products and Matrix Calculus with Applications, Ellis Horwood Series - Mathematics and its Applications, 1981

[27] Gull S F , Developments in maximum entropy data analysis, in Maximum Entropy and Bayesian Methods, J Skilling Ed , Boston Kluwer, 1989

[28] Hua Y , Estimating Two-Dimensional Frequencies by Matrix Enhancement and Matrix Pencil, ICASSP-91, pp 3073-76, Toronto, May 14-17, 1991

[29] Jain A K , Fundamentals of Digital Image Processing, Prentice-Hall, Englewood Cliffs, NJ, 1989

[30] Jain A K , Advances in Mathematical Models for Image Processing, Proc IEEE, vol 69, pp 502-528, May 1981

[31] Joseph P M and Spital R D, The exponential edge-gradient effect in x-ray computed tomography, Phys Med Biol pp 473-487, 1981

[32] Kartikeyan B and Sarkar A , An identification Approach for 2-D Autoregressive Models in Describing Textures, Computer Vision Graphics Image Process vol 53, no 2, pp 121- 131, March 1991

[33] Kashyap R L , Characterisation and Estimation of Two-Dimensional ARMA Models, IEEE Transactions on Information Theory, vol 30, no 5, pp 736-745, Sept 1984

[34] Kashyap R L , Finite Lattice Random Field Models for Finite Images, Proc Conf Information Sciences, John Hopkins University, Baltimore, MD, pp 215-220, March 1981

[35] Kashyap R L , Inconsistency of the AIC rule for estimating the order of autoregressive models, IEEE Trans Aut Control, AC-25, pp 996-997, Oct 1980

[36] Kashyap R L and Chellappa R , Estimation and Choice of Neighbors in Spatial-Interaction Models of Images, IEEE Trans Information Theory, Vol 29, no 1, pp 60-72, Jan 1983

[37] Kashyap R L , Chellappa R and Ahuja N , Decision Rules for Choice of Neighbors in Random Field Models of Images, Computer Graphics and Image Processing, vol 15, pp 301-318, 1981

[38] Kay S M , Modern Spectral Estimation Theory and Application, Prentice-Hall, Englewood Cliffs, NJ, 1988

[39] Kiernan P , Two-Dimensional Minimum Free Energy Spectral Estimation, to be published, IEE Proceedings, Vision, Image and Signal Processing, vol 142, no 3, June 1995

[40] Kiernan P , High Resolution Two-Dimensional Minimum Free Energy AR Spectral Estmation, to be published, Multidimensional Systems and Signal Processing, vol 6, pp 237-249, July 1995

[41] Kiernan P , Two-Dimensional Autoregressive Spectral Estimation using a Two-Dimensional Minimum Free Energy Method, Dublin City University, School of Computer Applications, Working Paper CA 0494, 1994

[42] Kiernan P , Two-Dimensional Spectral Estimation by Free Energy Minimisation, submitted for review, Digital Signal Processing, Feb 1995

[43] Kiernan P , Two-Dimensional Minimum Free Energy Autoregressive Spectral Estmation, submitted for review, IEEE Transactions on Signal Processmg, Oct 1994

[44] Kiernan P , Statistical Inference for Texture Characterisation using Second Order Statistics, Dublin City University, School of Computer Applications Working Paper CA 1093, 1993

[45] Kiernan P , SAR and Cepstral Stabilized SARMA Models for Texture Modelling and Synthesis, submitted IEEE Transactions on Signal Processing, 1993, unpublished

[46] Kiernan P , Analysis, Synthesis and Classification of Texture - An Overview, Dublin City University, School of Computer Applications Working Paper CA 2192, 1992

[47] Kimura H and Honoki Y , A Hybrid Approach to High Resolution Two-Dimensional Spectrum Analysis, IEEE Trans Acoust Speech, Signal Proc, vol 35, pp 1024-1036, July 1987

[48] Krantz S G , Functions of several complex variables, Encyclopaedia of Physical Science and Technology, vol 6, pp 803-828, Academic Press, 1992

[49] Krantz S G , Complex Analysis The Geometric Viewpoint, The Carus Mathematical Monographs Number Twenty-Three, The Mathematical Association of America, 1990

[50] Lim J , Two-Dimensional Signal and Image Processing, Chapter 6, Prentice-Hall Int , Inc , 1990

[51] Lim J S and Malik N A , A new algorithm for two dimensional maximum entropy power spectrum estimation, IEEE Trans Acoust , Speech, Signal Processmg, vol ASSP-29, pp 401-413, June 1981

[52] Marple S L , Digital Spectral Analysis with Applications, Prentice-Hall Signal Processing series, Englewood Cliffs, NJ, 1987

[53] MATLAB, The MathWorks Inc 21 Eliot Street, South Natick, MA 01760, USA

[54] McClellan J H , Multidimensional Spectral Estimation, Proc IEEE, vol 70, pp 1029-1039, Sept 1982

[55] McClellan J H and Purdy R J , Applications of digital signal processing to radar, in Applications of Digital Signal Processing, A V Oppenheim Ed , Englewood Cliffs, NJ Prentice-Hall, 1978

[56] McCormick B H and Jayaramamurthy S N , Time series model for texture synthesis, Internat J Comput Inform Sci 3, 1974, pp 329-343

[57] Narayan R and Nityananda R , Maximum entropy image restoration in astronomy, Annu Rev Astron Astrophys , vol 24, pp 127-170, 1986

[58] Nikias C L and Mendel J M , Signal Processing with Higher Order Spectra, IEEE Signal Processing, pp 10-37, July 1993

[59] Nikias C and Mendel J , Higher-Order Spectral Analysis, IEEE Video Tutorial HV0231-1, ICASSP-91, May 1991

[60] Nikias C L and Raghuveer M R , Multi-Dimensional Parametric Spectral Estimation, Signal Processing, vol 9, pp 191-205, Oct 1985

[61] Nikias C L , Scott P D and Siegel J H , Computer based two-dimensional spectral estimation for the detection of prearrhythmic states after hypothermic myocardial preservation, J Comp Med Biol, vol 14, pt 2, pp 159-78, 1984

[62] Park S K and Miller K W , Random number generators Good ones are hard to find, Comm ACM, vol 32, no 10, pp 1192-1201, Oct 1988

[63] Pickard R W , Gibbs Random Fields Temperature and Parameter Analysis, ICASSP-92, vol III, pp 45-48 1992

[64] Pickard R W , Elfadel I M and Pentland A , Markov/Gibbs Texture Modelmg Aura Matrices and Temperature Effects, Proc IEEE Conf on Computer Vision and Pattern Recognition, Maui, HI, pp 371-377, June 1991

[65] Pimbley J , Private communication, April 1994

[66] Pimbley J M , Recursive Autoregressive Spectral Estimation by Minimisation of the Free Energy, IEEE Trans Signal Processing, vol 40, no 6, pp 1518-1527, June 1992

[67] Pimbley J M and Silverstein S D , Recursive Minimum Free Energy Spectral Estimation, Proc 23rd Asilomar Conf Signals, Syst Comput pp 1051-1055, 1989

[68] Pinson L J and Childers D G , Frequency - Wavenumber Spectrum Analysis of EEG Multielectrode Array Data, IEEE Trans Biomed Eng, vol 21, pp 192-206, 1974

[69] Rabiner L R and Gold B , Theory and Application of Digital Signal Processing, Prentice-Hall, Englewood Cliffs, 1975

[70] Robinson E A and Treitel S , Digital signal processing in geophysics, in Applications of Digital Signal Processing, A V Oppenheim Ed , Englewood cliffs, NJ Prentice-Hall, 1978

[71] Rudin W , Function Theory in Polydiscs, W A Benjamin, New York, 1969

[72] Sacchini J J , Steedly W M and Moses R L , Two-Dimensional Prony Modeling and Parameter Estimation, IEEE Transactions on Signal Processing, vol 41, no 11, pp 3127-3137, Nov 1993

[73] Sibisi S , Regularization and Inverse Problems, in Maximum Entropy and Bayesian Methods, J Skilling Ed , Boston Kluwer, 1989

[74] Silverstein S D , Linear Minimum Free Energy Estimation A Computationally Efficient Noise Suppression Spectral Estimation Algorithm, IEEE Transactions on Signal Processing, vol 39, no 6, June 1991

[75] Silverstein S D , Carroll S M and Pimbley J M , Performance Comparisons of The Minimum Free Energy Algorithms with The Reduced Rank Modified Covariance Eigenanalysis Algorithm, ICASSP-89 Glasgow, Scotland, vol 4, pp 2270-2273, May 1989

[76] Silverstein S D and Pimbley J M , The Minimum Free Energy Method of Spectral Estimation, in - Advances in Spectral Analysis and Array Processing, S Haykin Ed, Englewood Cliffs, NJ Prentice-Hall, 1992

[77] Silverstein S D and Pimbley J M , Minimum-free-energy method of spectral estimation autocorrelation sequence approach, J Opt Soc Am A/vol 7, no 3, pp 356-372, March 1990

[78] Silverstein S D and Pimbley J M , Robust spectral estimation autocorrelation based minimum free energy method, Proc 22nd Asilomar Conference Signals Systems Computers, pp 209-213, Nov 1988

[79] Steedly W M and Moses R L , The Cramer-Rao Bound for Pole and Amplitude Estimates of Damped Exponential Signals in Noise, IEEE Intl Conf on Acoustics, Speech and Signal Proc , ICASSP-91, pp 3569-72, May 1991, Toronto, ON

[80] Swami A , Giannakis G B and Mendel J M , Linear Modeling of Multidimensional Non-Gaussian Processes Using Cumulants, Multidimensional Systems and Signal Processing, vol - 1, pp 11-37, Kluwer Academic Publishers, Boston, 1990

[81] Therrien C W , Relations between 2-D and Multichannel Linear Prediction IEEE Trans Acoustics, Speech and Signal Processing, vol 29, pp 454-456, June 1981

[82] Thompson A M , On the use of quadratic regularisation within maximum entropy image restoration, J Skilling Ed, Maximum Entropy and Bayesian Methods, pp 497-504, Kluwer Academic Publishers, 1989

[83] Ulrych T J and Walker C J , High Resolution 2-Dimensional Power Spectral Estimation Applied Time series Analysis II, D F Findley Ed , pp 71-99, Academic Press, Inc New York, 1981

[84] Zhang X -D , On the estimation of Two-Dimensional Moving Average Parameters, IEEE Trans on Automatic Control, vol 36, no 10, pp 1196-1199, Oct 1991

[85] Zhang X -D and Cheng J , High Resolution Two-Dimensional ARMA Spectral Estimation, IEEE Trans Signal Processing, vol 39, no 3, pp 765-770, March 1991

[86] Zou L and Liu B , On resolving two-dimensional sinusoids in white noise using different spectral estimates, IEEE Trans Acoust , Speech, Signal Processing, vol ASSP-36, pp 1338-1350, Aug 1988

Two-Dimensional Minimum Free Energy Spectral Estimation, P Kiernan, to be published, IEE Proceedings, Vision, Image and Signal Processing, vol 142, no 3, June 1995

Two-Dimensional Minimum Free Energy Spectral Estimation

Paul Kiernan

Abstract

We propose a 2-D extension of the Minimum Free Energy (MFE) parameter estimation method which may be used to determine autoregressive (AR) model parameters for 2-D spectral estimation. The performance of the technique for spectral estimation of 2-D sinusoids in white noise is demonstrated by numerical example It is seen that MFE can provide superior spectral estimation over that which can be achieved with the multidimensional Levinson algorithm with equivalent computational burden The performance of the technique in terms of computational expense and accuracy of spectral estimation over a number of simulation trials is compared with a modified covariance technique

1 Introduction

High resolution spectral estimation of 2-D homogeneous random fields is becoming increasingly important because of its role in various areas Such areas include analysis of space-space, space-time, and time-time data arrays Space-space data arrays are used in image processing [1], whereas space-time applications include sonar and seismic processing [2] Time-time arrays are typically used in the analysis of radar pulse repetition versus arrival time [3] As stated by McClellan [4] "The operation of spectral analysis arises in many fields of application Situations in which signals are inherently multidimensional can be found in geophysics, radio astronomy, sonar, and radar, to mention a few These multidimensional problems present a challenging set of theoretical and computational difficulties that must be tackled" Other areas of interest include biomedical imaging [5], geophysics [6], and radio astronomy [7] Any field in which the frequency spectrum of a directly measured quantity is of interest will benefit from continuing advances in power spectrum estimation [8]

We present a high resolution power spectrum estimation method. The Yule-Walker equation based Levinson recursion is an established method for deriving the parameters of a causal quarter plane (QP) AR model We show how model parameters for 2-D fields may be determined by the solution of 2-D Yule-Walker equations via a modified multidimensional Levinson algorithm The resulting models may be used for high resolution power spectrum estimation. We modify the multidimensional Levinson algorithm [9] by determining the reflection coefficient matrices via minimization of the free energy [10] rather than via minimization of the linear prediction error energy alone Our method is an efficient 2-D MFE spectral estimation technique based on extension of the method developed by Pinbley [8], and Pinbley and Silverstein [11] A 1-D MFE method is used in [12] along with a 1-D *periodogram as part* of a hybrid separable algorithm for 2-D spectral estimation Our method responds to the call in [12] for an efficient 2-D MFE algorithm

2 Theory

A simultaneous AR (SAR) model [13], may be represented by

$$\sum_{i=0}^{p1}\sum_{j=0}^{p2} a(i,j)y(m-i,n-j) = u(m,n) \tag{1}$$

where $\{y(m,n)\}$ is a finite set of observations on $1 \le m \le N$, $1 \le n \le N$ and is a homogeneous random field A toroidal model is assumed on this $N \times N$ lattice [14] $\{u(m,n)\}$ is uncorrelated Gaussian white noise with zero mean and variance σ^2 The autoregressive model parameters are given by $\{a\}$ over the $(p_1+1) \times (p_2+1)$ region of support It is assumed that $a(0,0) = 1$ The power spectral density of this model [15] may be written in normalised spatial frequency terms (ω_x, ω_y) where $|\omega_x| \le 1/2$, $|\omega_y| \le 1/2$ as

$$S(\omega_x,\omega_y) = \frac{\sigma^2}{\left|\sum_{k=0}^{p1}\sum_{l=0}^{p2} a_{kl} e^{-j(\omega_x k+\omega_y l)}\right|^2} \tag{2}$$

or $$S(f_x,f_y) = \beta \Big/ |A(f_x,f_y)|^2 \quad \text{where} \quad \beta = \sigma^2 \tag{3}$$

The Yule-Walker equations [9] are based on the autocorrelation estimates of the observed field and are given by

$$\sum_{i=0}^{p1}\sum_{j=0}^{p2} a(i,j) r_{yy}(k-i,l-j) = \sigma^2 \delta(k,l) \tag{4}$$

The RHS of this expression is zero for all points in QP' This covers the quarter plane area of model support QP except for the point at the origin

$$QP = QP' \cup (0\ 0) \tag{5}$$

The Yule-Walker equations are also given in matrix form [16] as

$$\mathbf{Ra} = \mathbf{h} \tag{6}$$

R is a block Toeplitz matrix that is symmetric and positive semi-definite The matrix is also made up of blocks **Ryy** that are Toeplitz in structure though not symmetric and have elements r_{yy} The multidimensional Levinson algorithm [9] may be used to solve (6) In this algorithm the reflection coefficients at stage m of the recursion are represented by a set of reflection

matrices $\mathbf{A}_m[m]$. If the order of the model used is *p1* x *p2*, then from the multidimensional Levinson algorithm [9] at the last *(p1-1)* recursion

$$\mathbf{A}_{p1}[p1]\,\mathbf{P}^{f}_{p1-1} + \Delta_{p1} = \mathbf{O} \tag{7}$$

where the Toeplitz structure of the autocorrelation matrices ensure that the covariance of the prediction error process is identical for the backward and forward AR process

$$\mathbf{P}^{f}_{p1} = \mathbf{P}^{b}_{p1} \tag{8}$$

The partial correlation matrix is given as

$$\Delta_{p1} = \left[\mathbf{I}\ \ \mathbf{A}_{P1-1}[1]\ \ \mathbf{A}_{P1-1}[2] \ldots\ldots \mathbf{A}_{P1-1}[p1-1]\right]\ \left[\mathbf{Ryy}[p1]\,\mathbf{Ryy}[p1-1] \ldots\ldots \mathbf{Ryy}[1]\right]^{T} \tag{9}$$

The prediction error covariance matrices are given by the expression

$$\mathbf{P}^{f}_{p1} = \left[\mathbf{I} - \mathbf{A}_{p1}[p1]\mathbf{A}^{T}_{p1}[p1]\right]\mathbf{P}^{f}_{p1-1}, \tag{10}$$

with initial condition $\mathbf{P}^{f}_{0} = \mathbf{Ryy}[0]$ (11)

The reflection coefficient matrices are given by

$$\mathbf{A}_{p1}[q] = \mathbf{A}_{p1-1}[q] + \mathbf{A}_{p1}[p1]\mathbf{A}^{T}_{p1-1}[p1-q-1] \quad \text{for} \quad 1 \le q \le p1-1 \tag{12}$$

Matrices in expressions (7) through (12) are of order p_2 x p_2.

Expression (7) gives optimisation of the reflection coefficients based on minimisation of prediction error energy. The AR parameters and white driving noise variance of the model are determined from the reflection coefficient and the prediction error covariance matrices.

We extend this algorithm by including an extra cost function based on entropy. The motivation behind this comes from statistical thermodynamics. The ground state in physical systems corresponds to the case in signal processing where parametric estimation is performed on the basis of minimisation of the prediction error energy alone. In this case fluctuations disappear and physical

systems reduce to their ground state In signal analysis this corresponds to zero input from the entropy energy term

"At nonzero temperature physical systems are neither in minimum energy states nor in maximum entropy states Rather, there exists a balance between low energy and high entropy Increasing the system temperature emphasizes the importance of entropy at the expense of energy Conversely, reduction of the temperature to absolute zero forces the system into its lowest energy state" [17] Hence, temperature acts as a control parameter for entropy or fluctuations in the system

The cost function in the 1-D MFE parametric estimation algorithm is based on extension of the least mean square criterion to include a noisy data cost element This extra cost element which minimises the free energy is due to an entropy term [8]

In the 2-D method we introduce an extra cost function due to the entropy This results in the minimisation of the resultant free energy, thereby providing better spectral estimation than that provided by minimisation of prediction error energy alone This extra cost function is given by the differential of a 2D Shannon-Burg type entropy term with respect to reflection matrix $\mathbf{A}_m[m]$ The Shannon-Burg entropy measure [17] is defined to within an arbitrary constant, hence for the 2-D entropy field H

$$H \propto \int_{-1/2}^{1/2}\int_{-1/2}^{1/2} \ln\left[\beta / |A(f_x, f_y)|^2\right] df_x df_y \qquad (13)$$

We require the differential of the 2-D entropy term with respect to the reflection coefficient matrix $\mathbf{A}_m[m]$ at stage m For real fields the reflection coefficient matrix $\mathbf{A}$ is real We express the differential of the entropy energy term, with respect to $\mathbf{A}$ as

$$\partial \alpha H / \partial \mathbf{A} = \alpha\left[\partial \ln(\beta) / \partial \mathbf{A} - \partial\left[\int_{-1/2}^{1/2}\int_{-1/2}^{1/2} \ln[|A(f_x, f_y)|^2]\, df_x df_y\right] / \partial \mathbf{A}\right] \qquad (14)$$

The entropy proportionality constant is absorbed into the signal processing temperature parameter α

At stage m of the recursion the RHS of expression (14) becomes

$$-\int_{-1/2}^{1/2}\int_{-1/2}^{1/2}\partial\left[\ln[A_m(f_x,f_y)A_m^*(f_x,f_y)]\right]/\partial\mathbf{A}_m[m]\,df_x df_y \tag{15}$$

$$=-\int_{-1/2}^{1/2}\int_{-1/2}^{1/2}(\partial\ln A_m(f_x,f_y)/\partial\mathbf{A}_m[m])+(\partial\ln A_m^*(f_x,f_y)/\partial\mathbf{A}_m[m])\,df_x df_y \tag{16}$$

At any frequency (f_x,f_y) the differential

$$\partial\ln A_m(f_x,f_y)/\partial\mathbf{A}_m[m] \tag{17}$$

is the differential of a scalar with respect to a matrix Applying matrix calculus [18] this may be expressed as a *(p2,p2)* matrix with any element $\mu(i,j)$ given by

$$\mu(i,j)=\partial\ln A_m(f_x,f_y)/\partial\,\tau(i,j)=A_m^{-1}\,\partial A_m(f_x,f_y)/\partial\,\tau(i,j) \tag{18}$$

where $\tau(i,j)$ is an element of the reflection matrix $\mathbf{A}_m[m]$ Then the integration becomes

$$\begin{aligned}&\int_{-1/2}^{1\,2}\int_{-1/2}^{1/2}[\,\partial A_m(f_x,f_y)/\partial\mathbf{A}_m[m]]/A_m(f_x,f_y)\,df_x df_y\\&+\int_{-1/2}^{1/2}\int_{-1/2}^{1/2}[\,\partial A_m^*(f_x,f_y)/\partial\mathbf{A}_m[m]]/A_m^*(f_x,f_y)\,df_x df_y\end{aligned} \tag{19}$$

The second part of this expression becomes

$$\int_{-1/2}^{1\,2}\int_{-1/2}^{1/2}\left(\partial\textstyle\sum_{k=0}^{p1}\sum_{l=0}^{p2}a_{kl}[m]e^{j(f_xk+f_yl)}/\partial\mathbf{A}_m[m]\right)/A_m^*(f_x,f_y)\,df_x df_y \tag{20}$$

This contour integral is taken about a surface in the 2-D complex frequency hyperplane The argument [8] may be extended so that the symmetry in the contour path reduces the contour integration to integrations at

(a)

$$[-1/2 \le \mathrm{Re}(f_x) \le +1/2, \mathrm{Im}(f_x) = -\infty],$$
$$[-1/2 \le \mathrm{Re}(f_y) \le +1/2, \mathrm{Im}(f_y) = -\infty]$$

and at

(b) (21)

$$[-1/2 \le \mathrm{Re}(f_x) \le +1/2, \mathrm{Im}(f_x) = 0],$$
$$[-1/2 \le \mathrm{Re}(f_y) \le +1/2, \mathrm{Im}(f_y) = 0]$$

The integration at (a) goes to zero as the numerator of the expression (20) contains a multiplicative exponential term Hence for $f_x = -j\infty$ and $f_y = -j\infty$ the integral vanishes

The integration at (21)(b) is now examined. A positive definite autocorrelation matrix may yield solutions to the Yule-Walker equations, though they may be unstable Hence the multidimensional method [9] which is a minimum prediction error method may yield unstable results Therefore $A(f_x, f_y)$ may not be minimum phase By sufficiently whitening the input data field we ensure that the autocorrelation falls off fast enough so that $A(f_x, f_y)$ tends to be minimum phase Given a minimum phase $A(f_x, f_y)$ all singularities i e zeroes of $A(z_x, z_y)$ or solutions of the equation $A(z_x, z_y) = 0$ are located within the unit bicircle Hence there are no zeros in the lower half of the 2-D complex frequency plane or outside the unit bicircle

The test for a bivariate polynomial can be reduced to testing for each variable when the other is fixed By fixing one variable and performing the contour integration with respect to the other the number of zeroes may be determined When double contour integration is performed one variable is set and the contour integral is evaluated with respect to the other variable Hence the integration on the region specified by (21) (b) goes to zero A similar argument may be made for the first integral in expression (19)

Continuing with expression (14), in terms of Levinson algorithm parameters at stage m of the recursion

$$\ln \beta_m = \ln[\mathbf{P}_m^f] = \ln\left[(\mathbf{I} - \mathbf{A}_m[m]\mathbf{A}_m^T[m])\mathbf{P}_{m-1}^f\right] \tag{22}$$

hence $$\partial(\ln \beta_m) / \partial \mathbf{A}_m[m] = \partial \ln\left[(\mathbf{I} - \mathbf{A}_m[m]\mathbf{A}_m^T[m])\mathbf{P}_{m-1}^f\right] / \partial \mathbf{A}_m[m] \quad (23)$$

We minimise this cost function at recursion m and signal processing temperature α by finding $\mathbf{A}_m[m]$ such that

$$\mathbf{A}_m[m]\mathbf{P}_{m-1}^f + \Delta_m - \alpha\left[\partial \ln(\mathbf{I} - \mathbf{A}_m[m]\mathbf{A}_m^T[m])\mathbf{P}_{m-1}^f / \partial \mathbf{A}_m[m]\right] = \mathbf{0} \quad (24)$$

3 Results

The resolution of sinusoids in white noise is a widely used standard simulation exercise for spectral estimation techniques [15] We used an unbiased autocorrelation function estimated from a realisation of sinusoids plus white noise

Using a single quarter plane spectral estimator results in elliptical contours of constant power spectral density (PSD) level This may be overcome by using a combined quarter plane estimator Another motivation for using a combined estimator is that spurious peaks are less likely to occur if quarter plane estimates are combined in 'parallel resistor' fashion [16] We combine first and fourth quarter plane estimates for all PSD estimates We note that spurious peaks which may occur for high order single quarter plane models are very effectively eliminated by using a combined quarter plane model

We take a 160x160 point data snapshot consisting of sinusoids at arbitrary unity normalised frequencies (0 1,0 2) and (0 3 0 4) of equal amplitude at arbitrary SNR of 6 dB in uncorrelated white Gaussian noise We compare the spectral estimate at temperature 0 074 with that at zero temperature This has special significance because at zero temperature our technique reverts to the multidimensional Levinson or Burg type technique The temperature of 0 074 was the optimal temperature for spectral estimation based on the average autocorrelation over 10 noise seeds This temperature also falls within a broad range of temperatures within which accurate spectral estimation was obtained Figure 1 (a) shows the combined first and fourth quarter plane normalised amplitude PSD plot in the x frequency direction $psd(f_x,0)$ $0 \le f_x \le 0.5$ derived using the MFE based AR

models of order 5x5 at temperature 0 074 Figure 1 (b) is a contour plot as used showing the spectral estimate in both frequency directions Corresponding plots for the spectral estimate of the two sinusoids at temperature zero are shown in figures 1 (c) and (d)

In figure 1 (a) we see sharp peaks at f_x = 0 1 and f_x = 0 3 The contour plot of figure 1 (b) clearly shows the spatial frequency peaks at (0 1,0 2) and (0 3 0 4) The sharpness of the peaks is illustrated by the 6 dB contours In figure 1 (c) we can see an number of peaks in the x frequency direction, however none are at the frequencies 0 1 and 0 3 Figure 1 (d) shows that the peaks are certainly not located at spatial frequencies (0 1,0 2) and (0 3,0 4) and therefore are incorrectly resolved We conclude that both frequency components are accurately resolved at temperature 0 074 whereas this is not the case at temperature zero using the multidimensional Levinson method

Extensive experimentation into the effect of model order variation has shown that the width of the peaks corresponding to sinusoid components in a spectral estimate decreases as the model order increases In one test we took a 160x160 point single snapshot of data consisting of 2 equal amplitude sinusoids at spatial frequencies (0 1,0 2) and (0 3,0 4) at 0 dB SNR. The data was subjected to spectral estimation using MFE models of order 3x3, 5x5, 7x7 and 9x9 We use a 2-D Q-factor to measure the sharpness of the peaks in the frequency domain The Q-factor is determined as the inverted product of the bandwidths in the x and y frequency direction across each spectral peak at a given amplitude We use the averaged Q-factor over the two spatial frequency components or peaks as a comparative measure of the sharpness of the peaks The average Q-factors at -21 dB for the 9x9, 7x7, and 5x5 model spectral estimates and at -3 dB for the 3x3 model are in the ratio 10 5 4 4 4 4 respectively We see that the Q-factor increases with model order indicating sharper peaks for higher model order We may apply a transformation [9],[16] on our 3x3 PSD estimate and thereby produce a modified PSD with sharper peaks Hence the Q-factor is not a measure of spectral resolution, however in applying this transformation the amplitude of one of the spectral components is attenuated significantly We conclude that better spectral estimation in terms of both peak width as quantified by the Q-factor and peak amplitude is achieved as the model order increases The only disadvantage of higher model order is added computational expense

We examined the bias and variance of spectral estimates produced by MFE and a modified covariance (MCV) method [16] We implemented both algorithms and made 25 simulation trials on each All trials used a single snapshot of data consisting of sinusoids at arbitrary unity normalised frequencies (0 1, 0 2) and (0 3 0 4) of equal amplitude at arbitrary SNR of 6 dB in uncorrelated white Gaussian noise To ensure a fair comparison, the same random number generator seed was used to initiate the 25 trials for both algorithms so that each simulation series contained an identical sequence of noise spectra This meant that the same set of 25 uncorrelated and independent noise fields were used for both algorithms The size of the sinusoid and white noise data fields were 40 x 40 points The MFE signal processing temperature was set at 0 05 This temperature was arbitrarily chosen from within a wide band of temperature which previous tests have indicated provides accurate spectral estimation Table 1 shows the bias and standard deviation of spectral estimates for both frequencies for each method. The PSD were calculated over 520x520 points and therefore the resolution of estimates is to 0 001 92 of unity normalised frequency The bias and variance statistics are comparable in the y frequency direction MCV provides better statistics in the x frequency direction The accuracy of AR model based spectral estimates depends on the size and shape of the model used [19] The x frequency statistics in this case may be improved by the use on a non symmetrical region of support for the AR model In general the statistics show that MFE provides accurate spectral estimation

Let us compare the computational expense of parameter estimation by a maximum likelihood method MLE [20], MCV and our MFE method The data set size is taken as M^2 and model order as p^2, where M >> p The cost function in MFE MCV and MLE are iteratively minimised at $O((p-1)(2p^4))$, $O(2(M-p)^2p^2)$ and $O(M^2p^2)$ multiplies respectively In MLE one of the elements is a trigonometric function MFE is computationally the least expensive It performed spectral estimation 12 times faster than MCV for any data snapshot in the comparative variance test above

4 Conclusions

A 2-D MFE parameter estimation technique has been proposed We have demonstrated the performance of the technique by performing MFE AR modelling and spectral estimation of closely spaced sinusoids in white noise We have seen that the better spectral estimation may be achieved at higher model order We have shown that it is possible to obtain superior spectral estimation, with equivalent computational burden, using MFE at a temperature greater than zero than at zero temperature using the multidimensional Levinson algorithm

We have compared MFE to a modified covariance technique over a number of simulation trials The results show that MFE provides accurate spectral estimation over a series of independent trials We have found that the bias and standard deviation of spectral estimates are comparable in the y frequency direction and better with MCV in the x frequency We have found that MFE is significantly faster than the modified covariance technique

References

[1] A K Jain Advances in Mathematical Models for Image Processing, Proc IEEE, vol 69, pp 502-528, May 1981

[2] J Capon, High Resolution Frequency-Wavenumber Spectrum Analysis, Proc IEEE, vol 57, pp 1408-1418, Aug 1969

[3] J H McClellan and R.J Purdy, Applications of digital signal processing to radar, in Applications of Digital Signal Processing, A V Oppenheim, Ed. Englewood Cliffs, NJ Prentice-Hall, 1978

[4] J H McClellan, Multidimensional Spectral Estimation, Proc IEEE, vol 70, pp 1029-1039, Sept 1982

[5] S Sibisi, J Skilling, R.G Brereton, E D Laue and J Staunton, Maximum entropy signal processing in practical NMR spectroscopy, Nature, vol 311, pp 446-447, Oct 1984

[6] E A Robinson and S Treitel, Digital signal processing in geophysics, in Applications of Digital Signal Processing, A V Oppenheim, Ed. Englewood cliffs, NJ Prentice-Hall, 1978

[7] R. Narayan and R. Nityananda, Maximum entropy image restoration in astronomy, Annu Rev Astron Astrophys , vol 24, pp 127-170, 1986

[8] J M Pimbley, Recursive Autoregressive Spectral Estimation by Minimisation of the Free Energy, IEEE Trans Signal Processing, vol 40, no 6, pp 1518-1527 June 1992

[9] S L Marple, Digital Spectral Analysis with Applications, Prentice-Hall Signal Processing series, NJ, 1987

[10] P Kiernan, Two-Dimensional Autoregressive Spectral Estimation using a Two-Dimensional Minimum Free Energy Method. Dublin City University working paper series CA-0494

[11] J M Pimbley and S D Silverstein Recursive Minimum Free Energy Spectral Estimation, Proc 23rd Asilomar Conf Signals, Syst Comput pp 1051-1055, 1989

[12] D K Cooper and J M Pimblev, A Minimum Free-Energy Hybrid Algorithm for 2-D Spectral Estimation, IEEE Trans Signal Processing, vol 42, no 3 pp 698-702, March 1994

[13] J A Cadzow and K Ogino Two-Dimensional Spectral Estimation. IEEE Transactions on Acoustics, Speech and Signal Processing, vol 29, no 3, pp 396-401, June 1981

[14] P Whittle, On Stationary Processes in the Plane, Biometrika, vol 41, pp 434-449, 1954

[15] X D- Zhang and J Cheng, High Resolution Two-Dimensional ARMA Spectral Estimation, IEEE Trans Signal Processing vol 39 no 3, pp 765-770 March 1991

[16] S M Kay, Modern Spectral Estimation Theory and Application, Prentice-Hall, NJ 1988

[17] S D Silverstein and J M Pimbley, The Minimum Free Energy Method of Spectral Estimation, in - Advances in Spectral Analysis and Array Processing, S Haykin Ed, NJ Prentice-Hall, 1992

[18] Alexander Graham, Kronecker Products and Matrix Calculus with Applications, Ellis Horwood Series - Mathematics and its Applications, 1981

[19] J Lim, Two-Dimensional Signal and Image Processing, Chapter 6, Prentice-Hall Int., Inc 1990

[20] R.L Kashyap, Characterization and Estimation of Two-Dimensional ARMA Models, IEEE Trans Information Theory, vol. 30, no 5, pp 736-745, Sept , 1984

Fig 1 MFE model based spectral estimates of sinusoids at normalised frequencies (0 1 0 2) and (0 3, 0 4) in white noise at temperature (a), (b) 0 074 and (c), (d) zero

(a) (c) Normalised amplitude spectral estimate on the x frequency axis, (b) (d) Contour plot in dB on x and y frequency axes

Table 1

	MFE		MCV	
f_x	Bias x 10^{-3}	Std x 10^{-3}	Bias x 10^{-3}	Std x 10^{-3}
0 1	-2 3	7 40	0 077	0 385
0 3	-2 5	9 96	0 0	0 544
f_y	Bias x 10^{3}	Std x 10^{-3}	Bias x 10^{-3}	Std x 10^{-3}
0 2	0 458	0 939	0 308	0 769
0 4	0 092	1 11	0 231	0 666

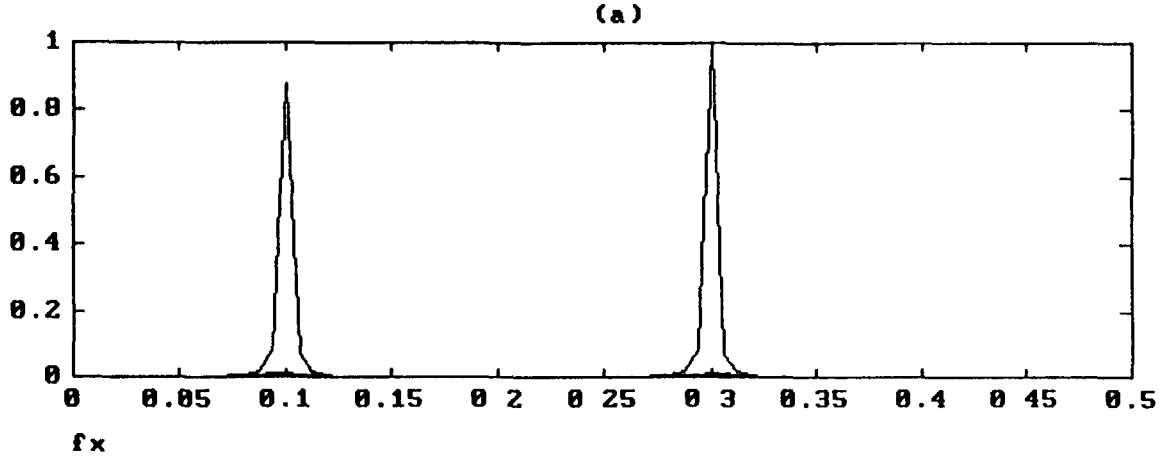
(a)
1
0.8
0.6
0.4
0.2
0
0
0.05
0.1
0.15
0 2
0 25
0 3
0.35
0.4
0 45
0.5
fx

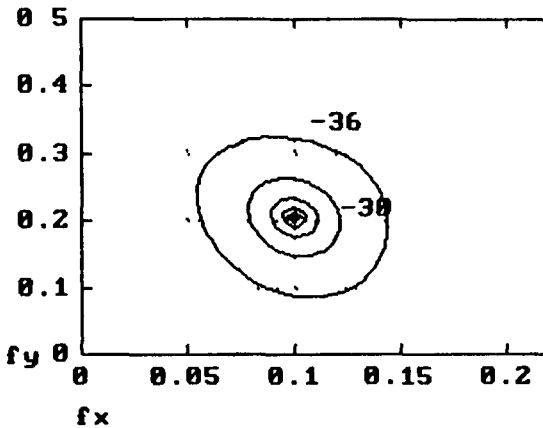
0 5
0.4
0.3
0.2
0.1
fy 0
0
0.05
0.1
0.15
0.2
fx
-36
-30

(b)

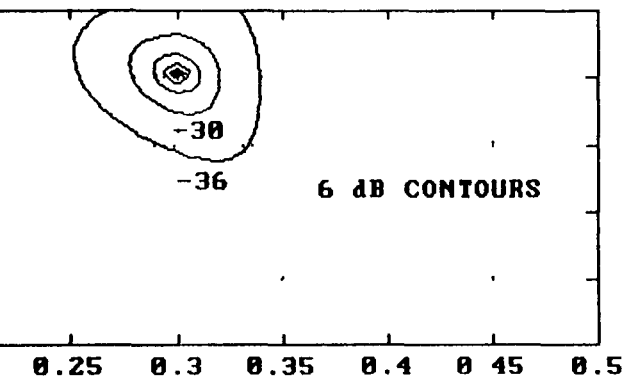

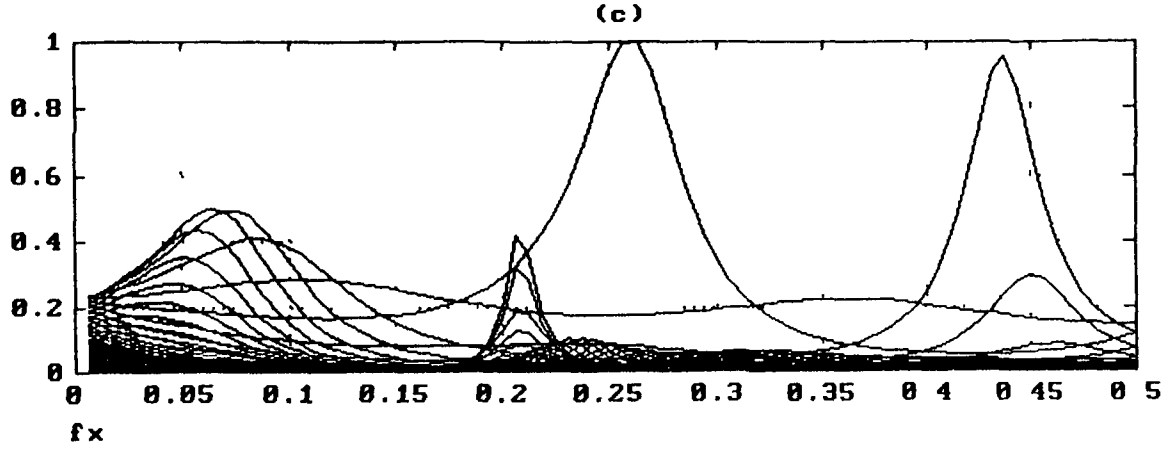
(c)
1
0.8
0.6
0.4
0.2
0
0
0.05
0.1
0.15
0.2
0.25
0.3
0.35
0 4
0 45
0 5
fx

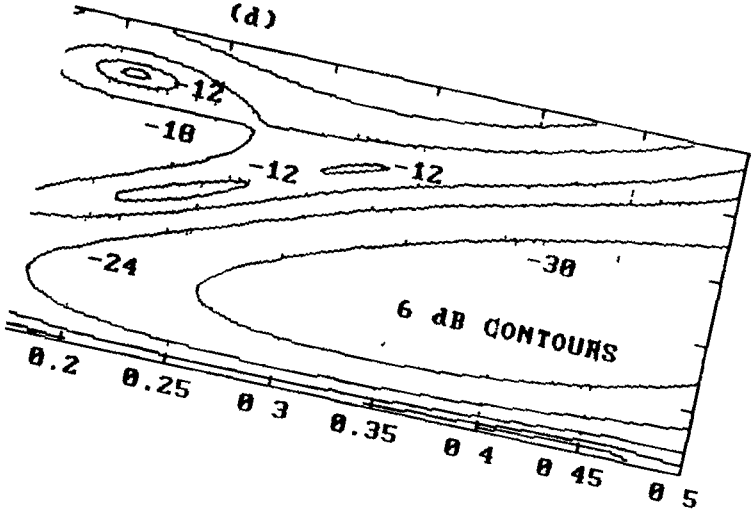
(d)
-12
-18
-12
-12
-24
-30
6 dB CONTOURS
0.2
0.25
0 3
0.35
0 4
0 45
0 5

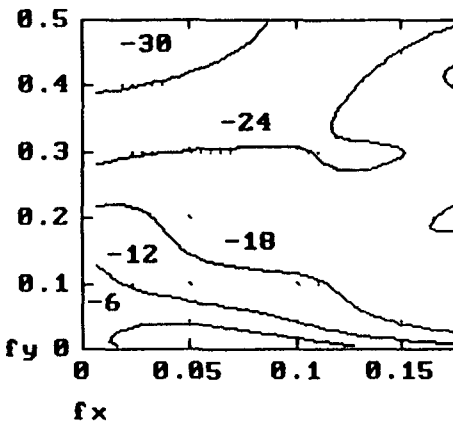
0.5
0.4
0.3
0.2
0.1
fy 0
-30
-24
-18
-12
-6
0
0.05
0.1
0.15
fx

High Resolution Two-Dimensional Minimum Free Energy AR Spectral Estimation, P Kiernan, to be published, Multidimensional Systems and Signal Processing, vol 6, pp 237-249, July 1995

High Resolution Two-Dimensional Minimum Free Energy AR Spectral Estimation

by

Paul Kiernan

Abstract - We extend the Minimum Free Energy (MFE) parameter estimation method to 2-D fields This 2-D MFE method may be used to determine autoregressive (AR) model parameters for spectral estimation of 2-D fields It may also be used to provide AR models for texture synthesis The performance of the technique for closely spaced sinusoids in white noise is demonstrated by numerical example Better results can be achieved than with the multidimensional Levinson algorithm

I Introduction

We are concerned with models with quarter plane (QP) parameter region of support which are a direct 2-D extension of the linear time series seasonal analysis models of Box and Jenkins [1] The Levinson recursion is an established autocorrelation based method for deriving the parameters of a causal AR model [2] We show how model parameters for 2-D fields may be determined by the solution of 2-D Yule-Walker equations via an MFE based modified multidimensional Levinson algorithm Our modification of the multidimensional Levinson algorithm [3] is based on determination of the reflection coefficient matrices by minimisation of the free energy rather than by minimisation of the forward and backward linear prediction error energy alone The proposed method is an 2-D extension of the method developed by Pimbley [4], and Pimbley and Silverstein [5] A second optimization loop may be introduced to determine the optimal signal processing temperature to achieve good parameter estimates To the authors knowledge, there have been no previous publications which extend the MFE method of parameter estimation to 2-D providing 2-D spectral estimation of closely spaced sinusoids

II Theory

The reflection coefficients in Levinson type algorithms are the negative normalized correlation coefficients between the forward and backward linear prediction errors (e^f e^b), with one unit of delay [3] In the Burg harmonic algorithm the error energy i e the sum of the forward and backward prediction error energy is minimized The reflection coefficients k_m at stage m $(1 \le m \le p)$ of a recursive algorithm, for model order p, and data sequence length N are given as

$$k_m = -2\Delta_m \,/\, (P^f_{m-1} + P^b_{m-1}) = -\Delta_m / P^f_{m-1} = a_m[m] \tag{1}$$

$$a_m[q] = a_{m-1}[q] + a_m[m]a_{m-1}[m-q] \quad 1 \le q \le m-1 \tag{2}$$

where $a_m[q]$ are the AR parameters and P^f and P^b are the forward and backward linear prediction error variances

$$P^f_{m-1} = \sum_{n=m+1}^{N} |e^f_{m-1}[n]|^2 \quad = \quad P^b_{m-1} = \sum_{n=m+1}^{N} |e^b_{m-1}[n-1]|^2 \tag{3}$$

$$\Delta_m = \sum_{n=m+1}^{N} e^f_{m-1}[n]\; e^b_{m-1}[n-1] \tag{4}$$

Hence $$\Delta_m + P^f_{m-1} k_m = 0 \tag{5}$$

In the MFE method [4] [5] the free energy F

$$F = u - \alpha H, \tag{6}$$

is minimized with respect to the reflection coefficients u is the prediction error energy, H is the entropy and α is the signal processing temperature If the power spectral density (psd) is given by

$$S(f) = \beta \,/\, |D(f)|^2 \tag{7}$$

where $$D(f) = 1 + \sum_{k=1}^{p} a(k)\; exp(-j2\pi fkT) \tag{8}$$

then $$H = \int_{-1/2}^{1/2} ln \left[\beta \; / \; |D(f)|^2 \right] df \qquad (9)$$

The energy due to the entropy is differentiated with respect to the real and imaginary parts of a reflection coefficient at stage m

In the 2-D case the reflection coefficients at stage m of the recursion are represented by a set of reflection matrices $\mathbf{A}_m[m]$ If the order of the model used is $(p1+1,\ p2+1)$, then from the multidimensional Levinson algorithm [3] at the last $(m = p1)$ recursion,

$$\mathbf{A}_{p1+1}[p1+1]\ \mathbf{P}^f_{p1} + \Delta_{p1+1} = 0 \qquad (10)$$

where

$$\Delta_{p1+1} = \left[\mathbf{I} \quad \mathbf{A}_{p1}[1]\ \mathbf{A}_{p1}[2] \quad \mathbf{A}_{p1}[p1] \right] \left[\mathbf{Ryy}[p1+1]\ \mathbf{Ryy}[p1] \quad \mathbf{Ryy}[1] \right]^T \qquad (11)$$

$$\mathbf{P}^f_{p1+1} = \left[\mathbf{I} - \mathbf{A}_{p1+1}[p1+1]\ \mathbf{A}^T_{p1+1}[p1+1] \right] \mathbf{P}^f_{p1} \qquad (12)$$

$$\mathbf{A}_{p1+1}[q] = \mathbf{A}_{p1}[q] + \mathbf{A}_{p1+1}[p1+1]\mathbf{A}^T_{p1}[p1-q] \quad \text{for} \quad 1 \le q \le p1 \qquad (13)$$

$\mathbf{Ryy}[\,]$ are the observed field autocorrelation matrices The derivation of these equations for the multidimensional case is based on the multichannel case and there is a direct correspondence between $\mathbf{A}_m[m]$ in multichannel and k_m for the single channel case Optimization of the reflection coefficients based on minimisation of prediction error energy is based on (10)

We now require the differential of the 2-D entropy term with respect to the reflection coefficient matrix at stage m, $(\partial \alpha H / \partial \mathbf{A})$ We are concerned with simultaneous AR models which may be represented by

$$\sum_{i=0}^{p1} \sum_{j=0}^{p2} a(i\ j) y(m-i, n-j) = u(m, n) \qquad (14)$$

We assume that $a(0,0)\equiv 1$, $\{y(m,n)\}$ is a finite set of observations on $1 \le m \le N$, $1 \le n \le N$ and u is a homogeneous random field A toroidal model is assumed on this $N \times N$ lattice [6] $\{u(m,n)\}$ is independent (uncorrelated) Gaussian white noise with zero mean and variance σ^2 The factorable SAR model in (14) is a special case of the conditional AR model $\{u\}$ is correlated for the conditional case The power spectral density of this model [7] may be written in normalised spatial frequency terms (ω_1, ω_2), where $|\omega_1| \le 1/2$ and $|\omega_2| \le 1/2$ as

$$S(\omega_1, \omega_2) = \frac{\sigma^2}{\left| \sum_{k=0}^{p1} \sum_{l=0}^{p2} a_{kl} e^{-j(\omega_1 k + \omega_2 l)} \right|^2} \qquad (15)$$

or $$S(f_1, f_2) = \beta \,/\, |D(f_1, f_2)|^2 \quad \text{where} \quad \beta = \sigma^2 \qquad (16)$$

The Yule-Walker equations are based on the autocorrelation estimates of the observed field and are given by

$$\sum_{i=0}^{p1} \sum_{j=0}^{p2} a(i,j) r_{yy}(k-i, l-j) = (\sigma^2 \text{ for } (k,l) = (0,0),\ 0 \text{ for } (k,l) \in QP')$$

where $$QP = QP' \cup (0,0) \qquad (17)$$

or in matrix form [8] as $$\mathbf{Ra} = \mathbf{h} \qquad (18)$$

R is a block Toeplitz matrix which is symmetric and positive semi-definite Furthermore the matrix is made up of blocks Ryy which are also Toeplitz in structure though not symmetric Hence (18) may be solved by the multidimensional Levinson algorithm which is derived from the multichannel Levinson algorithm [9] The solution yields the AR parameters and white driving noise variance of the model This method is the minimisation of prediction error energy method We extend this method by including an extra cost function based on entropy The motivation for inclusion of the extra cost function comes from statistical thermodynamics

There is a direct analogy between statistical thermodynamics and stochastic signal analysis The ground state in physical systems corresponds to the case in signal processing where parameter estimation is carried out on the basis of minimisation of the prediction error energy alone In this case fluctuations disappear and physical systems condense into their ground state In signal analysis this corresponds to zero input from the entropy term

"At nonzero temperature, physical systems are neither in minimum energy states nor in maximum entropy states Rather, there exists a balance between low energy and high entropy Increasing the system temperature emphasizes the importance of entropy at the expense of energy Conversely, reduction of the temperature to absolute zero forces the system into its lowest energy state" [10] Temperature, therefore, acts as a control parameter for the entropy or fluctuations in the system The cost function in the 1-D MFE parameter estimation algorithm is based on an extension of the least mean square (LMS) criterion to include a noisy data cost element This extra cost element is due to the entropy energy term The 2-D system is directly analogous in that there is an extra term due to the entropy

The result of adding this extra cost function is to minimize the resultant free energy, thereby providing better spectral estimation than that provided by minimization of prediction error energy alone The Shannon-Burg entropy measure is defined to within an arbitrary constant Therefore for the entropy field H

$$H \propto \int_{-1/2}^{1/2} \int_{-1/2}^{1/2} \ln \left(\beta \, / \, |D(f_1, f_2)|^2 \right) \, df_1 df_2 \qquad (19)$$

For purely real fields the reflection coefficient matrix **A** is real We

express the differential of the entropy energy term, with respect to **A** as

$$\partial\alpha H/\partial \mathbf{A} = \alpha \left[\partial \ln(\beta)/\partial \mathbf{A} - \partial \left(\int_{-1/2}^{1/2} \int_{-1/2}^{1/2} \ln \left(|D(f_1,f_2)|^2 \right) df_1 df_2 \right) / \partial \mathbf{A} \right] \qquad (20)$$

The entropy proportionality constant is absorbed into the temperature parameter α

At stage m of the recursion the RHS becomes

$$= - \int_{-1/2}^{1/2} \int_{-1/2}^{1/2} \partial \left[\ln \left[D_m(f_1,f_2) D_m^{*}(f_1,f_2) \right] \right] / \partial \mathbf{A}_m[m] \; df_1 df_2 \qquad (21)$$

$$= - \int_{-1/2}^{1/2} \int_{-1/2}^{1/2} \partial \ln D_m(f_1,f_2)/\partial \mathbf{A}_m[m] + \partial \ln D_m^{*}(f_1,f_2)/\partial \mathbf{A}_m[m] \; df_1 df_2 \qquad (22)$$

At any frequency (f_1,f_2) the differential

$$\partial \ln D_m(f_1,f_2)/\partial \mathbf{A}_m[m] \qquad (23)$$

is the differential of a scalar with respect to a matrix and may be expressed as a $(p1,p1)$ matrix with any element $\mu(i,j)$ given by

$$\mu(i,j) = \partial \ln D_m(f_1,f_2)/\partial \tau_{i,j} = D_m^{-1} \partial D_m(f_1,f_2)/\partial \tau_{i,j} \qquad (24)$$

where $\tau_{i,j}$ is an element of the reflection matrix $\mathbf{A}_m[m]$ The integration becomes

$$\int_{-1/2}^{1/2} \int_{-1/2}^{1/2} \left[\partial D_m(f_1,f_2)/\partial \mathbf{A}_m[m] \right] / D_m(f_1,f_2) \; df_1 \; df_2 \qquad (25)$$

$$+ \int_{-1/2}^{1/2} \int_{-1/2}^{1/2} \left[\partial D_m^{*}(f_1 f_2)/\partial \mathbf{A}_m[m] \right] / D_m^{*}(f_1,f_2) \; df_1 \; df_2 \qquad (26)$$

The second part of this expression becomes

$$\int_{-1/2}^{1/2}\int_{-1/2}^{1/2}\left[\partial\Big(\sum_{k=0}^{p1}\sum_{l=0}^{p2}a_{kl}[m]e^{J(f_1k+f_2l)}\Big)\,/\,\partial A_m[m]\right]\,/\,D^{*}_{m}(f_1,f_2)\,df_1\,df_2 \quad (27)$$

The contour integral is taken about a surface in the 2-D complex frequency hyperplane We extend the argument [4] that the symmetry in the contour path reduces the contour integration to integrations at

(a) $$\left[-1/2 \le Re(f_1) \le +1/2,\ Im(f_1) = -\infty\right],$$

$$\left[-1/2 \le Re(f_2) \le +1/2,\ Im(f_2) = -\infty\right]$$

and at

(b) $$\left[-1/2 \le Re(f_1) \le +1/2,\ Im(f_1) = 0\right],$$

$$\left[-1/2 \le Re(f_2) \le +1/2,\ Im(f_2) = 0\right] \quad (28)$$

The integration at (a) goes to zero as the numerator of the expression (27) contains a multiplicative exponential term which suggests that for $f_1 = -J\infty$ and $f_2 = -J\infty$, as in the 1-D case for $f = -J\infty$, the integral vanishes i e the numerator goes to zero, while the denominator reduces to unity

We now examine the integration at (b) A positive definite autocorrelation matrix may yield solutions to the Yule Walker equations, though they may not be stable Therefore the multidimensional method [3] which is a minimum prediction error method may yield unstable results Hence $D(f_1,f_2)$ may not be minimum phase However by sufficiently whitening the input field we may ensure that the autocorrelation falls off fast enough so that $D(f_1,f_2)$ tends to be minimum phase This results in a stable model which may also be used for field synthesis purposes such as texture generation Given that $D(f_1 f_2)$ is minimum phase then all singularities i e solutions of the equation $D(z_1,z_2) = 0$, or zeroes of $D(z_1,z_2)$ are within the unit bicircle Hence there are no zeros

outside the unit bicircle or in the lower half of the 2-D complex frequency plane

The test for a bivariate polynomial can be simplified to testing for each variable when the other is fixed, and the number of zeroes may be determined by fixing one variable and performing the contour integration with respect to the other In performing double contour integration one variable is fixed and the contour integral is evaluated with respect to the other variable Therefore Cauchy's integral formula applies to a double contour integral

$$\oint_{c1} \oint_{c2} f'(z_1, z_2)/f(z_1, z_2)\, dz_1 dz_2 = 0 \qquad (29)$$

Hence the integration on the region specified by (28) (b) goes to zero

In terms of the parameters within the Levinson algorithm

$$ln\ \beta_m = ln \left[\mathbf{P}^f_m \right] = ln \left[(\mathbf{I} - \mathbf{A}_m[m]\ \mathbf{A}_m[m])\ \mathbf{P}^f_{m-1} \right] \qquad (30)$$

$$\text{hence} \quad \partial(ln\ \beta_m) / \partial \mathbf{A}_m[m] = \partial ln \left[(\mathbf{I} - \mathbf{A}_m[m]\ \mathbf{A}_m[m])\ \mathbf{P}^f_{m-1} \right] / \partial \mathbf{A}_m[m] \qquad (31)$$

$$\text{If} \quad \mathbf{B}_m = \partial(ln\ \beta_m) / \partial \mathbf{A}_m[m] \qquad (32)$$

Then the cost function used at recursion m is given by finding a reflection matrix $\mathbf{A}_m[m]$ such that

$$\mathbf{A}_m[m]\ \mathbf{P}^f_{m-1} + \Delta_m - \alpha\ \mathbf{B}_m = 0 \qquad (33)$$

When $\alpha = 0$ the method reverts to the multidimensional Levinson algorithm A Nedler-Mead simplex [11] or Newton gradient [12] technique may be used to perform the minimisation depending on the model order and temperature range of interest

III Results

In this section we provide numerical examples in which the method outlined above has been applied These examples show power spectral estimates determined directly using MFE based AR model parameters The resolution of sinusoids in white noise is a widely used standard simulation exercise for spectral estimation techniques including AR model based techniques [7],[10] [13-17] We have used an autocorrelation estimated from a realisation of sinusoids in white noise This 160 x 160 point autocorrelation corresponds to a data set consisting of data samples over an 80 x 80 rectangular region of support

In the first example two closely spaced sinusoids at normalised frequencies (f_x, f_y) of (0 1, 0 2) and (0 11, 0 38) at 7 6 dB signal to noise ratio (SNR) in white noise are used We have established by experimentation that the best model order for this example is 5x5 It may be possible to determine the model order by use of the Akaike information criterion This has been proposed by Pimbley [4] and more recently by Cooper and Pimbley [18] However the Akaike information criterion is not a consistent decision rule for estimating the order of AR models [19] We use a simple and effective method of increasing the model order as long as the resolution of the resultant spectral estimate is improving The computational expense of the method depends on model order, hence there is a simple trade off between added computational expense and higher resolution

All psd are 80x80 point and are generated with (15) and the parameters from MFE AR models All frequencies are normalised for one cycle equal to unity The plots in figures 1 (a) and (b) were derived using the MFE based AR model of order 5x5 at zero temperature The plots in figures 1 (c) and (d) are for temperature 0 5

Figure 1 (a) shows the normalised amplitude psd estimate in the x frequency direction $psd\ (f_x, 0)\quad 0 \le f_x \le 0.5$ A number of spectral peaks occur however only one of them at $f_x = 0.09$ is close to the correct frequency $f_x = 0.1$ or $f_x = 0.11$ The contour plot [16] in figure 1 (b) shows the psd estimate in the x frequency direction $psd\ (f_x, 0)\quad 0 \le f_x \le 0.5$ and in y frequency direction $psd\ (0, f_y)\quad 0 \le f_y \le 0.5$ One peak is located near (0.1 0.2), there is no peak at (0.11,0.38) and several spurious peaks occur Thus at zero temperature neither of the spectral components at spatial frequencies (0.1 0.2) or (0.11, 0.38) are accurately resolved

Figure 1 (c) shows the normalised psd plot at temperature 0.5 in the x frequency direction $psd\ (f_x, 0)\quad 0 \le f_x \le 0.5$ Spectral peaks at frequencies $f_x = 0.1$ and $f_x = 0.11$ are clearly visible We can see in figure 1 (d) that the x frequency components at 0.1 and 0.11, and the y frequency components at 0.2 and 0.38 making up the two spatial frequencies (0.1, 0.2) and (0.11, 0.38) are accurately resolved Hence at the non zero temperature both spectral components at frequencies (0.1 0.2) and (0.11, 0.38) are accurately resolved However at zero temperature as shown in figures 1 (a) and (b) neither of the spectral components are accurately resolved

In the second example sinusoids at normalised frequencies (f_x, f_y) of (0.1 0.2) and (0.3, 0.4) at 6 dB SNR in white noise are used Figures 2 (a) and (b) show the normalised amplitude x frequency and 2-D contour psd plots derived using the MFE based AR model of order 5x5 at temperature zero Figures 2 (c) and (d) are for temperature 0.05 Figure 2 (c) shows that the estimated psd has spectral peaks at $f_x = 0.1$ and $f_x = 0.3$ The contour plot in figure 2 (d) shows that the two spectral components are accurately resolved at frequencies (0.1 0.2) and (0.3 0.4) Furthermore the sharpness of the peaks is illustrated by the 5 dB contours in the contour plot The spectral estimate at zero temperature

has two broad peaks Figure 2 (a) shows the two poorly resolved peaks The 1 dB contours of figure 2 (b) also illustrate these poorly resolved spectral peaks The peaks are not located at or near the spatial frequencies (0 1 0 2) and (0 3 0 4) We conclude that MFE provides accurate spectral estimation at temperature 0 05 whereas at zero temperature, using multidimensional Levinson method, the correct frequency components are not resolved

In the third example a sinusoid at normalised frequency (f_x, f_y) of (0 1 0 2) at 30 dB SNR in white noise is used Figures 3 (a) and (b) show the normalised amplitude x frequency and 2-D contour psd plots derived using the MFE based AR model of order 5x5 at temperature zero Figures 3 (c) and (d) are for temperature 0 5 They show that the spectral component is accurately resolved at (0 1 0 2) Figures 3 (a) and (b) show that at zero temperature no spectral peak occurs at the correct frequency and several spurious peaks occur

IV Conclusions

We have proposed a 2-D MFE parameter estimation technique We have demonstrated the performance of the technique by providing spectral estimation of closely spaced sinusoids in white noise We have shown by example that it is possible to obtain better spectral estimation at certain temperatures than at zero temperature, where at zero temperature our algorithm reverts to the multidimensional Levinson algorithm or Burg type technique

A method of identification of the best temperature range prior to or within the MFE parameter estimation algorithm should provide a computational advantage especially for high order models The cost function in MFE is minimized at $O((p-1)(2p^4))$ where the model order is p^2 Hence prior temperature determination would be significant at high model orders In order to address this issue we are investigating the

relationship between the reflection coefficient matrices in 2-D MFE and optimal signal processing temperature For optimal temperature spectral estimation the entropy term in the MFE cost function should ensure reflection matrices with elements of values less than unity

Gull [20] and Sibisi [21] present approaches for choosing signal processing temperature Sibisi determines the optimal Bayesian estimate for the signal processing temperature for the quadratic regularisation problem [18] The regularisation process corresponds to the additional cost element in MFE Gull also uses Bayesian analysis It may be possible to adapt these methods to 2-D MFE

It is also of interest to carry out experimental comparisons of performances of the technique above and approximate maximum likelihood techniques

Acknowledgement

The author would like to acknowledge and thank the anonymous reviewers for their valuable comments and suggestions

References

[1] G E P Box and G M Jenkins Time Series Analysis Forecasting and Control, Holden-Day, CA, 1976

[2] A K Jain, Fundamentals of Digital Image Processing, Prentice-Hall Englewood Cliffs, NJ, 1989

[3] S L Marple, Digital Spectral Analysis with Applications, Prentice-Hall Signal Processing series, Englewood cliffs NJ 1987

[4] J M Pimbley, Recursive Autoregressive Spectral Estimation by Minimisation of the Free Energy, IEEE Trans Signal Processing, vol 40, no 6 pp 1518-1527 June 1992

[5] J M Pimbley and S D Silverstein Recursive Minimum Free Energy Spectral Estimation Proc 23rd Asilomar Conf Signals, Syst Comput pp 1051-1055 1989

[6] P Whittle On Stationary Processes in the Plane Biometrika vol 41 pp 434-449 1954

[7] X D- Zhang and J Cheng High Resolution Two-Dimensional ARMA Spectral Estimation IEEE Trans Signal Processing, vol 39 no 3 pp 765-770 March 1991

[8] S M Kay Modern Spectral Estimation Theory and Application Prentice-Hall Englewood Cliffs, NJ 1988

[9] C W Therrien Relations between 2-D and Multichannel Linear Prediction, IEEE Trans Acoustics, Speech and Signal Processing, vol 29, pp 454-456, June 1981

[10] S D Silverstein and J M Pimbley, The Minimum Free Energy Method of Spectral Estimation, in - Advances in spectral Analysis and Array Processing, S Haykin ed, Englewood Cliffs NJ Prentice-Hall, 1992

[11] J E Dennis Jr and D J Woods, Optimization on Microcomputers The Nedler-Mead Simplex Algorithm New Computing Environments Microcomputers in Large-Scale Computing, A Wouk (Ed), SIAM, pp 116-122, 1987

[12] J E Dennis Jr and R B Schnabel, Numerical Methods for Unconstrained Optimization and Nonlinear Equations, Prentice-Hall 1983

[13] L Zou and B Liu, On resolving two-dimensional sinusoids in white noise using different spectral estimation, IEEE Trans Acoust Speech, Signal Processing, vol ASSP-36, pp 1338-1350, Aug 1988

[14] S D Silverstein and J M Pimbley Minimum-free-energy method of spectral estimation autocorrelation sequence approach J Opt Soc Am A/Vol 7 no 3 pp 356-372 March 1990

[15] X -D Zhang On the estimation of Two-Dimensional Moving Average Parameters IEEE Trans on Automatic Control, vol 36 no 10 pp 1196-1199, Oct 1991

[16] J Lim, Two-Dimensional Signal and Image Processing Chapter 6, Prentice-Hall Int , Inc, 1990

[17] T J Ulrych and C J Walker High Resolution 2-Dimensional Power Spectral Estimation Applied Time series Analysis II, D F Findley Ed pp 71-99, Academic Press, Inc New York, 1981

[18] D K Cooper and J M Pimbley A Minimum Free Energy Hybrid Algorithm, for 2-D Spectral Estimation, IEEE Trans on Signal Processing, vol 42, no 3, pp 698-702, March 1994

[19] R L Kashyap, Inconsistency of the AIC rule for estimating the order of autoregressive models, IEEE Trans Aut Control, AC-25, pp 996-997, Oct 1980

[20] S F Gull, Developments in maximum entropy data analysis, in Maximum Entropy and Bayesian Methods, J Skilling, Ed Boston Kluwer, 1989

[21] S Sibisi Regularization and inverse problem, in Maximum Entropy and Bayesian Methods J Skilling Ed Boston Kluwer, 1989

Fig 1 Spectral estimates of sinusoids at normalised frequencies (0 1, 0 2) and (0 11 0 38) at 7 6 dB SNR in white noise derived using MFE based AR models of order 5x5

(a) Normalised amplitude spectral estimate on the x frequency axis at zero temperature (b) Contour plot in dB for spectral estimate at zero temperature (c) Normalised amplitude spectral estimate on the x frequency axis at temperature 0 5 (b) Contour plot in dB for spectral estimate at temperature 0 5

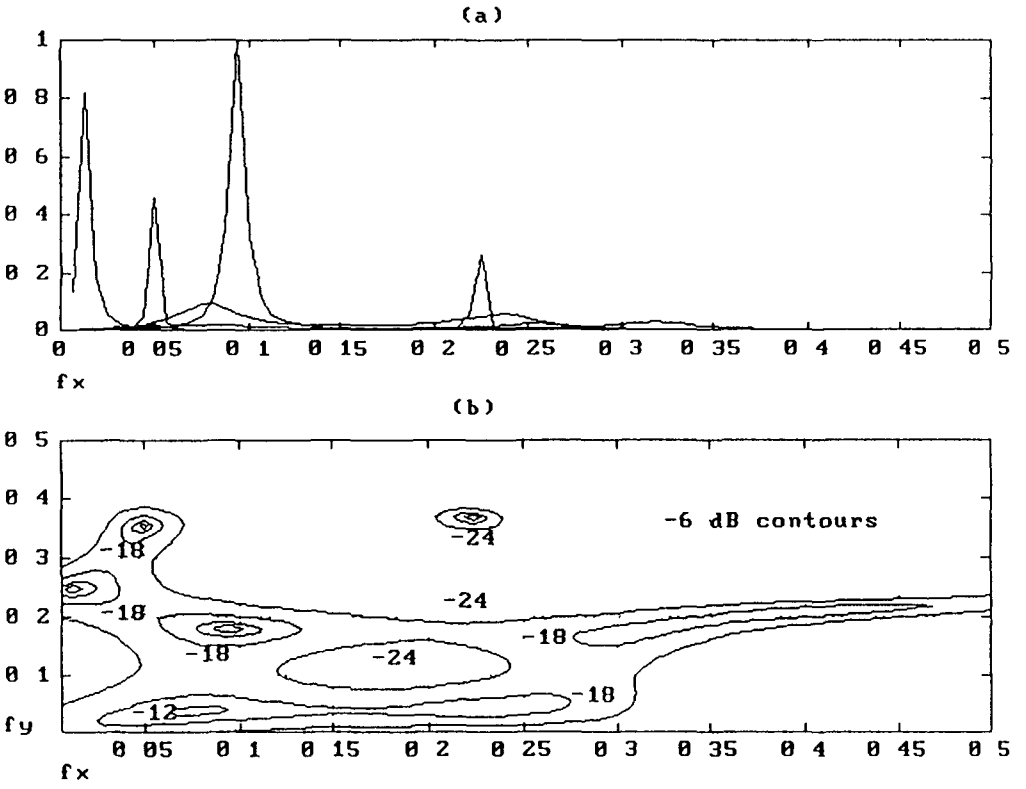
(a)
1
0 8
0 6
0 4
0 2
0
0 0 05 0 1 0 15 0 2 0 25 0 3 0 35 0 4 0 45 0 5
f x
(b)
0 5
0 4
0 3
0 2
0 1
f y
-6 dB contours
-18
-24
-18
-24
-18
-18
-24
-18
-12
0 0 05 0 1 0 15 0 2 0 25 0 3 0 35 0 4 0 45 0 5
f x

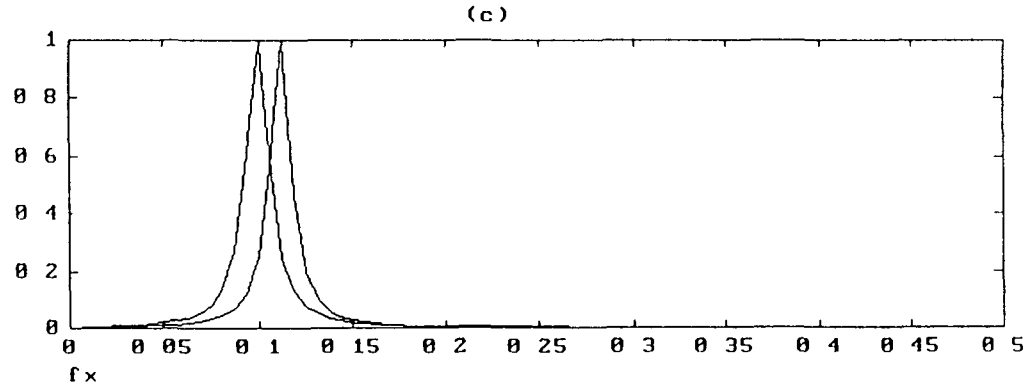
(c)
1
0 8
0 6
0 4
0 2
0
0
0 05
0 1
0 15
0 2
0 25
0 3
0 35
0 4
0 45
0 5
f x

(d)

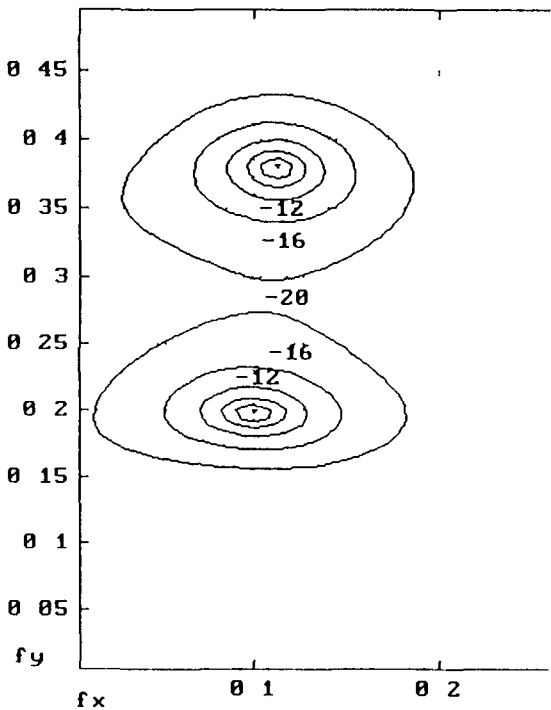

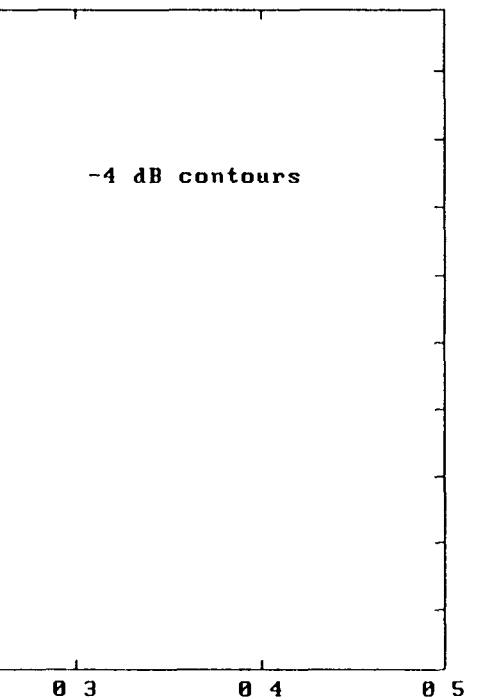
-4 dB contours
0 3
0 4
0 5

Fig 2 Spectral estimates of sinusoids at normalised frequencies (0 1 0 2) and (0 3 0 4) at 6 dB SNR in white noise derived using MFE based AR models of order 5x5

(a) Normalised amplitude spectral estimate on the x frequency axis at zero temperature (b) Contour plot in dB for spectral estimate at zero temperature (c) Normalised amplitude spectral estimate on the x frequency axis at temperature 0 05 (d) Contour plot in dB for spectral estimate at temperature 0 05

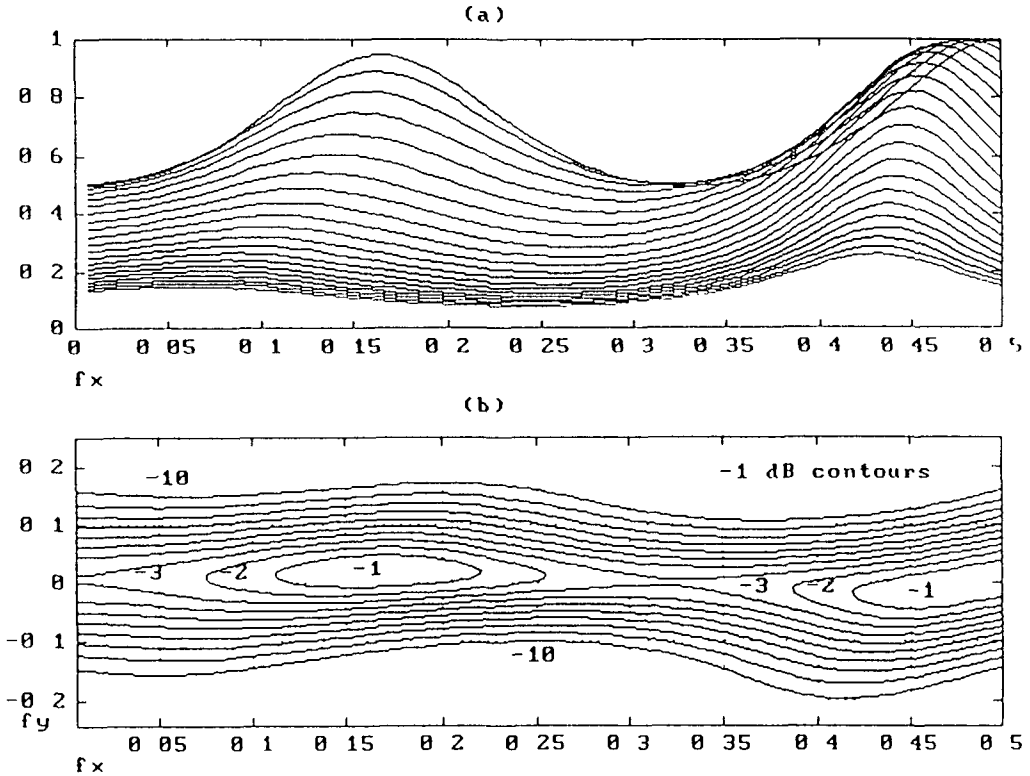
(a)
1
0 8
0 6
0 4
0 2
0
0 0 05 0 1 0 15 0 2 0 25 0 3 0 35 0 4 0 45 0 5
f x
(b)
0 2
0 1
0
-0 1
-0 2
f y
-10
-1 dB contours
-3
-2
-1
-3
-2
-1
-10
0 05 0 1 0 15 0 2 0 25 0 3 0 35 0 4 0 45 0 5
f x

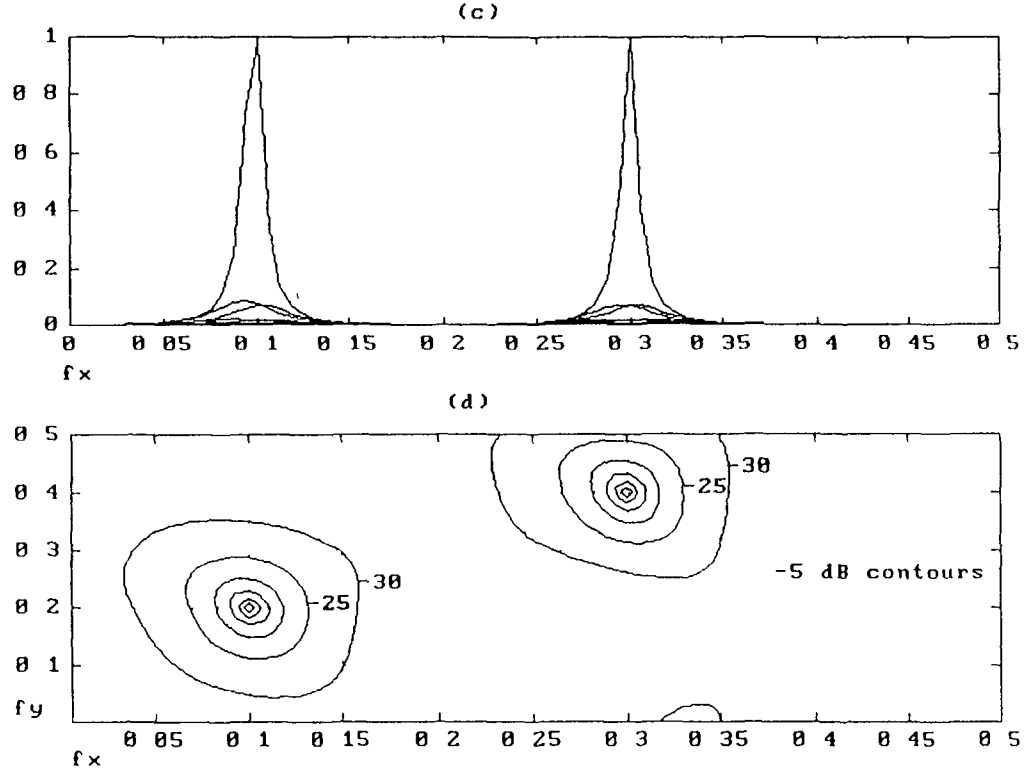
(c)
1
0 8
0 6
0 4
0 2
0
0 0 05 0 1 0 15 0 2 0 25 0 3 0 35 0 4 0 45 0 5
f x
(d)
0 5
0 4
0 3
0 2
0 1
f y
30
25
30
25
-5 dB contours
0 0 05 0 1 0 15 0 2 0 25 0 3 0 35 0 4 0 45 0 5
f x

Fig 3 Spectral estimates of sinusoid at normalised frequency (0 1 0 2) at 30 dB SNR in white noise derived using MFE based AR models of order 5x5

(a) Normalised amplitude spectral estimate on the x frequency axis at zero temperature (b) Contour plot in dB for spectral estimate at zero temperature (c) Normalised amplitude spectral estimate on the x frequency axis at temperature 0 5 (d) Contour plot in dB for spectral estimate at temperature 0 5

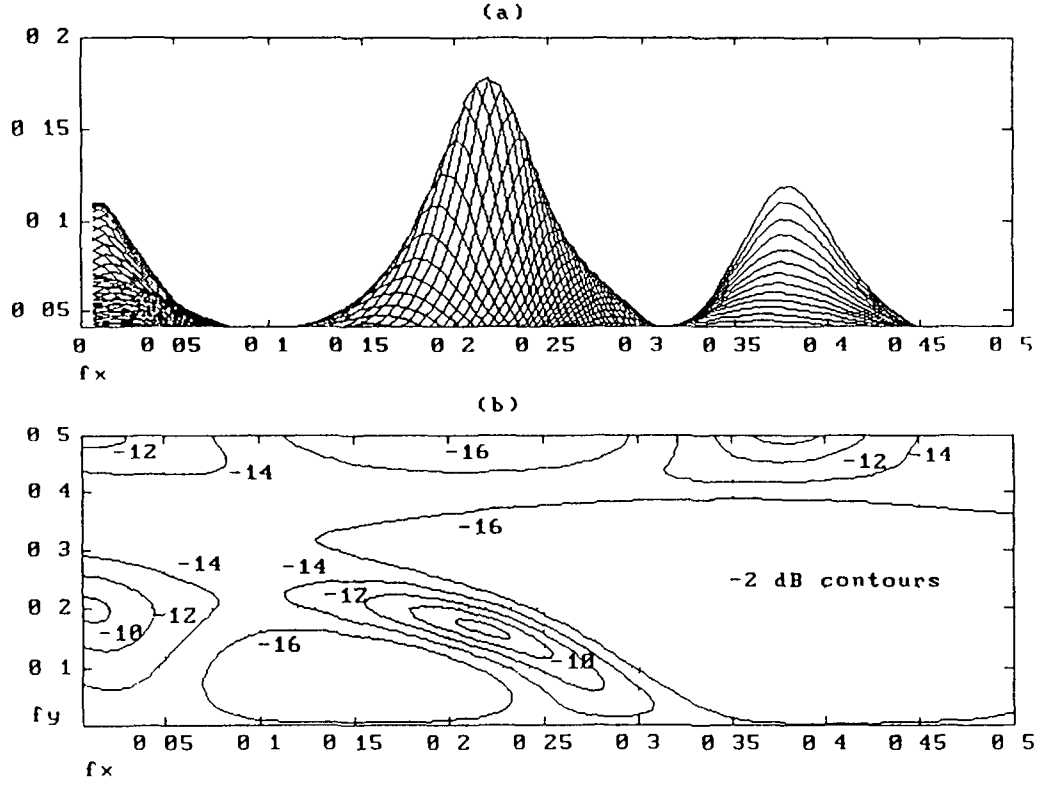
(a)
0 2
0 15
0 1
0 05
0
0 05
0 1
0 15
0 2
0 25
0 3
0 35
0 4
0 45
0 5
fx
(b)
0 5
0 4
0 3
0 2
0 1
fy
-12
-14
-16
-12
-14
-16
-14
-14
-12
-2 dB contours
-10
-12
-16
-10
0 05
0 1
0 15
0 2
0 25
0 3
0 35
0 4
0 45
0 5
fx

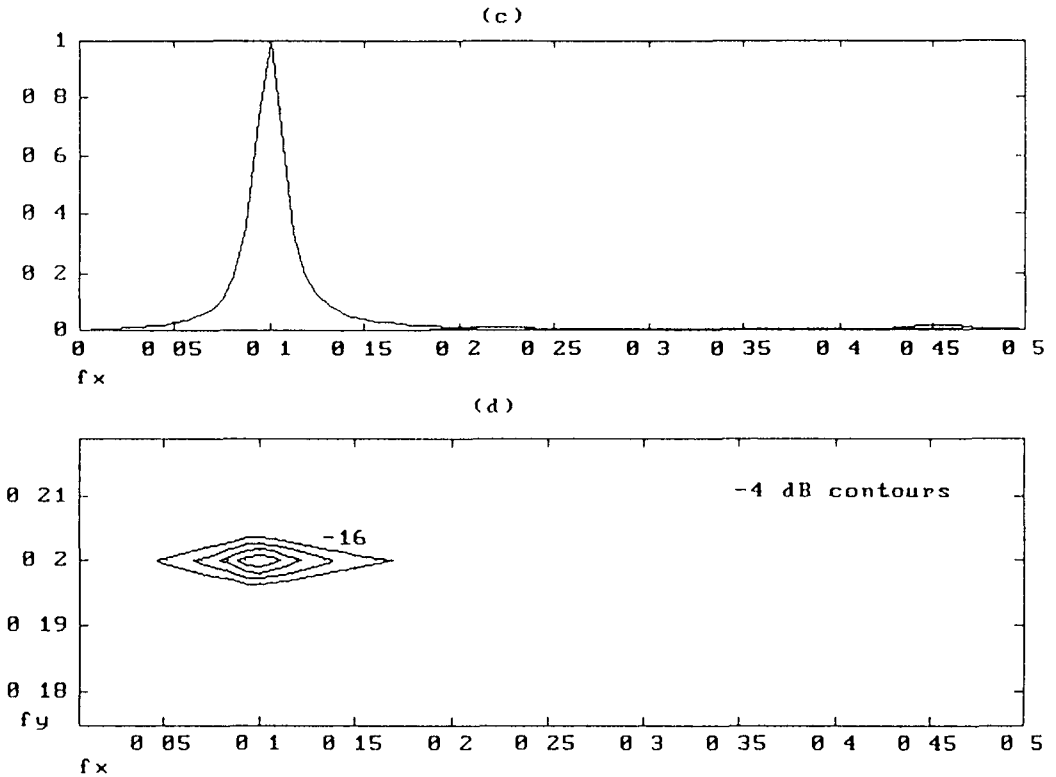
(c)
1
0 8
0 6
0 4
0 2
0
0 0 05 0 1 0 15 0 2 0 25 0 3 0 35 0 4 0 45 0 5
f x
(d)
0 21
0 2
0 19
0 18
f y
-4 dB contours
-16
0 0 05 0 1 0 15 0 2 0 25 0 3 0 35 0 4 0 45 0 5
f x